NASA Contractor Report 187546

(NASA-CR-187546) SIGNAL PROCESSING OF
AIRCRAFT FLYOVER NOISE (Lockheed
Engineering and Sciences Corp.) 86 p
CSCL 20A
G3/7
N91-2434
Unclas
0019371

Signal Processing of Aircraft Flyover Noise

Jeffrey J. Kelly

Lockheed Engineering & Sciences Company
Hampton, Virginia

Contract NAS1-19000
May 1991

National Aeronautics and
Space Administration

Langley Research Center
Hampton, Virginia 23665

TABLE OF CONTENTS

LIST OF TABLES

LIST OF FIGURES

LIST OF FIGURES (cont'd)

LIST OF SYMBOLS AND ABBREVIATIONS

A_n	signal amplitude
ANOPP	aircraft noise prediction program
c_o	ambient speed of sound
f	frequency
f_c	filter cut-off frequency
f_R	Doppler shifted frequency
f_s	source frequency
$f_R^{(1)}$	upper bound of Doppler shift
$f_R^{(2)}$	lower bound of Doppler shift
FFT	fast Fourier transform
G_{pp}	power spectral density function
h	altitude
HSR	high speed research
HST	high speed transport
L	sound-pressure level
L_{OA}	overall sound-pressure level
$\mathbf{M}$	Mach number vector ($=\mathbf{U}/c_o$)
N	block size
n_d	number of records
$\mathbf{n}_r(\tau)$	unit vector in the direction of $\mathbf{r}(\tau)$
OASPL	overall sound-pressure level
p	acoustic pressure
P	Fourier transform of pressure
p_{ref}	reference pressure (20 μPa)

Q	source strength
$\mathbf{r}(\tau)$	position vector between source and receiver at time τ
r_R	magnitude of receiver position vector ($=\lvert\mathbf{x}_R\rvert$)
SPL	sound-pressure level
t	reception time
T	window duration
$\mathbf{U}$	source velocity vector
w_n	window function
x_{in}	signal samples
$\mathbf{x}_R$	position vector of receiver
$\mathbf{x}_S$	position vector of source
Δf	bin width
Δt	sample rate
$\Delta\theta$	smear angle
θ,ϕ	source directivity angles
θ_1	initial emission angle
θ_2	final emission angle
τ	emission time

ABSTRACT

A detailed analysis of signal processing concerns for measuring aircraft flyover noise is presented. Development of a de-Dopplerization scheme for both corrected time history and spectral data is discussed along with an analysis of motion effects on measured spectra. A computer code was written to implement the de-Dopplerization scheme. Input to the code is the aircraft position data and the pressure time histories. To facilitate ensemble averaging, a level uniform flyover is considered in the study but the code can accept more general flight profiles. The effects of spectral smearing and its removal are discussed. Using test data acquired from an XV-15 tilt-rotor flyover, comparisons are made between the measured and corrected spectra. Frequency shifts are accurately accounted for by the de-Dopplerization procedure. It is shown that by correcting for spherical spreading and Doppler amplitude along with frequency can give some idea about noise source directivity. The analysis indicated that smearing increases with frequency and is more severe on approach than recession. Simulated spectra were generated using a moving point source model with frequency content similar to the XV-15 data. The results from the simulation corroborated the observations obtained from the analysis of the actual flight data.

INTRODUCTION

Until recently, only 1/3 octave spectra were produced from flyover tests. The effect of Doppler shifts was difficult to assess with these spectra. Tonal resolution and the frequency dependence of any broadband noise was often poor. Rapid advances in digital techniques pertaining to both algorithms and hardware have greatly influenced acoustic testing in recent years. This has enhanced resolution in spectra and allowed greater flexibility in signal processing. But these advantages of digital methods require some knowledge of the theory behind them in order to make the most of their features.

This paper describes some of the concerns and goals of signal processing procedures regarding aircraft flyover noise measurements. The emphasis now placed on HSR has produced increased interest in flyover noise measurements and its attendant data analysis. Since HSR developmental funding is linked to environmental issues, one of which is noise, accurate acoustic acquisition and signal analysis on aircraft that emulate the HST is of paramount importance. Due to higher speeds envisaged throughout its flight envelope, motion effects will be more pronounced on acoustic data for the HST than for conventional aircraft.

Nonstationarity in aircraft noise and its subsequent signal restoration have been addressed previously. One study [1] develops two-dimensional (frequency-time) spectral descriptions which are based on time variant linear filter theory. This is a more accurate approach in theory to nonstationary analysis in the sense that it does not begin with any stationarity assumptions. In practice nonstationary theory increases the complexity involved in data analysis procedures. Nonstationary signal analysis is still in a developing stage and its theory is not well-known in the acoustics community. The Lorentz transformation is employed in another investigation [2] to relate a stationary moving source to its measured data which provided an estimated autocorrelation function. De-Dopplerization schemes that compensate for motion effects in the signal time history are the topics of other studies [3,4]. An approach similar to this is adopted in this paper but greater detail in the signal processing schemes and parameters is given along with an analysis of smearing effects on the measured data.

Both the actual measured ground spectra and the de-Dopplerized versions for a particular aircraft are of value in determining its impact on community noise. The characteristics of the measured noise are what people find objectionable. But aircraft noise is usually quantified by static tests, thus the need for de-Dopplerized spectra. This would provide some idea of a particular offending noise component where sound abatement should be applied. Also, the measured spectra can be used to validate current prediction programs (i.e. ANOPP) and to construct exposure contours which depends on an array of microphones. In this study, a highly nonstationary signal case is considered (=250 ft., M=.33). Using data acquired from a XV-15 Tilt-Rotor flyover test in the airplane mode an assessment is made of the signal processing and de-Dopplerization techniques

SIGNAL PROCESSING PROCEDURES

For aircraft flyover measurements, the acoustic signal will appear nonstationary to a ground based observer. Thus the Fourier transform of the signal will be time dependent. A short-time Fourier transform with a sliding window function [5] was employed to deal with this. A trade-off is made here though between time resolution and frequency resolution. One function of the window is to limit the duration of the time signal so that the spectral characteristics are reasonably stationary over the duration of the window. For a rapidly varying signal, a reduced window length is required. But reducing the window duration also reduces the frequency resolution. Increasing the window duration can lead to spectral smearing. This problem is less severe for de-Dopplerized data.

The detailed steps that were used in the data analysis scheme are given in Ref. 6. A brief description of these steps follows. To prevent aliasing, the bandwidth of the spectrum is first selected and the sample rate determined by

$$\Delta t = \frac{1}{2.5\ f_c} \qquad (1)$$

which satisfies the Nyquist criterion. Also, to avoid aliasing, the signal must be fed through a low-pass filter with cut-off frequency f_c. Equation (1) along with the block size, N, determine the record length which is equal to the window duration and the bin width which are given by, respectively

$$T = N\Delta t \tag{2}$$

and

$$\Delta f = \frac{1}{T} \tag{3}$$

The FFT of the signal can be expressed as [7]

$$P_i(f_k) = \Delta t P_{ik} = \Delta t \sum_{n=0}^{N-1} x_{in} w_n \exp\left[-\frac{i2\pi kn}{N}\right] \tag{4}$$

where P_{ik} is the actual output from the FFT algorithm and the subscript i designates the particular record. The discrete frequencies, which are the bin center frequencies, are given by

$$f_k = \frac{k}{T} \quad , \qquad k = 0,1,2,\ldots\ldots,\frac{N}{2} \tag{5}$$

With the FFT components computed, the power spectral density function can be evaluated from

$$G_{pp}(f_k) = \frac{2}{n_d T} \sum_{i=1}^{n_d} |P_i(f_k)|^2 \qquad , \; k=0,1,2,\ldots\ldots,\frac{N}{2} \tag{6}$$

Using equation (6), the time-averaged pressure for the bin with center frequency f_k and width Δf can be approximated by

$$\overline{p^2(f_k,\Delta f)} = G_{pp}(f_k)\Delta f = \frac{2}{n_d T^2}\sum_{i=1}^{n_d} \left|P_{ik}(f_k)\right|^2 \tag{7}$$

Thus, the sound-pressure level for the k-th bin is

$$L(f_k) = 10\log\left[\frac{\overline{p^2(f_k,\Delta f)}}{p_{ref}^2}\right] \tag{8}$$

and the overall sound-pressure level for a particular band is

$$L_{OA} = 10\log\left[\frac{\sum_{k=0}^{n_b} \overline{p^2(f_k,\Delta f)}}{p_{ref}^2}\right] \tag{9}$$

MOTION EFFECTS ON MEASURED SPECTRA

The usual model for source motion characterization is the nonhomogeneous wave equation i.e.

$$c_o^{-2}\frac{\partial^2 p}{\partial t^2} - \nabla^2 p = q(\mathbf{x},t) \tag{10}$$

In this expression, the forcing function, $q(\mathbf{x},t)$, accounts for the source motion. The solution to equation (10) can be stated in terms of a volume integral [8] as

$$p(\mathbf{x},t) = \frac{1}{4\pi} \int_{|\mathbf{y}-\mathbf{x}|<c_o t} \frac{q(\mathbf{y},t-\frac{|\mathbf{y}-\mathbf{x}|}{c_o})}{|\mathbf{y}-\mathbf{x}|} dV(\mathbf{y}) \tag{11}$$

The source is contained within the region V and $\mathbf{y}$ is the position vector to each source element. Assuming the source is concentrated at the single moving point $\mathbf{x}=\mathbf{x}_s(t)$ allows $q(\mathbf{x},t)$ to be expressed as

$$q(\mathbf{x},t) = Q(\theta,\phi,t)\ \delta[\mathbf{x}-\mathbf{x}_s(t)] \tag{12}$$

where the angles θ and ϕ describe the directionality of the source. Equation (11) will then reduce [9] to

$$p(\mathbf{x}_R,t) = \left(\frac{r_m}{|\mathbf{r}(\tau)|}\right) \frac{p_m(\theta,\phi,\tau)}{1-\mathbf{M}\cdot\mathbf{n}_r} \tag{13}$$

Here, $p_m(\theta,\phi,\tau)$has been introduced to describe the source structure in terms of pressure at the reference distance r_m. A geometrical description of this situation is shown in Figure 1. Equation (13) is valid for a general flight trajectory since no assumption of uniform motion was made in its derivation. It is important to distinguish between reception time t and emission or retarded time τ in equation (13) which are related by

$$t = \tau + \frac{|\mathbf{r}(\tau)|}{c_o} \tag{14}$$

In the above expressions, τ is the time of signal emission and t is the time of signal reception. The position vector $\mathbf{x}_R$ designates the receiver location at reception time t. Also, the instantaneous Mach number vector, **M**, and the angles θ, ϕ correspond to me τ. Equation (14) describes the well-known signal compression and expansion d to source motion. It is seen from equation (13) that amplitude modulation of the signal ill occur not only through **r**(τ) and the Doppler factor (1-**M**·**n**$_r$) but also by way of the sour e directionality. The next step considered is the Fourier transform of equation (3).

Since p($\mathbf{x}_R$,t) is the measured acoustic quantity in flyover tests, the Fo rier transform of equation (13) with respect to reception time, t, is now developed n order to ascertain the effects of motion on the received spectra. The Fourier transform f equation (13) is

$$P(\mathbf{x}_R,f) = \int_{-\infty}^{\infty} p(\mathbf{x}_R,t)\, e^{-i2\pi ft}\, dt$$

$$= r_m \int_{-\infty}^{\infty} \frac{p_m(\theta,\phi,\tau)e^{-i2\pi ft}}{|\mathbf{r}(\tau)|\left[1-\mathbf{M}(\tau)\cdot\mathbf{n}_r(\tau)\right]}\, dt \qquad (15)$$

where the dependence on times t and τ has been clearly shown since it is critic l in evaluating the transform. For the level flyover situation at constant velocity a shown in Figure 2, equation (15) becomes

$$P(\mathbf{x}_R,f) = r_m \int_{-\infty}^{\infty} \frac{p_m(\theta,\phi,\tau)e^{-i2\pi ft}}{|\mathbf{r}(\tau)|\left(1-M\cos\theta\right)}\, dt \qquad (16)$$

Here ϕ and M are constant. From the geometry, the following relation for the mission angle is easily derived

$$\cos\theta = \frac{x_R - U\tau}{|\mathbf{r}(\tau)|} \tag{17}$$

The variable of integration can be changed to the emission time τ by means of equation (14), i.e.

$$dt = \left(1 - M\frac{x_R - U\tau}{|\mathbf{r}(\tau)|}\right) d\tau \tag{18}$$

Substituting these relations into equation (16) will result in

$$P(\mathbf{x}_R, f) = r_m \int_{-\infty}^{\infty} \frac{e^{-i2\pi f \frac{|\mathbf{r}(\tau)|}{c_o}}}{|\mathbf{r}(\tau)|} p_m(\theta,\phi,\tau) e^{-i2\pi f\tau} d\tau \tag{19}$$

where $\mathbf{r}(\tau)$ can be explicitly expressed as

$$\mathbf{r}(\tau) = \sqrt{(x_R - U\tau)^2 + y_R^2 + z_R^2} \tag{20}$$

Suppose the source structure is such that p_m can be separated i.e.

$$p_m(\theta,\phi,t) = d(\theta)g(t) \tag{21}$$

where $d(\theta)$ is the directivity factor and $g(t)$ is some characteristic time signature of the source. Note that d can be expressed as a function of τ through equation (17). Thus equation (19) can be written as

$$P(\mathbf{x}_R,f) = \int_{-\infty}^{\infty} h(\tau)g(\tau)e^{-i2\pi f t}\,d\tau \tag{22}$$

and h(τ) is defined as

$$h(\tau) = \frac{e^{-i2\pi f\frac{|\mathbf{r}(\tau)|}{c_o}}}{\left(\frac{|\mathbf{r}(\tau)|}{r_m}\right)}\,d(\tau) \tag{23}$$

Therefore, $P(\mathbf{x}_R,f)$ is the convolution of the Fourier transforms of h(t) and g(t), namely

$$P(\mathbf{x}_R,f) = \int_{-\infty}^{\infty} H(\alpha)G(f-\alpha)\,d\alpha \tag{24}$$

As a final consideration of some of the theoretical aspects of ground-based spectra, approximate relations for a short-time Fourier transform will be given. The accuracy of these approximations is very much dependent on source velocity. Assuming that t is short enough such that $U\tau \ll |\mathbf{r}_R|$ permits the following approximations to be made

$$|\mathbf{r}(\tau)| \approx r_R - \frac{U x_R \tau}{r_R} \tag{25}$$

and

$$\cos\theta \approx \frac{x_R}{r_R} \tag{26}$$

Substituting these expressions into equation (19) results in

$$P(x_R,f) = \frac{e^{-i\frac{2\pi f}{c_o} r_R}}{\left(\frac{r_R}{r_m}\right)} \int_0^T p_m(\theta,\phi,\tau) e^{-i2\pi f(1-M\cos\theta)\tau}\, d\tau \qquad (27)$$

If the smear angle, $\Delta\theta$, is small, a characteristic source spectrum can be defined as

$$P_m(\theta,\phi,f) = \int_0^T p_m(\theta,\phi,\tau) e^{-i2\pi f\tau}\, d\tau \qquad (28)$$

So that equation (27) can be expressed as

$$P(x_R,f) = \frac{e^{-i\frac{2\pi f}{c_o} r_R}}{\left(\frac{r_R}{r_m}\right)} P_m[\theta,\phi,f(1-M\cos\theta)] \qquad (29)$$

For a pure tone of amplitude A and frequency f_o, P_m is

$$P_m(\theta,\phi,f) = AT\frac{\sin[\pi(f-f_o)T]}{\pi(f-f_o)T} e^{-i\pi(f-f_o)T} \qquad (30)$$

which is the well-known result describing spectral broadening due to a finite time duration. Introduction of equation (30) into equation (29) produces

$$P(x_R,f) = AT\frac{e^{-i\beta}}{\left(\frac{r_R}{r_m}\right)} \frac{\sin\{\pi[f(1-M\cos\theta)-f_o]T\}}{\pi[f(1-M\cos\theta)-f_o]T} \qquad (31)$$

The phase angle β is given by

$$\beta = \frac{2\pi f}{c_o} r_R + \pi[f(1-M\cos\theta)-f_o]T \tag{32}$$

From equation (31), it is seen that its first zero occurs at

$$f_1 = \frac{\frac{1}{T} + f_o}{1-M\cos\theta} \tag{33}$$

For an approaching source (subsonic case) $1-M\cos\theta<1$ and for a receding source $1-M\cos\theta>1$. Thus, f_1 is greater in the approach regime and this indicates spectral smearing is more pronounced in this portion of the flight path.

DE-DOPPLERIZATION SCHEME

Equation (13) can be re-written as

$$p_m(\theta,\phi,\tau) = \left(\frac{|\mathbf{r}(\tau)|}{r_m}\right)\left(1-\mathbf{M}\cdot\mathbf{n}_r\right)p(\mathbf{x}_R,t) \tag{34}$$

Taking the Fourier transform of equation (34) with respect to τ will result in the source spectrum with corrections for amplitude and frequency, viz.

$$p_m(\theta,\phi,f) = \int_{-\infty}^{\infty} \frac{|\mathbf{r}(\tau)|}{r_m}\left(1 - \mathbf{M}\cdot\mathbf{n}_r\right) p(\mathbf{x}_R,t)\, e^{-i2\pi f\tau}\, d\tau \tag{35}$$

So that, in principle p_m can be evaluated using the measured data. The tracking data determines $\mathbf{r}(\tau)$ and $\mathbf{M}$ while the measured acoustic data provides $p(\mathbf{x}_R,t)$. Equation

(14) allows p to be expressed as a function of the emission time τ. The specific steps used in this study to compute equation (35) were as follows. First, at a particular microphone location a start time is chosen to begin the analysis. Then the tracking data is searched for this time where linear interpolation is used to determine $\mathbf{r}(\tau)$ and $\mathbf{M}(\tau)$. That is, this start time is emission time. The acoustic data, $p(\mathbf{x}_R,t)$, is in a digital format consisting of equally-spaced samples. Equation (14) is employed to compute the reception time t that corresponds to the emission time τ. Linear interpolation is performed on the p vs. t time history to determine $p(\mathbf{x}_R,t)$. Incrementing τ by the designated sample rate Δt generates an equally-spaced pressure time history which is the required form for the FFT algorithm. These steps are summarized in Figure 3. A word of caution concerning aliasing in this signal reconstruction process. For an approaching aircraft, the measured signal is compressed with the highest frequency limited to f_c by the anti-aliasing filter. The reconstructed signal will appear to be expanded and its highest frequency will be less than f_c. Thus, there is no problem with aliasing. But for a receding aircraft the measured signal is expanded and the restored signal will appear to be compressed. Therefore it could have spectral content above f_c. In this situation aliasing could occur. If significant power is expected above f_c then the reconstructed signal should be low-pass filtered or re-sampled at a higher rate.

So far in the above discussion no stipulation has been made for a level, constant velocity flyover. To implement an ensemble average the uniform, level flyover as shown in Figure 4 is considered. An ensemble average is performed across four equally-spaced measurement locations beneath the flight path. The records used in the average are taken at approximately the same emission angles and smear angles. A description of the test and the data acquisition for the XV-15 is given in Ref. 10.

Flush mounted microphones were employed which had a frequency re ponse of 0.01-40,000 Hz with a maximum sound-pressure level of 160 dB. The signal were band-passed filtered between 16-16,000 Hz and then FM-recorded at 15 ips which g ves a dynamic range of about 46 dB. The recorded signals were then low-pass filte ed at 12.5 kHz and digitized at a sample rate of 25 kHz. All of the results presented in th s study were developed from one flyover measurement of the XV-15 in the airplane mode (≈250 ft., M≈.33). The aircraft track is shown in Figure 5 which is determined by a lase tracking system. Since the sample rate is set, the only way to vary the bin width is thro gh the block size N. For the first group of results discussed N is set to N=2048. Th s corresponds to a window duration of T=.08192s and a bin width of Δf=12.2 Hz. Also, averaging was performed within each microphone measurement and then the r sulting spectra averaged across the four microphones [10]. At each measurement loca ion, the acquired time history was divided into five contiguous records. Thus in these cases n_d=20. Spectra were produced from seven measurement intervals of the flight path. T ble 1 contains the averaged emission angles, smear angles and frequency shifts for t is data. The frequency parameters, f_R and Δf_R are calculated from the following

$$f_R = \frac{f_S}{1-M\cos\theta} \tag{36}$$

and

$$\Delta f_R = \frac{f_R^{(1)} - f_R^{(2)}}{f_S} = \frac{1}{1-M\cos\theta_1} - \frac{1}{1-M\cos\theta_2} \tag{37}$$

which are the Doppler shift relations for uniform motion. Equation (37) gives a quantitative idea about spectral smearing for a window duration that spans the mear angle given by

$$\Delta\theta = \theta_2 - \theta_1 \qquad (38)$$

Figures 6 and 7 show the time histories that correspond to microphone no.1 for $\theta_1=16.25°$. In Figure 6, the measured pressure is illustrated. Figure 7 depicts the corrected signal using equations (14) and (34). Here, $r_m=62.5$ ft. which is 5x the propeller radius of the XV-15. Also, the plot in Figure 7 was constructed using equally-spaced samples. The signal compression in the measured data is clearly seen by comparing the figures. For this test flight, the propellers were operated at 589 rpm which yields a blade passage frequency of 29.45 Hz. Notice that an effective period of .039s can be ascribed to the signal in Figure 7 which yields a fundamental of 25.64 Hz. Measurements to the rear of the aircraft are presented in Figures 8 and 9 which were taken by microphone no.1 for $\theta_1=141.15°$. These are similar to the previous figures in that Figure 8 is the measured signal and Figure 9 is the de-Dopplerized signal. Now, expansion of the signal in the measured data is evident by comparing the figures. Though the time histories differ in structure between fore and aft measurement locations they do exhibit the same characteristic period of .039s. Thus the de-Dopplerization procedure is accurately accounting for signal compression and expansion.

Figures 10-16 describe the measured (shifted) spectra for a bandwidth of 10 kHz. These spectra confirm [10] that most of the power and structure of the signal in the airplane mode is concentrated below 1 kHz. A dominant tone occurs in the neighborhood of the blade passage frequency. The de-Dopplerized spectra are shown in Figures 17-23. The apparent tonal structures at 8.56 kHz in Figure 17, 8.7 kHz in Figure 18 and 9 kHz in Figure 19 are artifacts due to the low-pass filter. In each of these cases, these frequencies yield a Doppler shifted frequency of 12.5 kHz, which is the Nyquist frequency for the data. Thus, for these figures, the portion of the spectra above these respective frequencies should be ignored since they represent the transition zone of the filter.

The spectra in Figures 17-20 represent radiation to the fore of the propeller plane. They were determined from a sweep of θ through the range 16.25°-65.03° The four spectra show little change. There is a slight increase in the fundamental as the propeller plane is approached. Table 2 contains the peak and overall sound-pressure levels for all seven blocks for both Doppler and de-Dopplerized spectra. In the fore region of the propeller, it appears that the directivity pattern remains relatively uniform through this range of θ. Figures 22 and 23 depict sound propagation to the aft of the propeller plane. These spectra and Table 2 indicate greater variability in the radiation pattern in the aft region compared to the fore region. Since the peak and overall sound-pressure levels are less in this portion of the acoustic field, suggests that the energy radiated to the aft of the aircraft is less than to the front. Also, as is the case in the fore direction, the levels decrease as the propeller axis is approached.

After this analysis an attempt to improve the resolution of the spectra by increasing the block size, N, was performed. Choosing N=16384 produces a window duration of T=.65536s and a bin width of Δf=1.53 Hz. Due to the increased window duration no averaging was attempted within each microphone measurement but only across the four acquisition locations so that n_d=4. As before, spectra were constructed from seven measurement intervals of the flight path. Table 3 shows the greater smear angles that result for this increased resolution. Figures 24-30 contain the spectra of the measured signals for these cases for a bandwidth of 500 Hz. Likewise, Figures 31-37 contain the de-Dopplerized spectra. Table 4 presents the sound-pressure levels. The fact that for some cases in Table 4 the overall levels are greater than those shown in Table 2 even though the frequency range is less can be attributed to the finer frequency resolution. In the Doppler spectra smearing is evident beginning with the 4th harmonic in Figure 26 and the 2nd harmonic in Figures 27-29. Also note the broadening of the fundamental in these figures.

In general, the first seven harmonics are easily identified in the de-Dopplerized spectra, Figures 31-37. The pronounced smearing that was evident in the first three overtones in the measured spectra is absent in these figures. Though the amplitudes of the harmonics vary during the flyover, they do retain their spectral location in each spectrum. The fundamental occurs at approximately 25 Hz. As expected, since most of the energy is contained in the lower end of the spectrum, the same trends emerge that were produced for a 10 kHz bandwidth and Δf=12.21 Hz. That is, the levels increase toward the propeller plane with more energy radiated to the front of the aircraft and greater variation in the radiation pattern to the rear of the aircraft. An important feature brought out by the finer resolution of this data is the difference in the fundamental and the overtones in the fore and aft directions. As Figures 31-34 show the fundamental dominates the peak overtone by 18-21 dB in the forward direction. But, Figures 36 and 37 show that to the rear of the aircraft the 2nd harmonic is approximately only 2 dB less than the fundamental.

SIMULATED SPECTRA

To complete the study, an analysis of some computer simulated spectra is now presented. With known source distribution and flight path, a pressure time history can be constructed at the observation point by way of equation (13). Therefore, a simulated spectrum is generated at the measurement location of the moving source. All the cases depicted were produced using a level flyover (h=250 ft.) and U=222.3 knots (M=.33). The idea being to mimic as closely as possible the situation in the previous section. An omnidirectonal source was chosen whose frequency content consisted of a summation of harmonics. Thus the form of $p_m(\theta,\phi,\tau)$ is given by

$$p_m(\theta,\phi,\tau) = \sum_{n=1}^{N_H} A_n \cos\left[2\pi f_n \tau + (n-1)\frac{\pi}{2}\right] \tag{39}$$

where

$$f_n = n f_1 \qquad , n=1,2,\ldots,N_H \tag{40}$$

This yields a periodic signal with a fundamental frequency of f_1. By choosing f_1=25 Hz and A_1 equivalent to a 115 dB tone (re 62.5 ft.) yields similar characteristics to the real data. The amplitudes of the overtones monotonically decreased with each harmonic 25 percent less than the previous one (A_n=.75A_{n-1}) and the number of harmonics in the signal was set to N_H=100. As before time series were generated in seven blocks of the flight path where each block began at the same emission angles given in Tables 1 and 3. Since the frequency content of the source is known it is easily seen how well the signal analysis scheme is performing.

Using altitude, velocity and initial emission angle, θ_0, as input, the position vectors can be expressed as

$$\mathbf{x}_S(\tau) = x_S\mathbf{i}+y_S\mathbf{j}+z_S\mathbf{k} = U\tau\,\mathbf{i} \tag{41}$$

and

$$\mathbf{x}_R = x_R\mathbf{i}+y_R\mathbf{j}+z_R\mathbf{k} = h\cot\theta_0\mathbf{i} - h\mathbf{j} \tag{42}$$

Also, equation (14) can be solved explicitly for τ in terms of t

$$\tau = \frac{c_0 t - M x_R - \sqrt{(x_R - Ut)^2 + (1-M^2)\,y_R^2}}{c_0\,(1-M^2)} \tag{43}$$

Equation (43) is needed for signal processing based on reception time (contains Doppler shifts) since FFT algorithms require equally-spaced samples. For the results now presented, a bandwidth of 500 Hz and a bin width of Δf=1.53 Hz was again chosen. Figure 38 illustrates the pressure time history based on emission time which is given by equation (39). This can be compared to the received signals computed from equation (13) shown in Figures 39 and 40. Signal compression for an approaching source is illustrated in Figure 39 for θ_1=16.25°. Signal expansion for a receding source is depicted in Figure 40 for θ_1=141.15°. Figures 41-47 contain the spectra of the seven data blocks and Table 5 shows some of the pertinent characteristics of the spectra. The increase in spectral smearing with frequency is evident. It is more severe on approach becoming apparent on the lower harmonics as the smear angle increases. From Figure 41 it is seen that tonal broadening first becomes significant at the 7th harmonic. But Figure 47 which was constructed as the source receded (θ_1=141.15°) shows that the harmonics are discernible through the 11th harmonic. On approach, notice how the smearing of the higher-order harmonics takes on the appearance of band-pass white noise.

CONCLUSIONS

A detailed analysis of signal processing concerns for measuring aircraft flyover noise has been presented in this paper. The effects of spectral smearing and its removal (de-Dopplerization) were considered. Using test data acquired from an XV-15 tilt-rotor flyover, comparisons were made between the measured and corrected spectra. Frequency shifts are accurately accounted for by the de-Dopplerization scheme. It was shown in the study that by correcting for spherical spreading and Doppler amplitude along with frequency can give some idea about noise source directivity. Also, the analysis indicated that smearing increases with frequency and is more severe on approach than recession. Simulated spectra were generated using a moving point source model with frequency content similar to the XV-15 data. The results from the simulation corroborated the observations obtained from the analysis of the actual flight data.

REFERENCES

1. Tsao, Y. H. and Hammond, J. K.: "Nonstationarity in Acoustic Fields." Journal of the Acoustical Society of America **74,** 827- 839, 1983.

2. Chow, P. L and Maestrello. L.: "Statistical Estimation of Correlation For Nonstationary Aircraft Noise." Journal of the Acoustical Society of America **70,** 735-739, 1981.

3. Verhas, H. P.: "A Restoration Procedure For (Nonstationary) Signals From Moving Sources." Journal of Sound and Vibration **89,** 487-497, 1983.

4. Howell, G. P., Bradley, A. J., McCormick, M. A., and Brown, J. D.: "De-Dopplerization and Acoustic Imaging of Aircraft Flyover Noise Measurements." Journal of Sound and Vibration **105**, 151-167, 1986.

5. Oppenheim, A. V. and Schafer, R. W.: "Discrete-Time Signal Processing." Prentice Hall, Engelwood Cliffs, NJ, 1989.

6. Bendat, J. S. and Piersol, A. G.: "Random Data: Analysis and Measurement Procedures." Wiley-Interscience, New York, 1986.

7. Cadzow, J. A. and Van Landingham, H. F.: "Signals, Systems and Transforms." Prentice Hall, Engelwood Cliffs, NJ, 1985.

8. John, F.: "Partial Differential Equations." Springer-Verlag, New York, 1975.

9. Dowling, A. P. and Ffowcs Williams, J. E.: "Sound and Sources of Sound." Ellis Horwood, Chichester, England, 1983.

10. Golub, R. A., Becker, L. E., Rutledge, C. K., Smith, R. A., and Conner, D. A. "Some Far-Field Acoustics Characteristics of the XV-15 Tilt-Rotor Aircraft." AIAA Paper No. 90-3971, 1990.

```
      PROGRAM BBAND
      IMPLICIT REAL*8 (A-H,O-Z)
      REAL STI(32766),SPR(40000),SFREQ(2048),SSR(2048)
      REAL SIR(50000),SIT(50000)
      DIMENSION PR(32766),SR(2048),FREQ(2048),IWK(20)
      DIMENSION TI(32766),SR1(2048),TSO(4,9)
      DIMENSION TR(50000),PRE(50000),PRT(50000)
      DIMENSION TIM(2048),X(2048),Y(2048),Z(2048)
      DIMENSION VX(2048),VY(2048),VZ(2048),NRD(4)
      DIMENSION SX(2048),SR1X(2048)
      COMPLEX*16 ZS(16384),ZX(16384)
      OPEN(UNIT=20,FILE='FLYOR.OUT',STATUS='NEW')
      OPEN(8,FILE='KRAD0200.909',FORM='FORMATTED',ACCESS=
     +'SEQUENTIAL',STATUS='OLD')
C
C *************************************************************
C   OPEN ACOUSTIC FILES
C *************************************************************
C
      IBLK=24000
      IBUF=1
      TSO(1,1)=36349.7006D0
      TSO(2,1)=36350.2354D0
      TSO(3,1)=36350.7716D0
      TSO(4,1)=36351.3041D0
      OPEN(1,FILE='KA02009A.DAT',
     +     FORM='UNFORMATTED',
     +     RECORDTYPE='FIXED',BLOCKSIZE=IBLK,BUFFERCOUNT=IBUF,
     +     ACCESS='DIRECT',RECL=2048,ASSOCIATEVARIABLE=IPLACE,
     +     STATUS='OLD')
      OPEN(2,FILE='A020010A.DAT',
     +     FORM='UNFORMATTED',
     +     RECORDTYPE='FIXED',BLOCKSIZE=IBLK,BUFFERCOUNT=IBUF,
     +     ACCESS='DIRECT',RECL=2048,ASSOCIATEVARIABLE=IPLACE,
     +     STATUS='OLD')
      OPEN(3,FILE='A020011A.DAT',
     +     FORM='UNFORMATTED',
     +     RECORDTYPE='FIXED',BLOCKSIZE=IBLK,BUFFERCOUNT=IBUF,
     +     ACCESS='DIRECT',RECL=2048,ASSOCIATEVARIABLE=IPLACE,
     +     STATUS='OLD')
      OPEN(4,FILE='A020012A.DAT',
     +     FORM='UNFORMATTED',
     +     RECORDTYPE='FIXED',BLOCKSIZE=IBLK,BUFFERCOUNT=IBUF,
     +     ACCESS='DIRECT',RECL=2048,ASSOCIATEVARIABLE=IPLACE,
     +     STATUS='OLD')
   39 FORMAT(/,1X,'NREC=',I5)
      DO 300 K=1,4
      CALL HEADER_BUFFER(K,NREC)
      WRITE(20,39)NREC
  300 NRD(K)=NREC
C
C  READ RADAR DATA
C  TSTART=1ST ACOUSTIC TIME MARK
C
      TSTART=36349.7006D0
      MS=1
    1 READ(8,101,END=654)TIM(MS),X(MS),Y(MS),Z(MS),
     +VX(MS),VY(MS),VZ(MS)
  101 FORMAT(1X,F11.1,6F10.1)
      IF(TIM(MS).LT.(TSTART-.3D0))GO TO 1
      X(MS)=-X(MS)
      VX(MS)=-VX(MS)
      MS=MS+1
```

```
      GO TO 1
  654 MS=MS-1
C ***************************************************
C  SIGNAL PROCESSING PARAMETERS
C  FC=BANDWIDTH, NPTS=NO. OF SAMPLES, NR=NO. OF CHANNELS
C  DT=SAMPLE RATE, TO=TEMPERATURE(C)
C  XR,YR,ZR=MICROPHONE LOCATION
C ***************************************************
      FC=500.DO
      M=14
      NPTS=2**M
      NR=4
      COEF=2.DO/DFLOAT(NR*NPTS**2) !BOXCAR WINDOW
      DT=4.E-5
      PREF=2.E-4 !SIGNAL IN DYNES/CM**2
      RREF=62.5DO !REF. DISTANCE IN FT
      IP=0
      IX=0
      IY=0
      BW=1.DO/(DT*DFLOAT(NPTS))
      TO=21.9DO
      YR=0.DO
      ZR=0.DO
      WRITE(20,50)TO
   50 FORMAT(//,1X,'TO=',F5.1,'C',//)
      CO=DSQRT(401.8DO*(TO+273.16DO))/.3048DO
      WRITE(20,60)DT,BW,NR,MS
   60 FORMAT(//,1X,'DT=',E9.3,'SEC',2X,'BW=',F5.2,'HZ',2X,
     *'NR=',I3,2X,'#PTS=',I5,//)
      LI=FC/BW
      DO 25 K1=1,LI
      FREQ(K1)=DFLOAT(K1-1)*BW
   25 SFREQ(K1)=SNGL(FREQ(K1))
      CALL PSEUDO
      CALL PSE(11)
C
C  GENERATE DIGITAL INPUT SIGNAL
C
      DO 5 NT=1,8
      DO 20 LM=1,LI
      SX(LM)=0.DO
   20 SR(LM)=0.DO
      SUM=0.DO
      SUMX=0.DO
      XR=0.DO
      NSS=32765
      IF(NT.GE.5)NSS=32765
      IF(NT.EQ.8)NSS=22730
      IMEMLOC=1+(NT-1)*12500
      DO 6 ICHAN=1,4
      CALL DATA_BUFFER(ICHAN,NRD(ICHAN),IMEMLOC,NSS,SPR)
      TSO(ICHAN,NT)=TSO(ICHAN,1)+.5DO*DFLOAT(NT-1)
      DO 45 NN=1,NSS
      PR(NN)=DBLE(SPR(NN))
   45 TI(NN)=TSO(ICHAN,NT)+DFLOAT(NN-1)*DT
      NX=1
      NY=1
      DO 51 MX=1,NPTS
      IF(TI(MX).GE.TIM(MS))STOP
      CALL NTRPOL8VEC(X,Y,Z,VX,VY,VZ,TIM,MS,TI(MX),
     +RX,RY,RZ,RVX,RVY,RVZ,NX,MS)
      RDX=XR-RX
      RDY=YR-RY
      RDZ=ZR-RZ
      R=DSQRT(RDX**2+RDY**2+RDZ**2)
      UX=RDX/R
```

```
        UY=RDY/R
        UZ=RDZ/R
        DP=UX*RVX+UY*RVY+UZ*RVZ
        DENOM=1.DO-DP/CO
        IF(MX.EQ.1.OR.MX.EQ.NPTS)THEN
        THE=DACOSD(DP/DSQRT(RVX**2+RVY**2+RVZ**2))
        WRITE(20,75)THE,ICHAN
   75   FORMAT(/,1X,'THETA=',F5.1,2X,'MIC=',I2)
        ENDIF
        TR(MX)=TI(MX)+R/CO
        PRT(MX)=0.DO
        PRE(MX)=0.DO
        IF(TR(MX).GE.TI(NSS))GO TO 51
        CALL NTRPOL8(PR,TI,32766,TR(MX),RESULT,NY,NSS)
        PRT(MX)=RESULT
        PRE(MX)=RESULT*(R/RREF)*DENOM
   51   CONTINUE
C
C  PLOT TIME HISTORY (MEASURED SIGNAL)
C
        IF(IP.EQ.0)GO TO 4
        DO 100 II=1,NSS
  100   STI(II)=SNGL(TI(II)-TI(1))
        CALL PLOTR(1,0,NSS,STI,SPR,0.,0.,0.,0.,'TIME(SEC)',9,.16,
       *'P(DYNES/CM**2)',14,.16,
       *'MEASURED TIME HISTORY',21,.16,0,0.,10.,1.5,13.6,7.,1.,
       *10.4,0,1)
        CALL ERASE
C
C  PLOT TIME HISTORY (RECEPTION TIME)
C
        IF(IX.EQ.0)GO TO 4
        DO 200 II=1,NPTS
        SIT(II)=SNGL(TR(II)-TR(1))
  200   SIR(II)=SNGL(PRT(II))
        CALL PLOTR(1,0,NPTS,SIT,SIR,0.,0.,0.,0.,'TIME(SEC)',9,.16,
       *'P(DYNES/CM**2)',14,.16,
       *'RECEPTION TIME HISTORY',22,.16,0,0.,10.,1.5,13.6,7.,1.,
       *10.4,0,1)
        CALL ERASE
C
C  PLOT TIME HISTORY (EMISSION TIME)
C
        IF(IY.EQ.0)GO TO 4
        DO 205 II=1,NPTS
  205   SIR(II)=SNGL(PRE(II))
        CALL PLOTR(1,0,NPTS,STI,SIR,0.,0.,0.,0.,'TIME(SEC)',9,.16,
       *'P(DYNES/CM**2)',14,.16,
       *'EMISSION TIME HISTORY',21,.16,0,0.,10.,1.5,13.6,7.,1.,
       *10.4,0,1)
        CALL ERASE
C
C COMPUTE SPL FOR EACH BIN AND OASPL
C
    4   DO 2 J=1,NPTS
        ZX(J)=DCMPLX(PR(J),0.DO)
        ZS(J)=DCMPLX(PRE(J),0.DO)
    2   CONTINUE
        CALL FFTD(ZX,M,IWK)
        CALL FFTD(ZS,M,IWK)
        DO 3 JK=1,LI
        SRX=(CDABS(ZX(JK)))**2
        SRT=(CDABS(ZS(JK)))**2
        SX(JK)=SX(JK)+SRX
    3   SR(JK)=SR(JK)+SRT
    6   XR=XR-200.DO
```

```
      DO 30 LS=1,LI
      SR1X(LS)=COEF*SX(LS)
      SUMX=SUMX+SR1X(LS)
      SR1(LS)=COEF*SR(LS)
      SUM=SUM+SR1(LS)
      SX(LS)=10.DO*DLOG10(SR1X(LS)/PREF**2)
   30 SR(LS)=10.DO*DLOG10(SR1(LS)/PREF**2)
      OASPL=10.DO*DLOG10(SUM/PREF**2)
      OASPLX=10.DO*DLOG10(SUMX/PREF**2)
C
C  PLOT SPECTRUM (DOPPLER SPECTRUM)
C
      DO 105 II=1,LI
  105 SSR(II)=SNGL(SX(II))
      CALL PLOTR(1,0,LI,SFREQ,SSR,0.,0.,0.,0.,'FREQ(HZ)',8,.16,
     *'SPL(dB)',7,.16,'DOPPLER SPECTRUM',16,
     *.16,0,0.,10.,1.5,13.6,7.,1.,10.4,0,1)
      CALL ERASE
C
C  PLOT SPECTRUM (DE-DOPPLERIZED SPECTRUM)
C
      DO 106 II=1,LI
  106 SSR(II)=SNGL(SR(II))
      CALL PLOTR(1,0,LI,SFREQ,SSR,0.,0.,0.,0.,'FREQ(HZ)',8,.16,
     *'SPL(dB)',7,.16,'DE-DOPPLERIZED SPECTRUM',23,
     *.16,0,0.,10.,1.5,13.6,7.,1.,10.4,0,1)
      CALL ERASE
      WRITE(20,70)OASPLX,OASPL,NT
   70 FORMAT(/,1X,'OASPLX=',F4.0,'dB',2X,'OASPL=',F4.0,'dB',2X,
     *'NT=',I2)
    5 CONTINUE
      CALL CALPLT(0.,0.,999)
      CALL PSC
      CLOSE(20)
      STOP
      END
C
C  INTERPOLATION SUBROUTINE
C
      SUBROUTINE NTRPOL8(VC1,VC2,N,REF,RESULT,I,M)
      IMPLICIT REAL*8 (A-H,O-Z)
      DIMENSION VC1(N),VC2(N)
      IKEEP=0
    1 IF((VC2(I)/REF).LE.1.DO)THEN
      IKEEP=I
      IF(IKEEP.EQ.M)STOP
      I=I+1
      GO TO 1
      ENDIF
      I=I-1
      IF(IKEEP.EQ.0)STOP
      V2DIFF=VC2(IKEEP+1)-VC2(IKEEP)
      V1DIFF=VC1(IKEEP+1)-VC1(IKEEP)
      RESULT=(V1DIFF/V2DIFF)*(REF-VC2(IKEEP+1))+VC1(IKEEP+1)
      RETURN
      END
C
C    RADAR DATA INTERPOLATION
C
      SUBROUTINE NTRPOL8VEC(VC1,VC2,VC3,VC4,VC5,VC6,VC7,
     +N,REF,RES1,RES2,RES3,RES4,RES5,RES6,I,M)
      IMPLICIT REAL*8 (A-H,O-Z)
      DIMENSION VC1(N),VC2(N),VC3(N),VC4(N),VC5(N)
      DIMENSION VC6(N),VC7(N)
    1 IF((VC7(I)/REF).LE.1.DO)THEN
      IKEEP=I
```

```
      IF(IKEEP.EQ.M)STOP
      I=I+1
      GO TO 1
      ENDIF
      I=I-1
      IF(IKEEP.EQ.0)STOP
      V7DIFF=VC7(IKEEP+1)-VC7(IKEEP)
      V6DIFF=VC6(IKEEP+1)-VC6(IKEEP)
      V5DIFF=VC5(IKEEP+1)-VC5(IKEEP)
      V4DIFF=VC4(IKEEP+1)-VC4(IKEEP)
      V3DIFF=VC3(IKEEP+1)-VC3(IKEEP)
      V2DIFF=VC2(IKEEP+1)-VC2(IKEEP)
      V1DIFF=VC1(IKEEP+1)-VC1(IKEEP)
      DTA=(REF-VC7(IKEEP+1))/V7DIFF
      RES1=V1DIFF*DTA+VC1(IKEEP+1)
      RES2=V2DIFF*DTA+VC2(IKEEP+1)
      RES3=V3DIFF*DTA+VC3(IKEEP+1)
      RES4=V4DIFF*DTA+VC4(IKEEP+1)
      RES5=V5DIFF*DTA+VC5(IKEEP+1)
      RES6=V6DIFF*DTA+VC6(IKEEP+1)
      RETURN
      END

C
C     SUBROUTINE TO EMULATE CALLING MECHANISM TO GRANDLE'S A/D BUFFERS
C
C
C
C      VARIABLE     RANGE          DESCRIPTION
C      --------    ---------       --------------------------------
C      ICHANNEL    0-5             (WHICH MIC-CHANNEL TO USE)
C                                  THERE WILL CONCEPTUALLY BE
C                                  FIVE ROUTINES LIKE THIS , EACH
C                                  CAN ACCESS ONLY 6 CHANNELS.
C                                  THIS IS THE CASE SO AS TO MIMMICK
C                                  THE HARDWARE CONSTRAINT.
C
C      IFIRST      0,16777215      INTEGER ARGUMENT INDICATING WHICH
C                                  ELEMENT IN THE DATA STREAM TO BE
C                                  ACCESSED.
C
C      IHOWMANY    0,32765         AT ANY ONE CALL THIS SUBROUTINE
C                                  WILL RETURN THIS MANY ELEMENTS
C                                  IN THE DATA ARRAY.
C
C      DATA                        ARRAY WHICH CONTAINS DATA.
C
C
C
C
      SUBROUTINE header_buffer(ichannel,norif)
*==================================================!header read entry point
      READ(ICHANNEL'1) NORIF                       !NUMBER OF RECORDS IN FILE
     return                                        !return to main prog
     end
*=============================================================================*


      subroutine data_buffer(ichannel,nrec,ifirst,ihowmany,data)
*==================================================!data read entry point
      dimension data(40000)
      data nvpr / 2048 /


      IFREC2RD = INT(IFIRST/NVPR) + 2              !FIRST RECORD TO READ FROM
                                                   !THE FILE
```

```
       ILREC2RD = INT((IFIRST-1+IHOWMANY)/NVPR) + 2 !LAST RECORD TO READ FROM
                                                              !THE FILE

       NUMRECS = ILREC2RD + 1 - IFREC2RD            !TOTAL NUMBER OF RECORDS
                                                    !TO READ

*
*     issue error diagnostic if attempt to read beyond file limits
*     ------------------------------------------------------------
*
       IF((IFREC2RD + NUMRECS - 1) .GT. nrec) THEN
             TYPE *,' ATTEMPT TO READ BEYOND EOF  CHANNEL READ FAILED'
             RETURN
       ENDIF

*
*     READ THE PERTINENT DATA FROM THE DIRECT ACCESS FILE INTO THE DATA ARRAY
*     -----------------------------------------------------------------------
       K = 1
       DO irecp = IFREC2RD,ILREC2RD
             L = K + NVPR - 1
             READ(ICHANNEL'irecp) (DATA(J),J=K,L)
             K = K + NVPR
       ENDDO


*
*     THROW AWAY DATA IN THE BEGINNING OF THE ARRAY THAT WAS NOT REQUESTED
*     --------------------------------------------------------------------
*

       IFRSTNREC = (IFREC2RD - 2)*NVPR !0-2047 INDEX SCHEME ID FOR THE FIRST
                                       !ELEMENT OF THE DATA ARRAY

       INC = IFIRST - IFRSTNREC - 1    !SHIFTING INCREMENT CONSTANT
*
*     fill data array with requested data
*     -----------------------------------
*
       DO I = 1,IHOWMANY
       DATA(I) = DATA(INC + I)
       ENDDO


       RETURN
       END
```

Table 1

Emission angles and Doppler shifts for $\Delta f = 12.2$ Hz

block no.	θ_1 (deg)	θ_2 (deg)	$\Delta\theta$ (deg)	Δf_R
1	16.25	19.25	3.0	.001
2	20.3	25.98	5.68	.026
3	27.6	38.53	10.93	.065
4	41.9	65.03	23.13	.164
5	72.0	107.78	35.78	.205
6	114.7	137.73	23.03	.075
7	141.15	152.1	10.95	.021

Table 2

sound-pressure levels
for $\Delta f = 12.2$ Hz

block no.	Doppler spectrum		de-Dopplerized spectrum	
	peak spl (dB)	oaspl (dB)	peak spl (dB)	oaspl (dB)
1	90	91	114	115
2	94	95	115	116
3	98	99	116	117
4	103	104	117	118
5	102	107	115	117
6	100	102	109	113
7	90	94	103	108

Table 3

Emission angles and Doppler shifts for
$\Delta f = 1.53$ Hz

block no.	θ_1 (deg)	θ_2 (deg)	$\Delta\theta$ (deg)	Δf_R
1	16.25	22.5	6.25	.025
2	20.3	31.03	10.73	.054
3	27.6	48.93	21.33	.137
4	41.9	85.25	43.35	.164
5	72.0	125.1	53.1	.205
6	114.7	146.1	31.4	.09
7	141.15	156.25	15.1	.02

Table 4

sound-pressure levels
for $\Delta f = 1.53$ Hz

block no.	Doppler spectrum		de-Dopplerized spectrum	
	peak spl (dB)	oaspl (dB)	peak spl (dB)	oaspl (dB)
1	92	92	114	115
2	95	96	115	116
3	98	100	117	117
4	100	105	116	118
5	98	106	112	116
6	96	101	105	111
7	88	92	102	106

Table 5

Emission angles and sound-pressure levels for simulated spectra, $\Delta f = 1.53$ Hz

block no.	θ_1 (deg)	θ_2 (deg)	$\Delta\theta$ (deg)	peak spl (dB)	oaspl (dB)
1	16.25	26.51	10.26	96	101
2	20.3	37.6	17.06	98	103
3	27.6	59.05	31.45	98	105
4	41.9	91.95	50.05	97	107
5	72.0	121.69	49.69	97	106
6	114.7	141.82	27.12	95	102
7	141.15	153.54	12.39	95	99

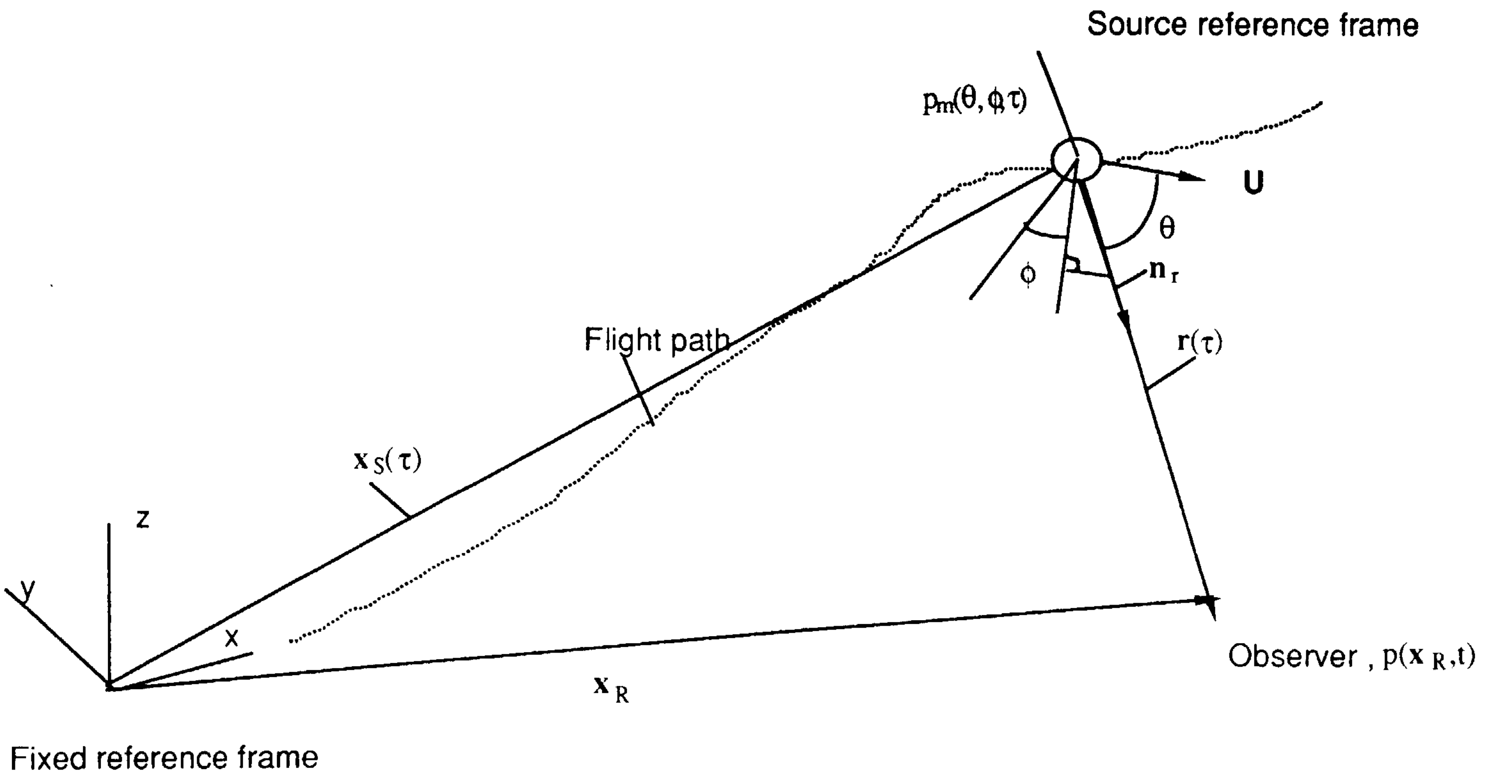

Figure 1: Flight geometry and parameter description

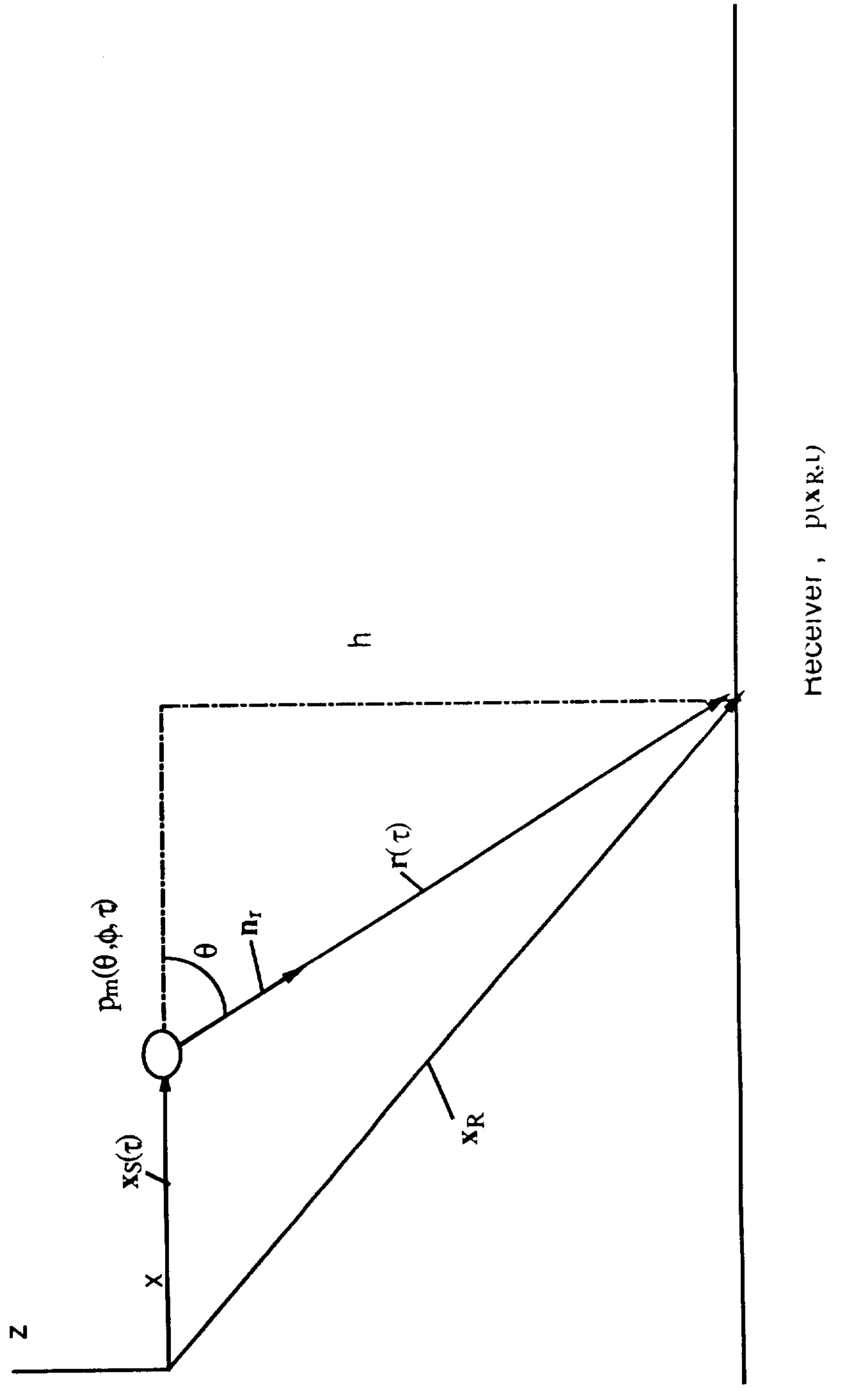

Figure 2: Level flyover geometry

Figure 3. Time history restoration scheme

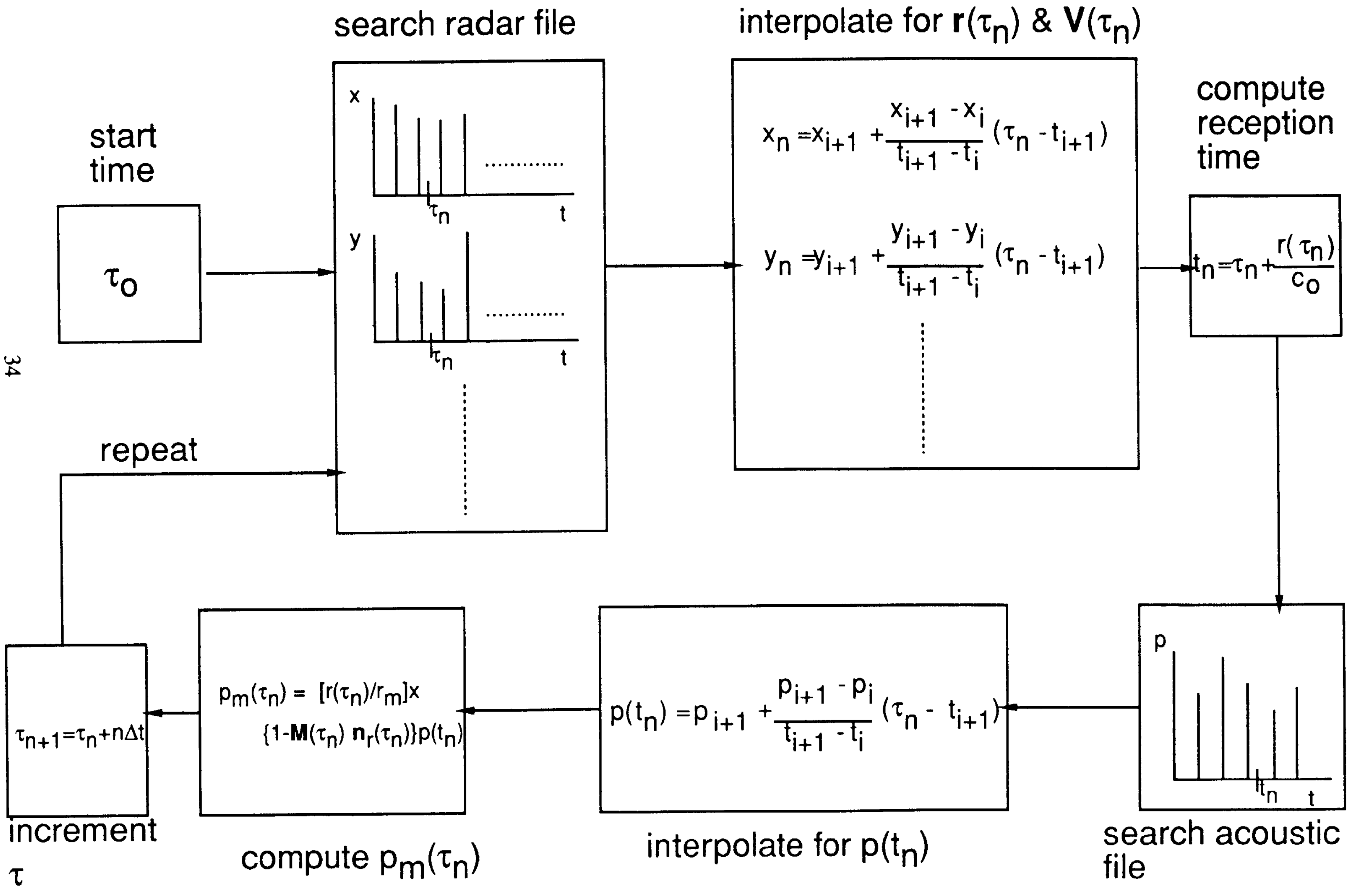

Figure 4. Level flyover configuration for ensemble average

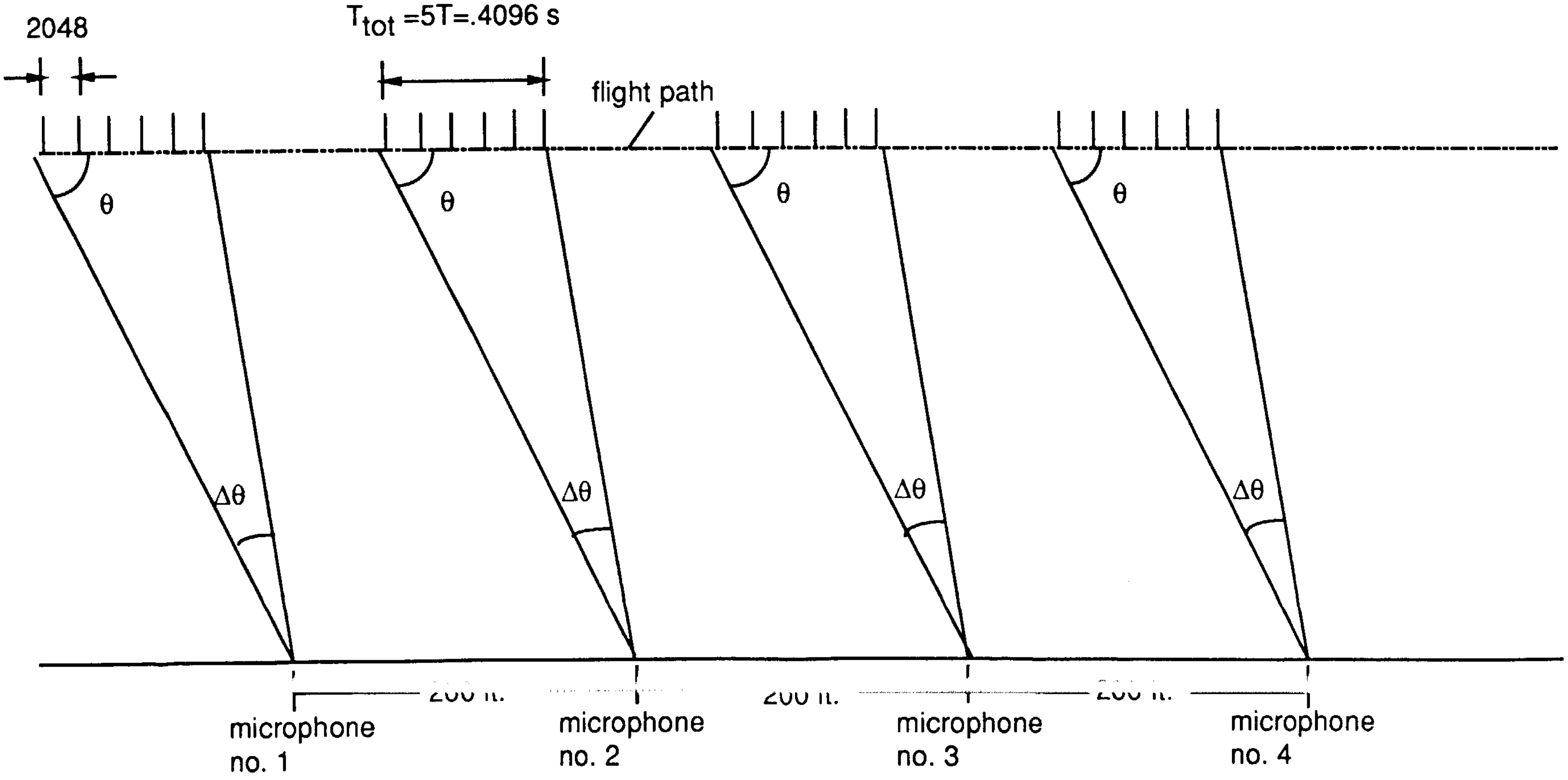

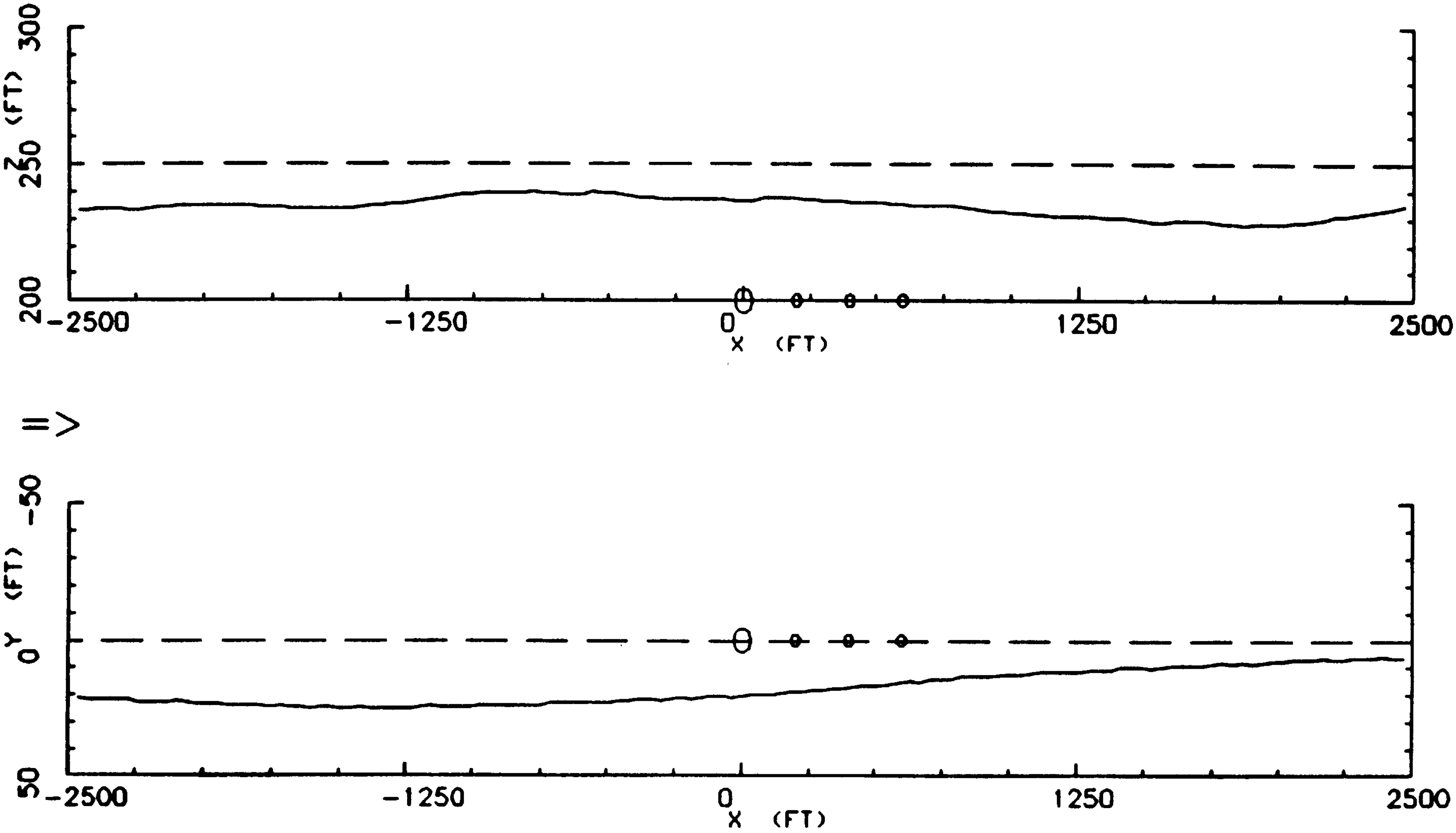

Figure 5: Nasa/Bell XV-15 position data - level flyover run

Figure 6. Measured time history; microphone no. 1; $\theta_1=16.25^\circ$; $\Delta\theta=3.0^\circ$.

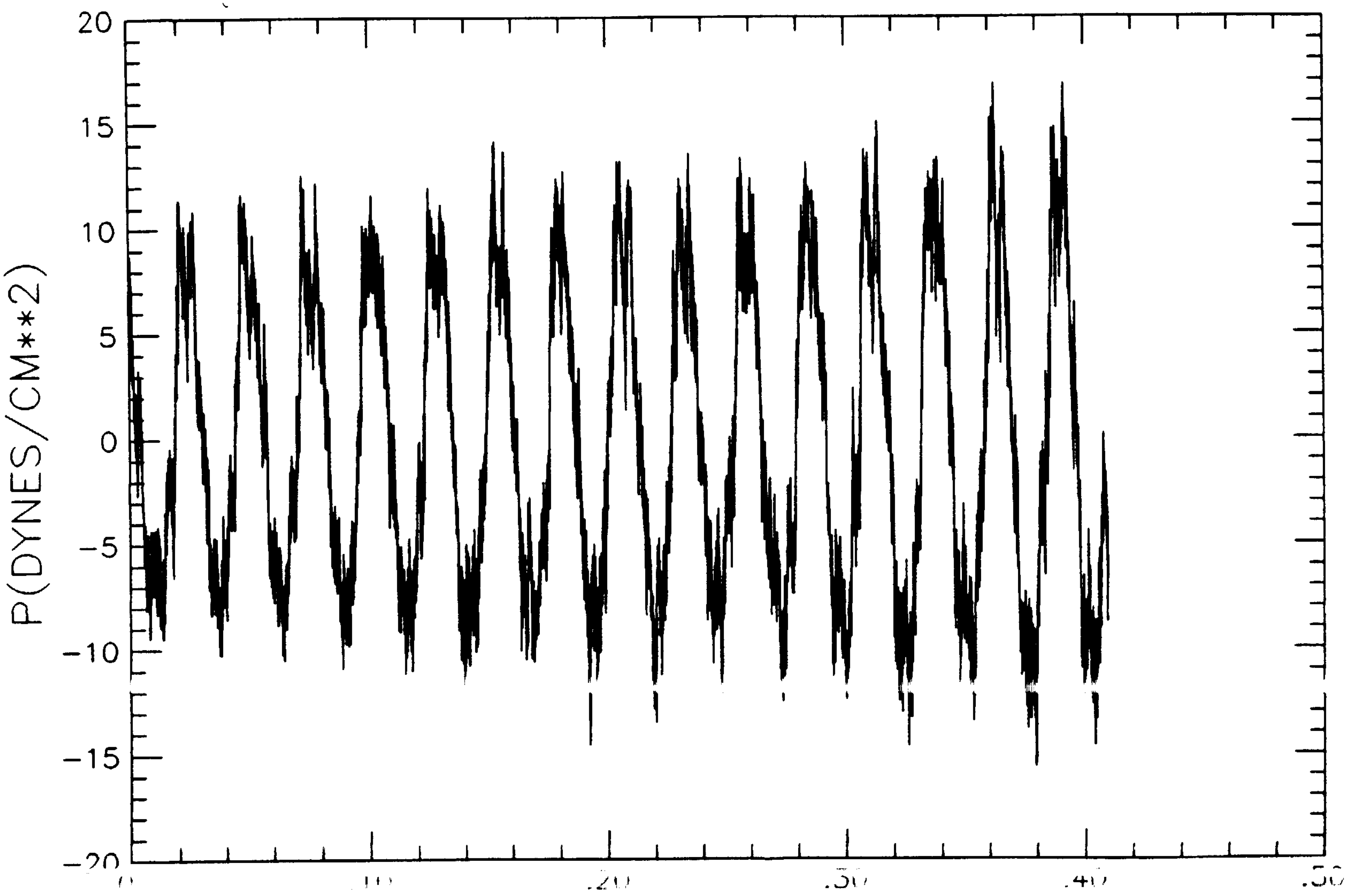

Figure 7. Emission time history; microphone no. 1; $\theta_1=16.25^o$; $\Delta\theta=3.0^o$.

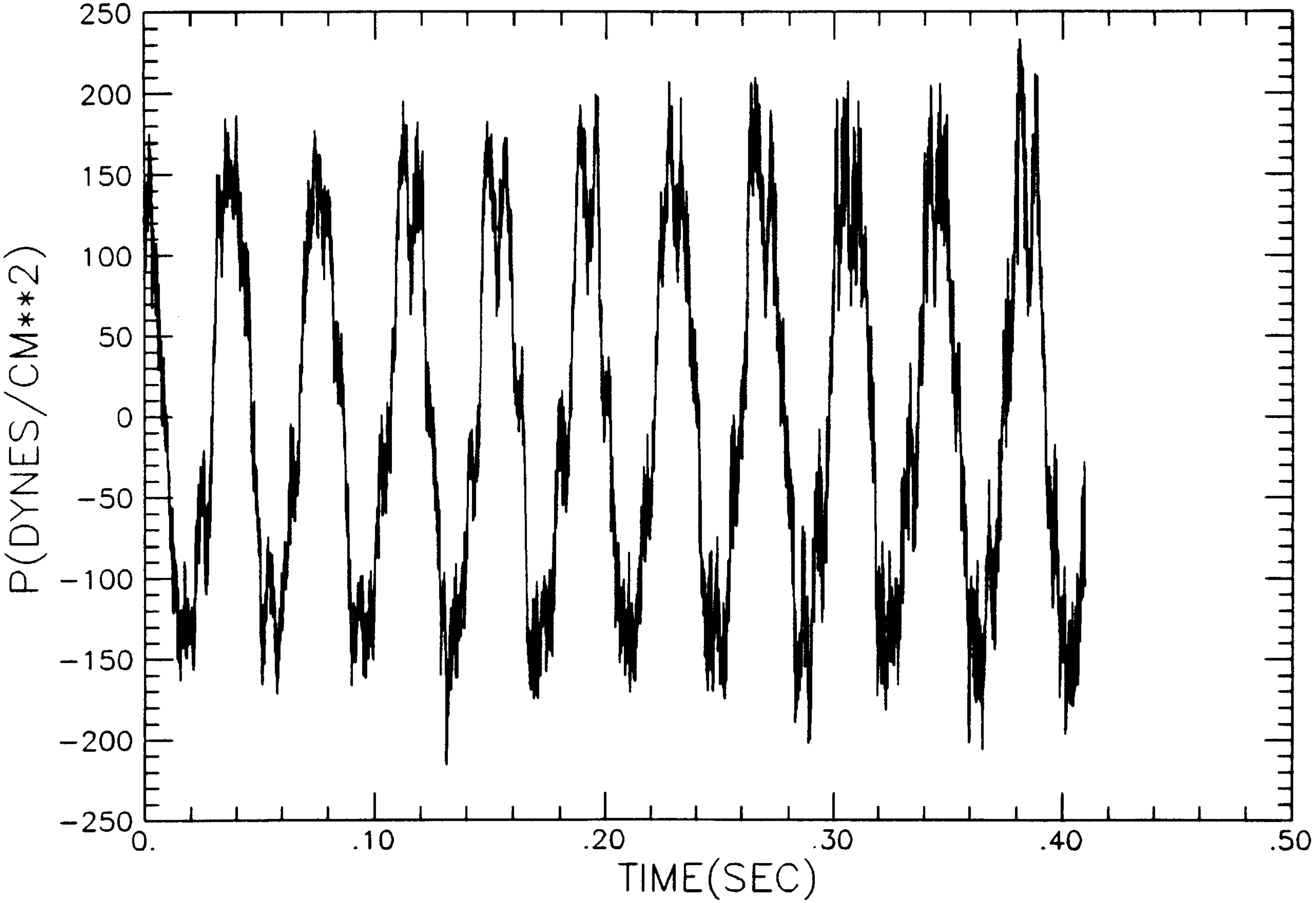

Figure 8. Measured time history; microphone no. 1; $\theta_1=141.15°$; $\Delta\theta=10.95°$.

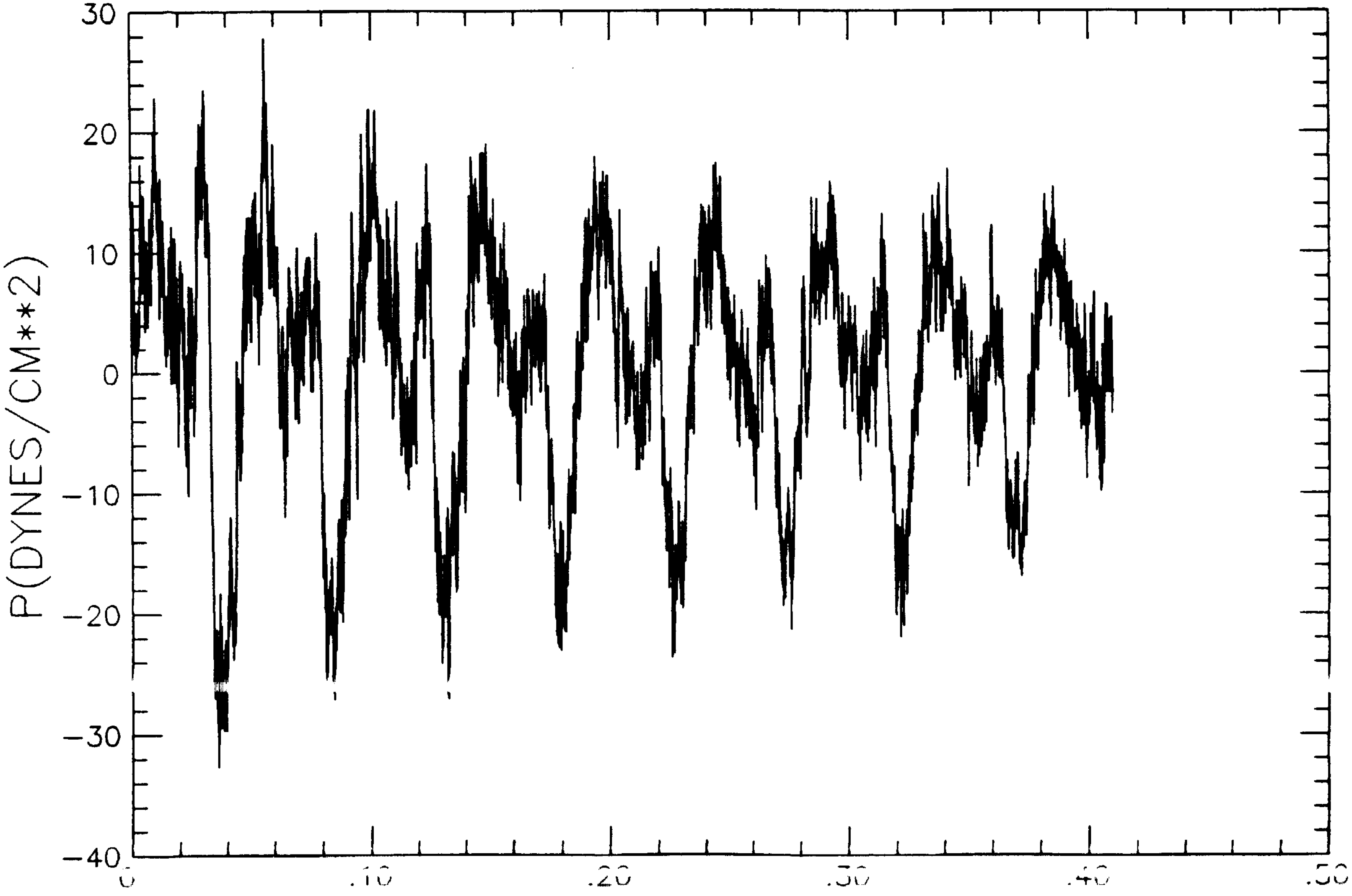

Figure 9. Emission time history; microphone no. 1; $\theta_1=141.15^{\circ}$; $\Delta\theta=10.95^{\circ}$.

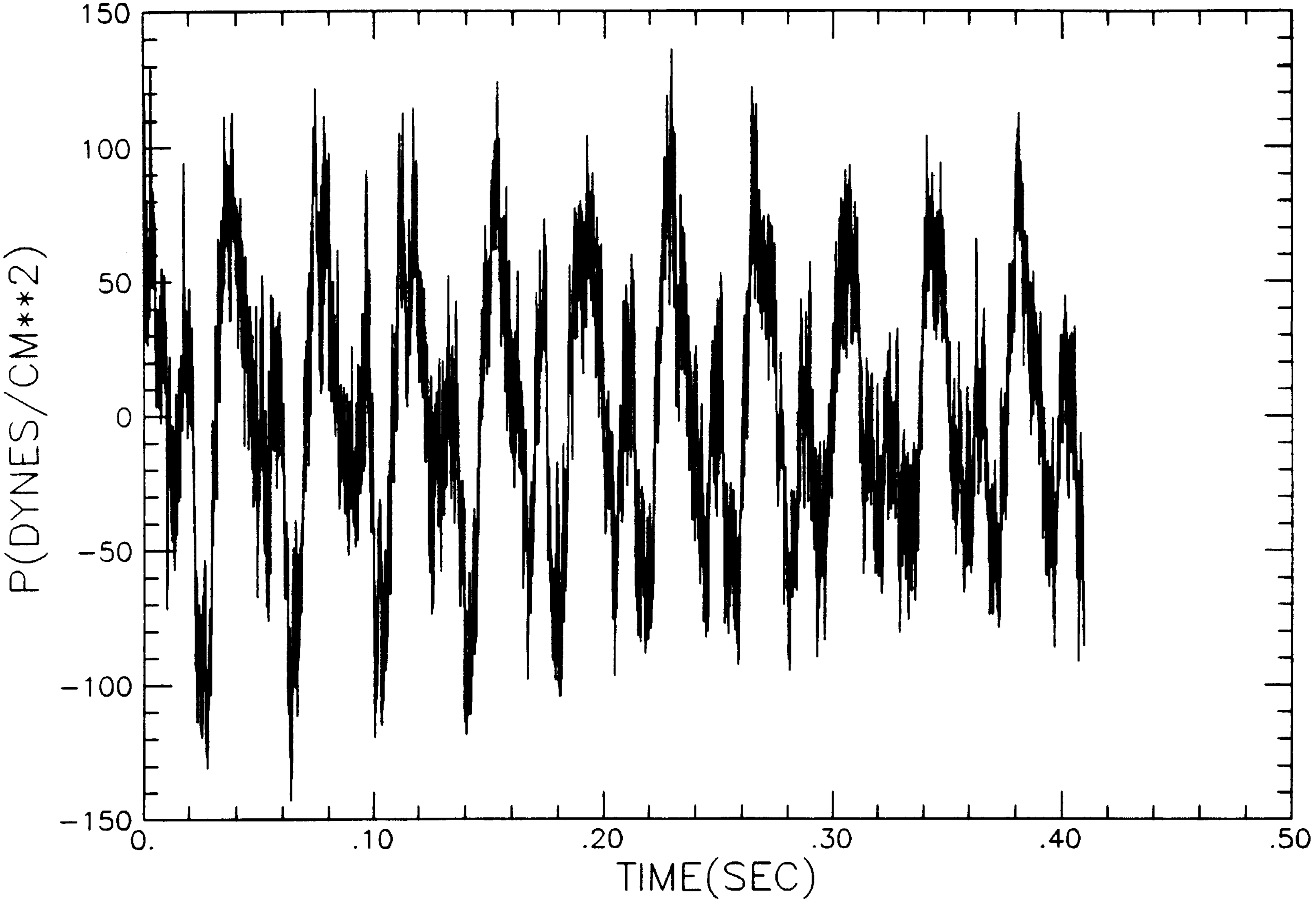

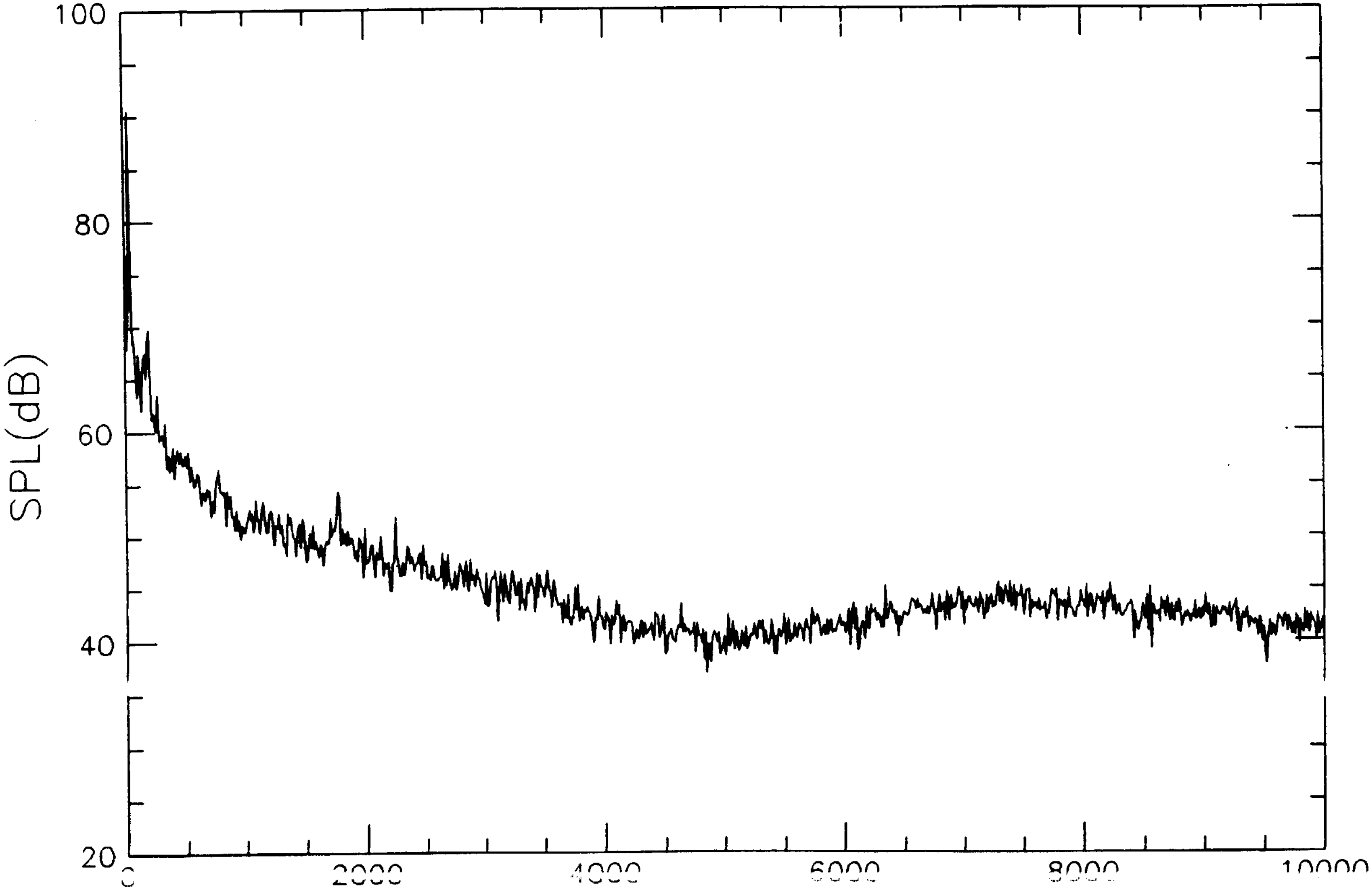

Figure 10. Doppler spectrum; $\Delta f=12.2$ Hz; $\theta_l=16.25^{o}$; $\Delta\theta=3.0^{o}$.

Figure 11. Doppler spectrum; $\Delta f=12.2$ Hz; $\theta_1=20.3^{\circ}$; $\Delta\theta=5.68^{\circ}$.

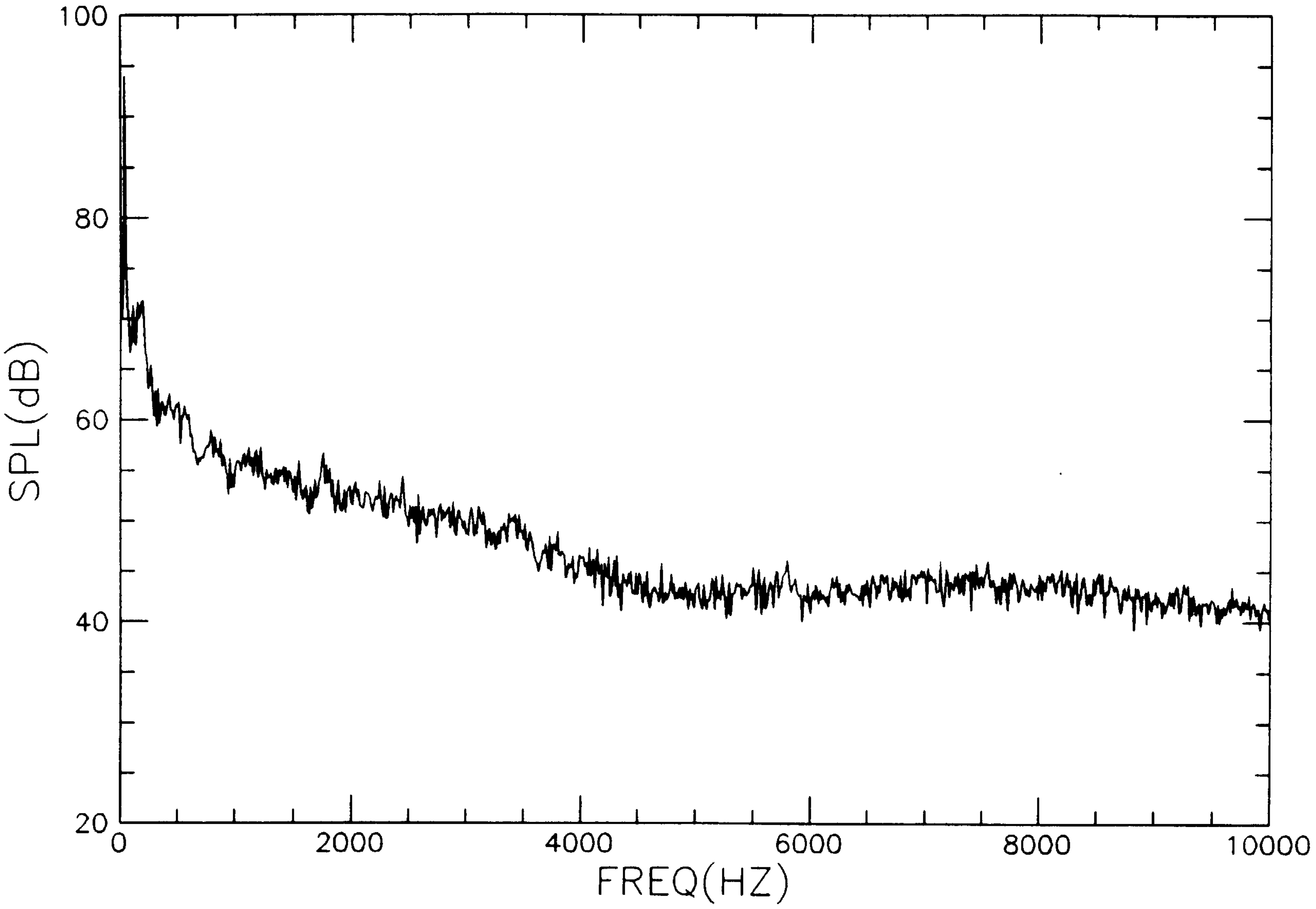

Figure 12. Doppler spectrum; $\Delta f=12.2$ Hz; $\theta_1=27.6^\circ$; $\Delta\theta=10.93^\circ$.

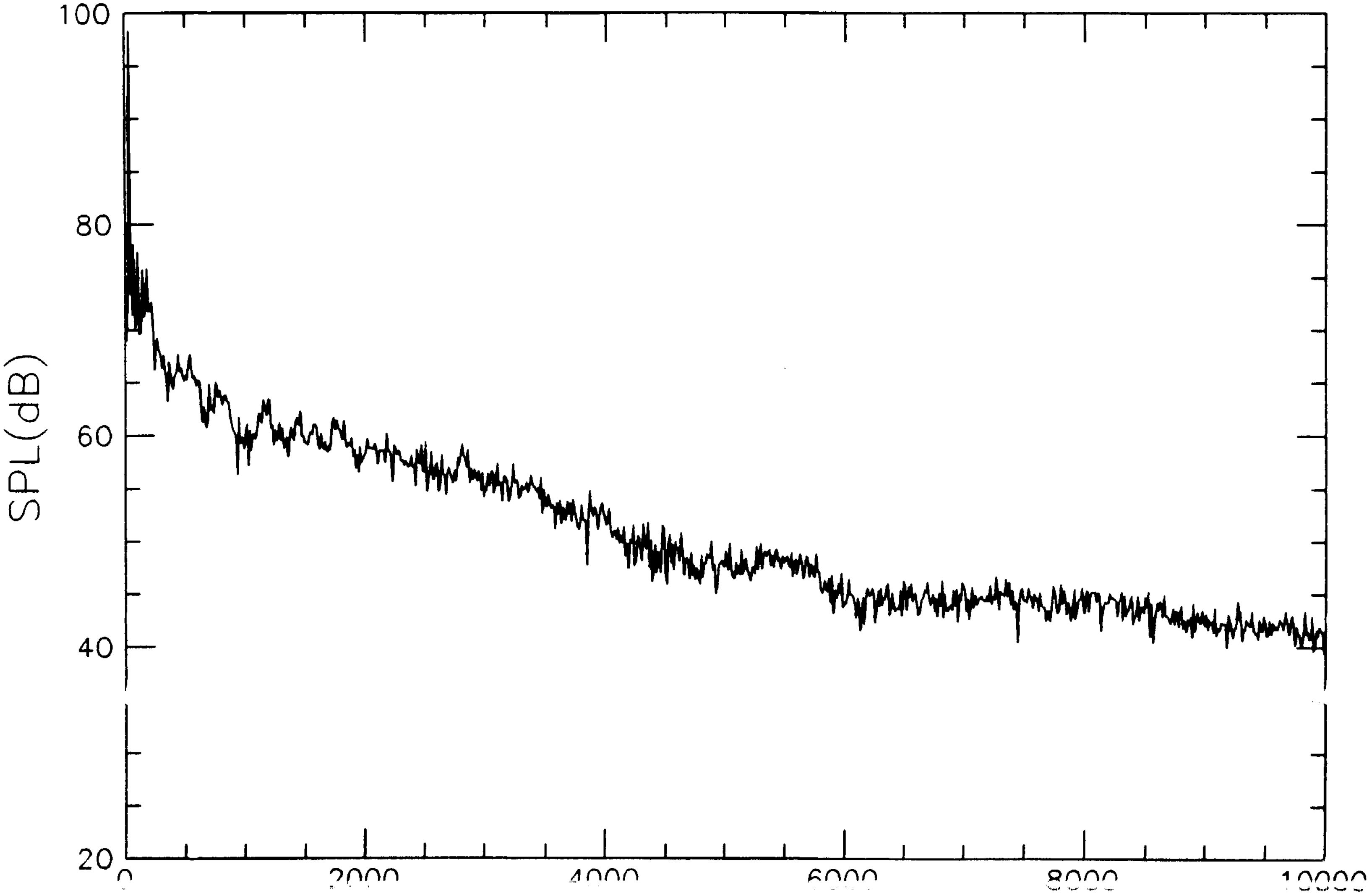

Figure 13. Doppler spectrum; $\Delta f=12.2$ Hz; $\theta_1=41.9^o$; $\Delta\theta=23.13^o$.

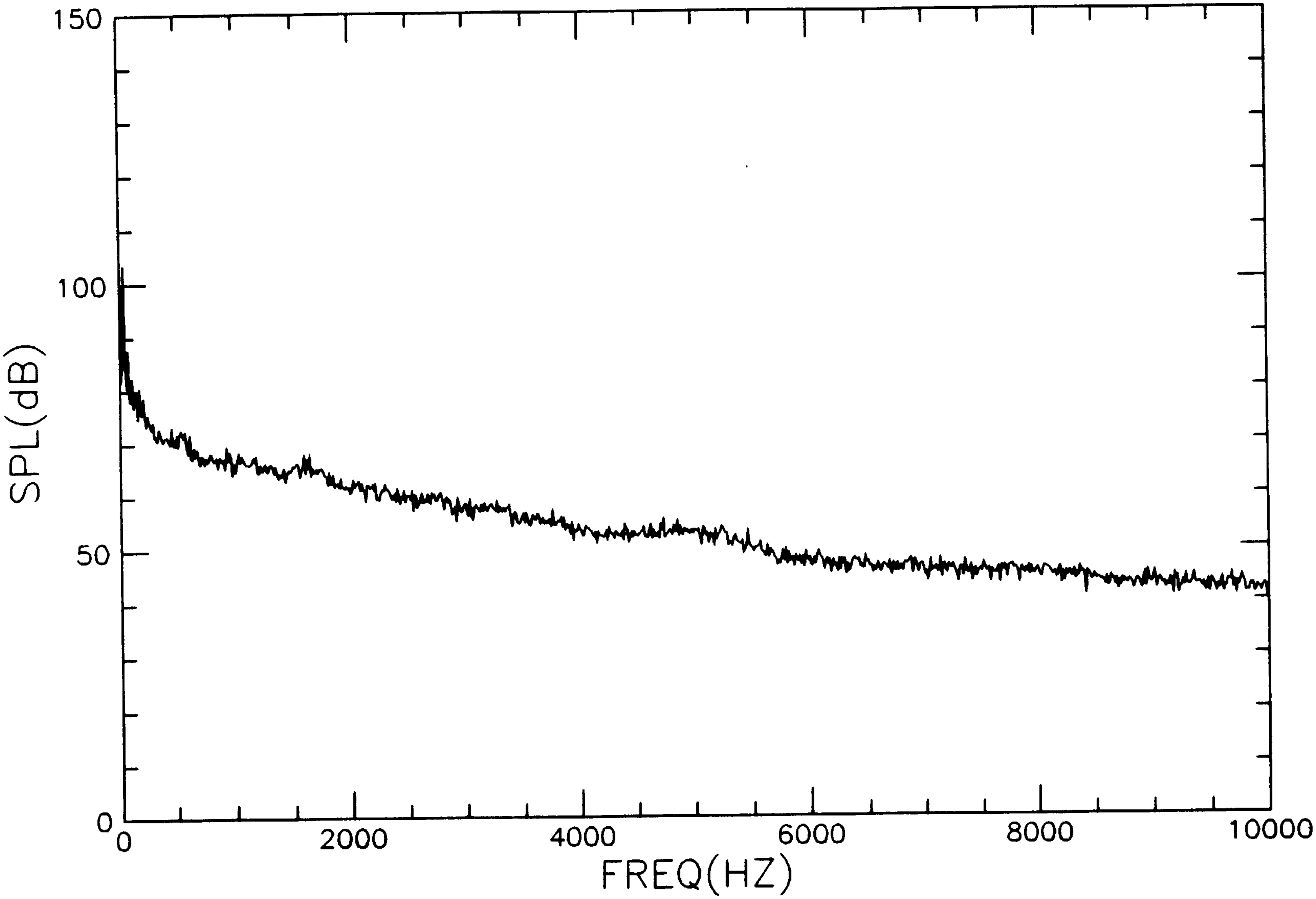

Figure 14. Doppler spectrum; $\Delta f=12.2$ Hz; $\theta_1=72.0^{\circ}$; $\Delta\theta=35.78^{\circ}$.

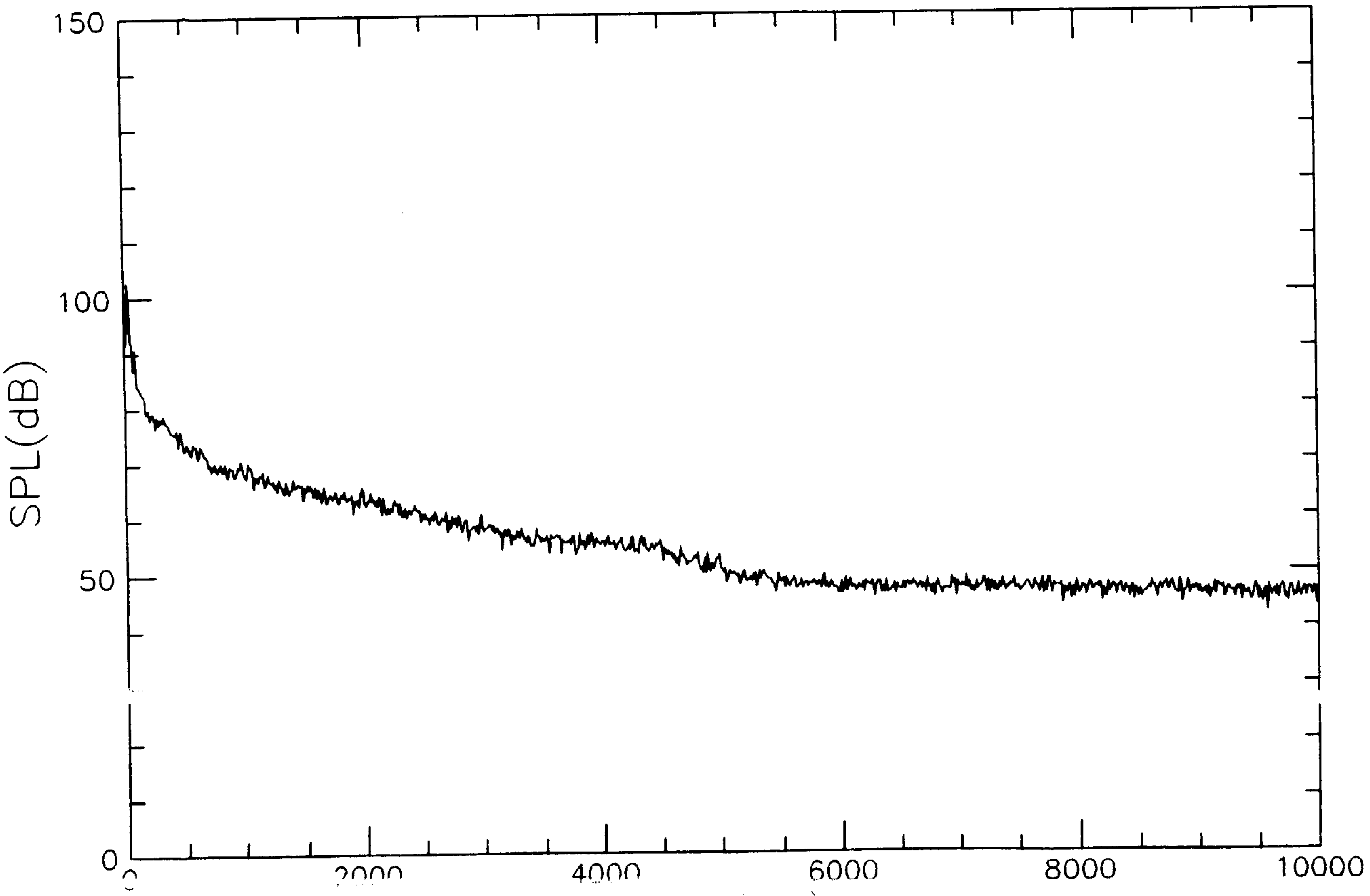

Figure 15. Doppler spectrum; $\Delta f=12.2$ Hz; $\theta_1=114.7^{\circ}$; $\Delta\theta=23.03^{\circ}$.

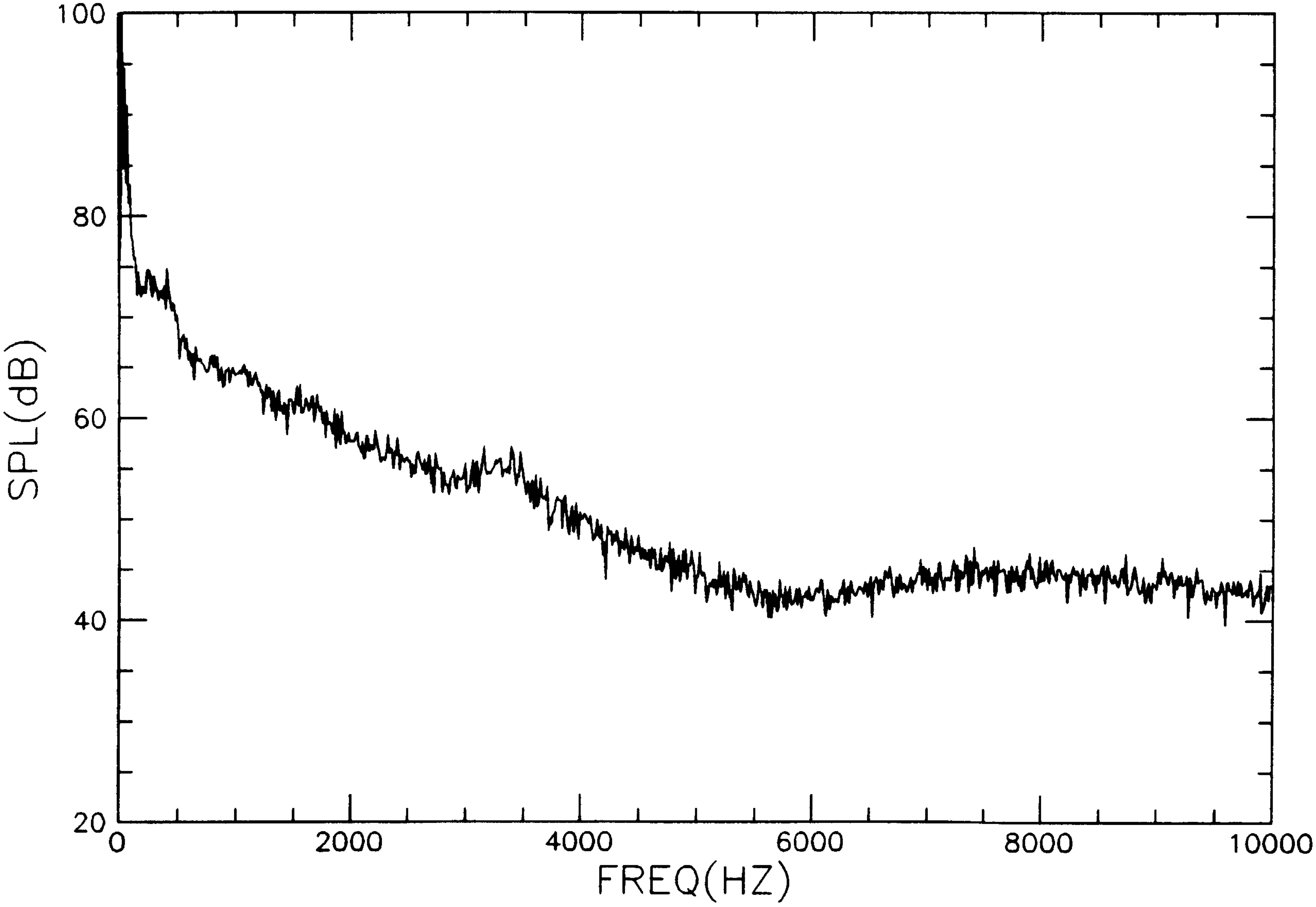

Figure 16. Doppler spectrum; Δf=12.2 Hz; θ_l=141.15°; Δθ=10.95°.

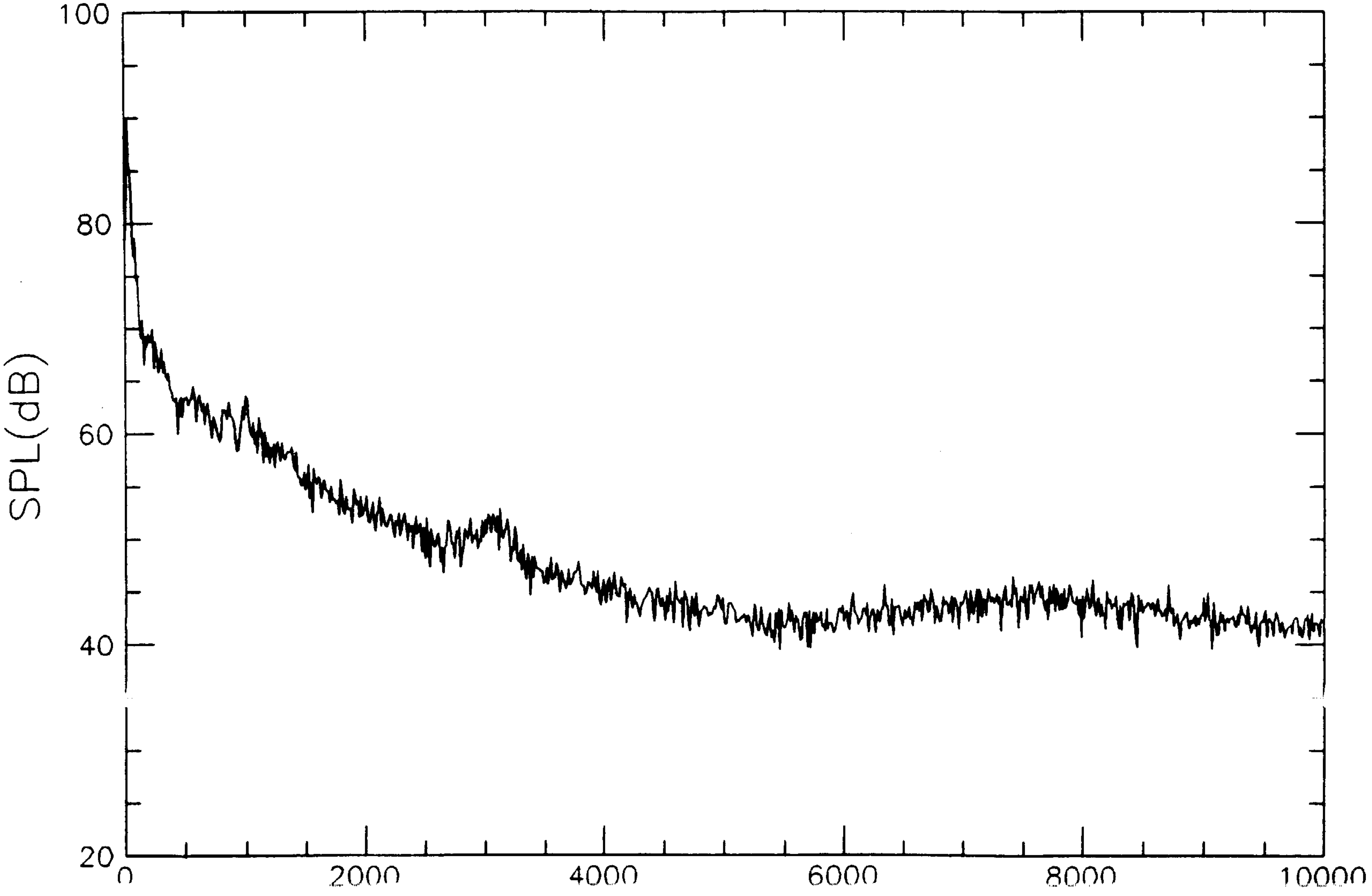

Figure 17. De-Dopplerized spectrum; $\Delta f=12.2$ Hz; $\theta_1=16.25^o$; $\Delta\theta=3.0^o$.

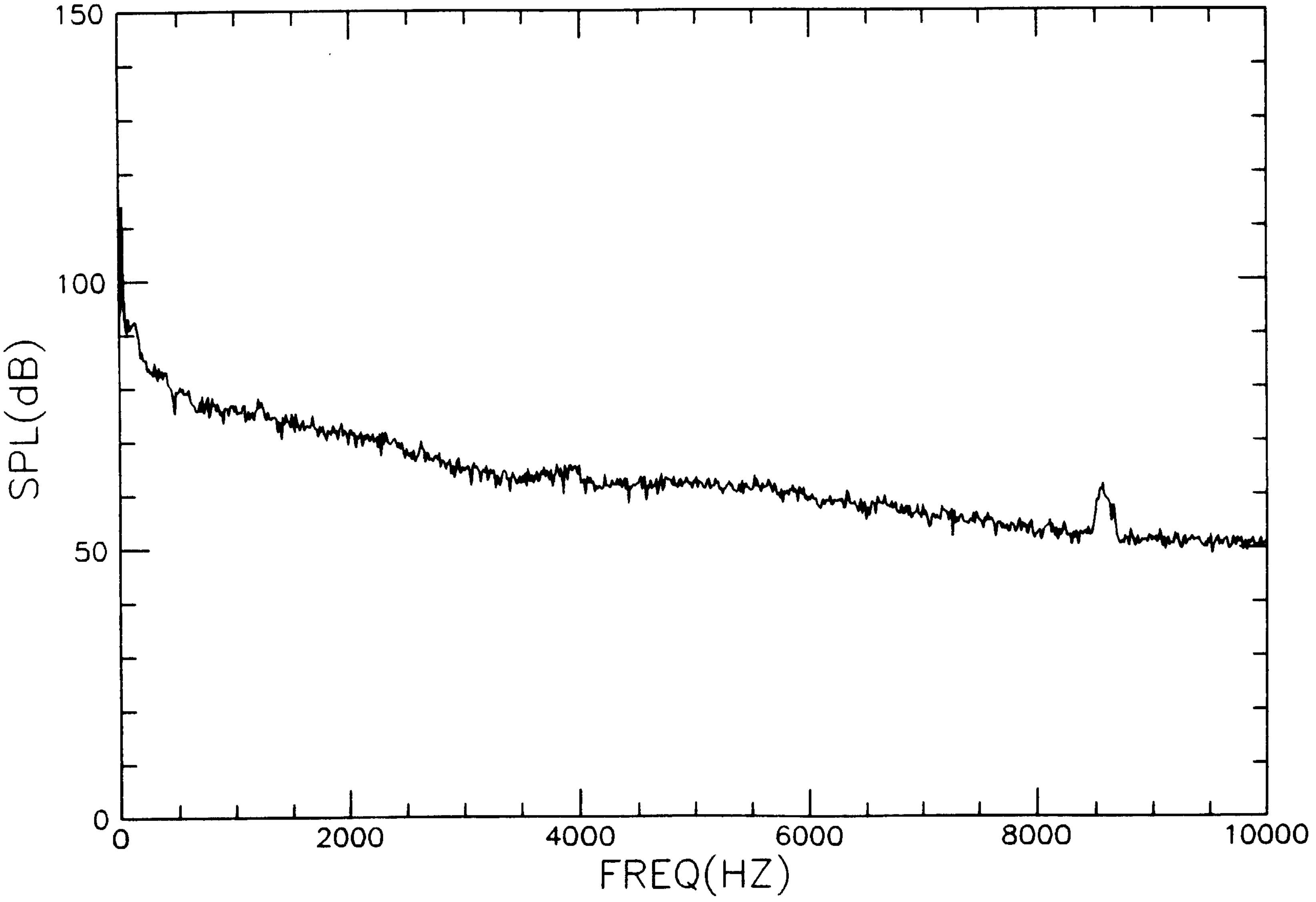

Figure 18. De-Dopplerized spectrum; Δf=12.2 Hz; θ_1=20.3°; Δθ=5.68°.

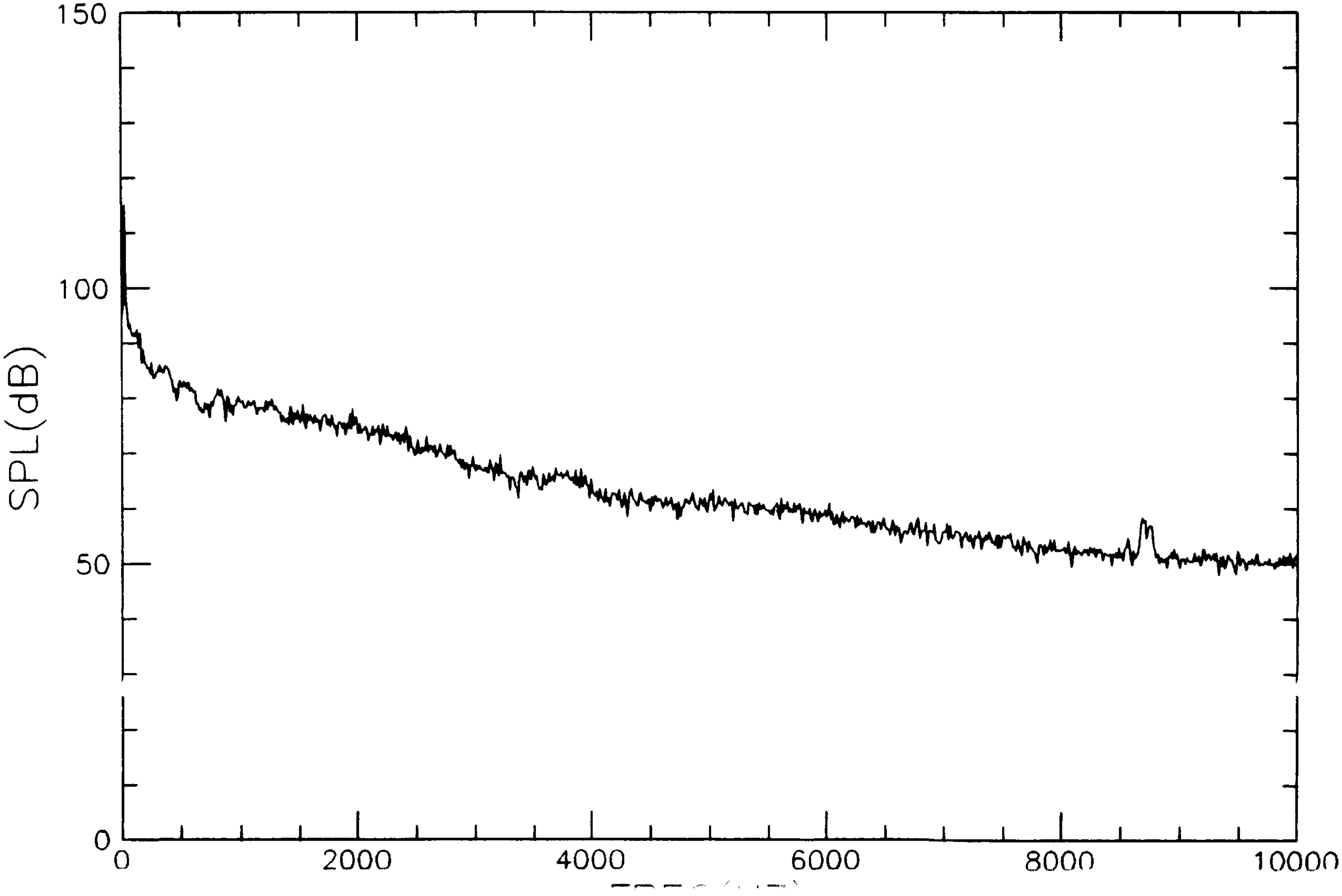

Figure 19. De-Dopplerized spectrum; Δf=12.2 Hz; θ_1=27.6°; $\Delta\theta$=10.93°.

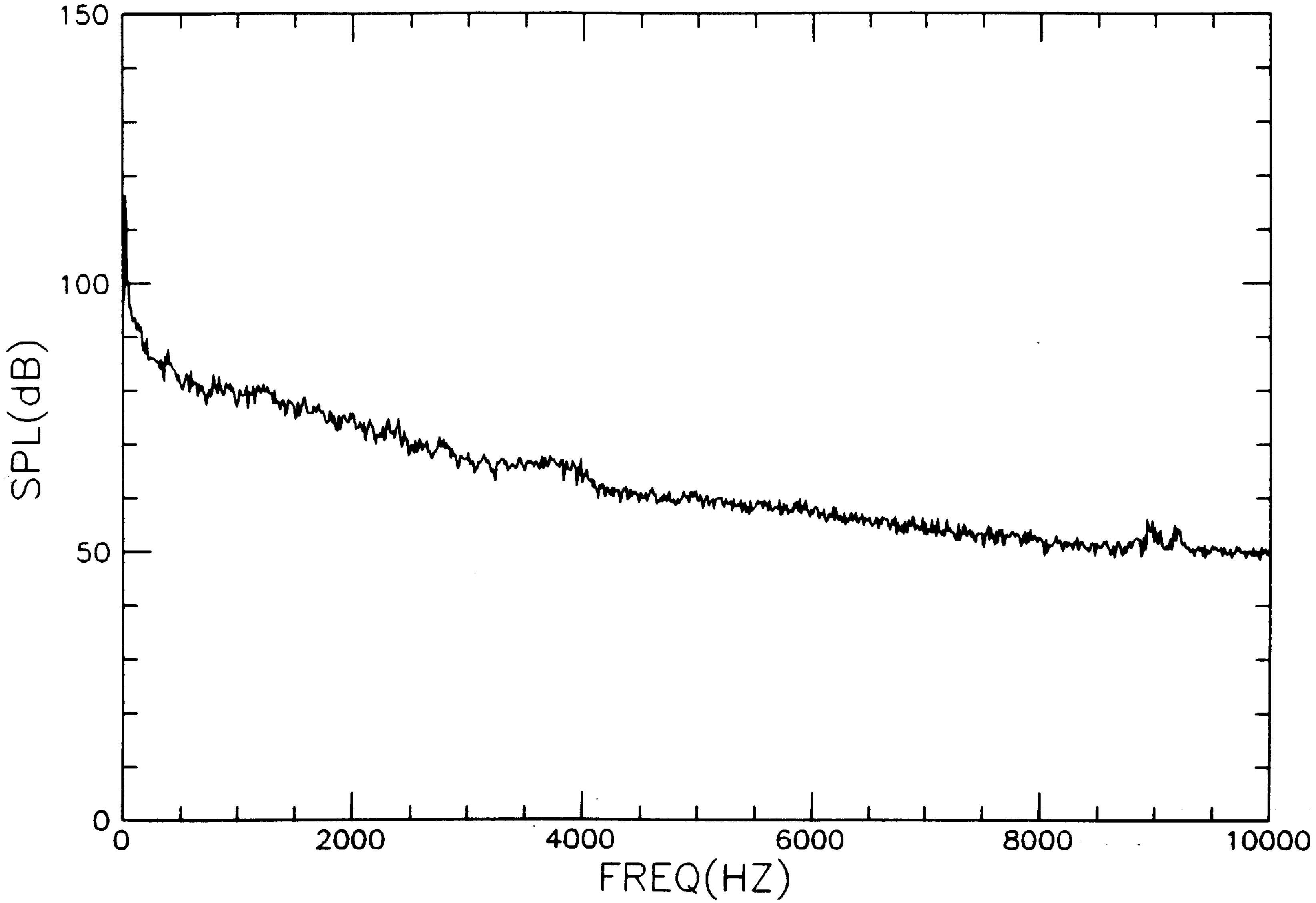

Figure 20. De-Dopplerized spectrum; $\Delta f=12.2$ Hz; $\theta_1=41.9^{\circ}$; $\Delta\theta=23.13^{\circ}$.

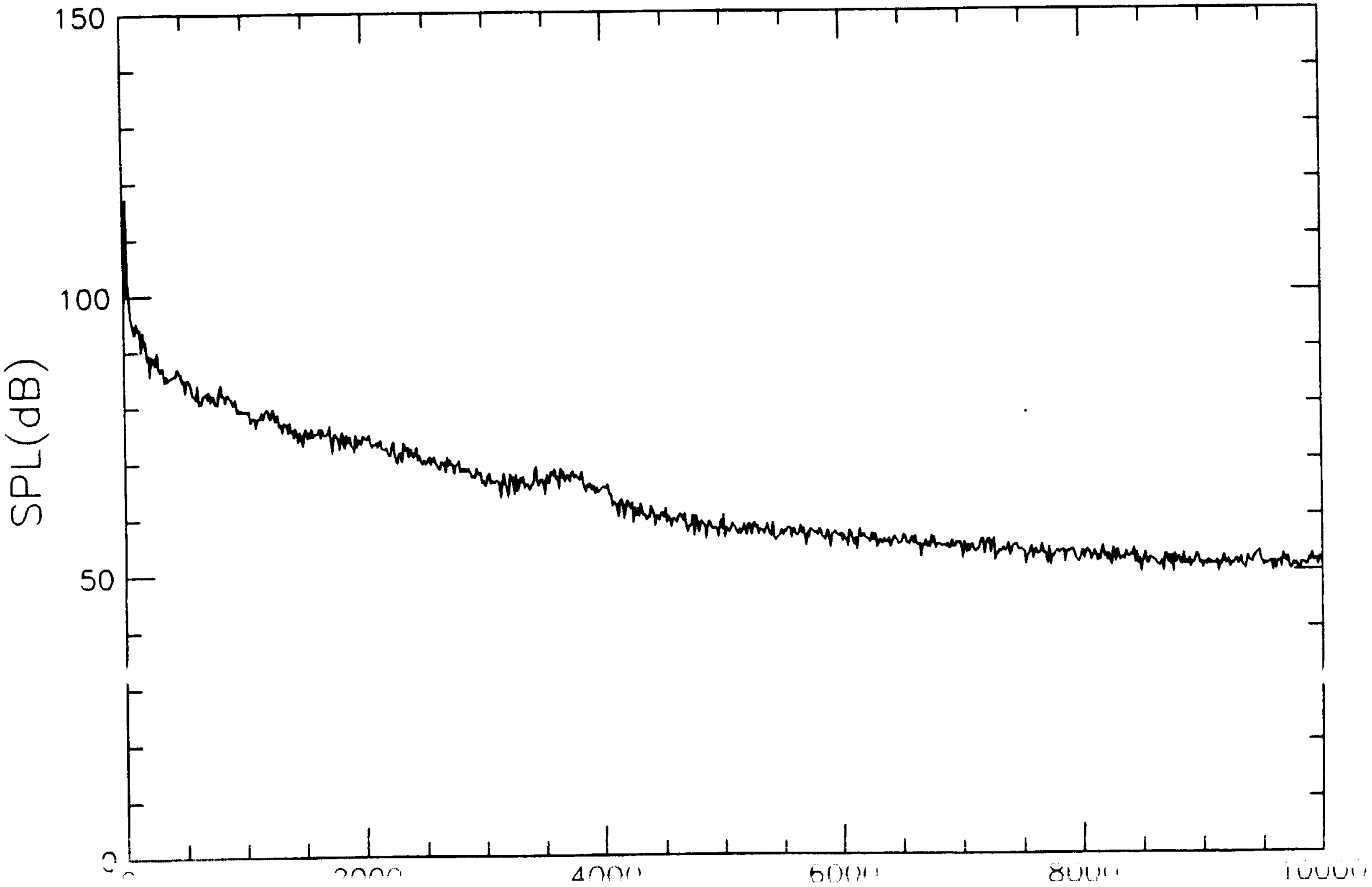

Figure 21. De-Dopplerized spectrum; $\Delta f=12.2$ Hz; $\theta_1=72.0°$; $\Delta\theta=35.78°$.

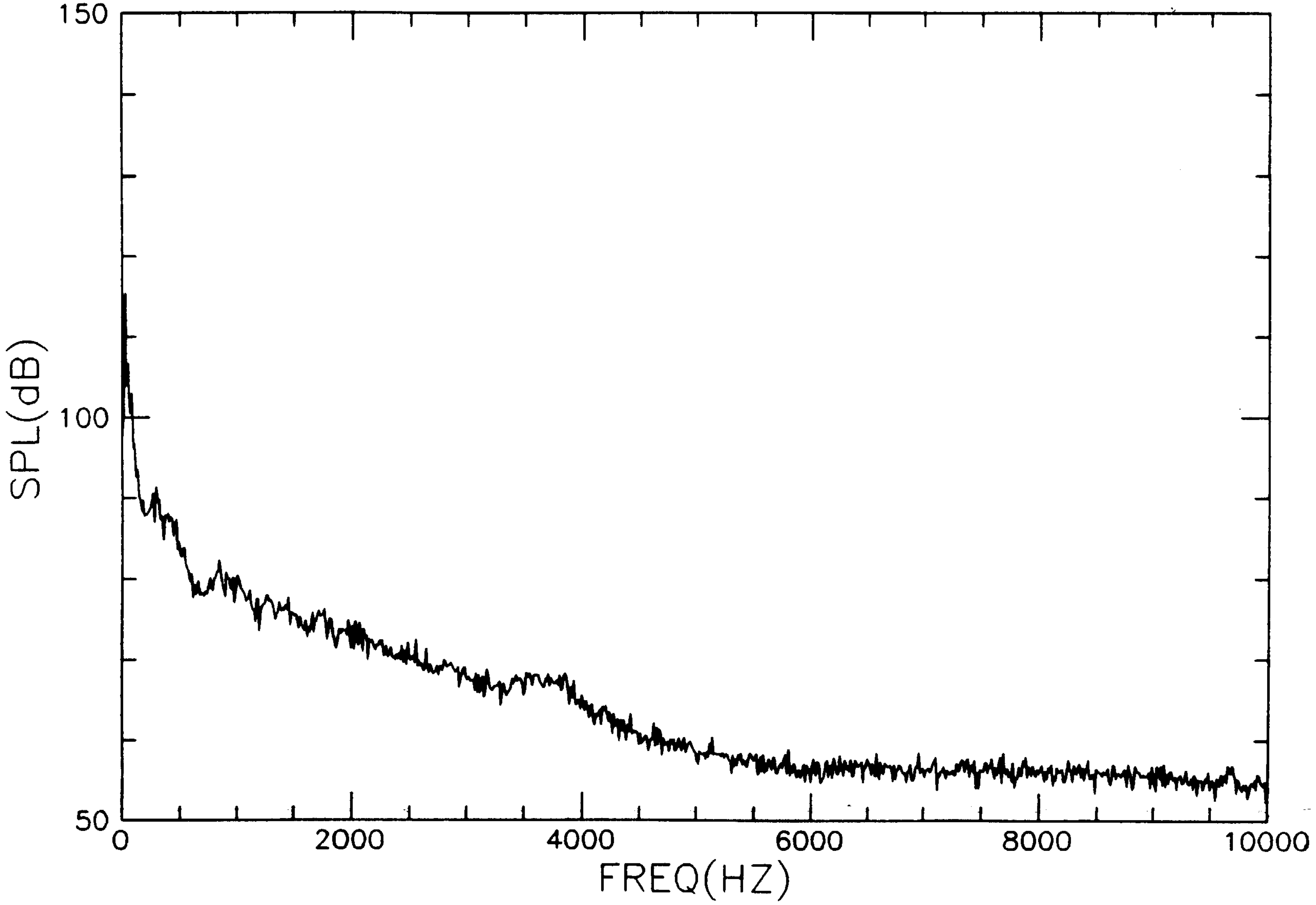

Figure 22. De-Dopplerized spectrum; $\Delta f=12.2$ Hz; $\theta_1=114.7^{\circ}$; $\Delta\theta=23.03^{\circ}$.

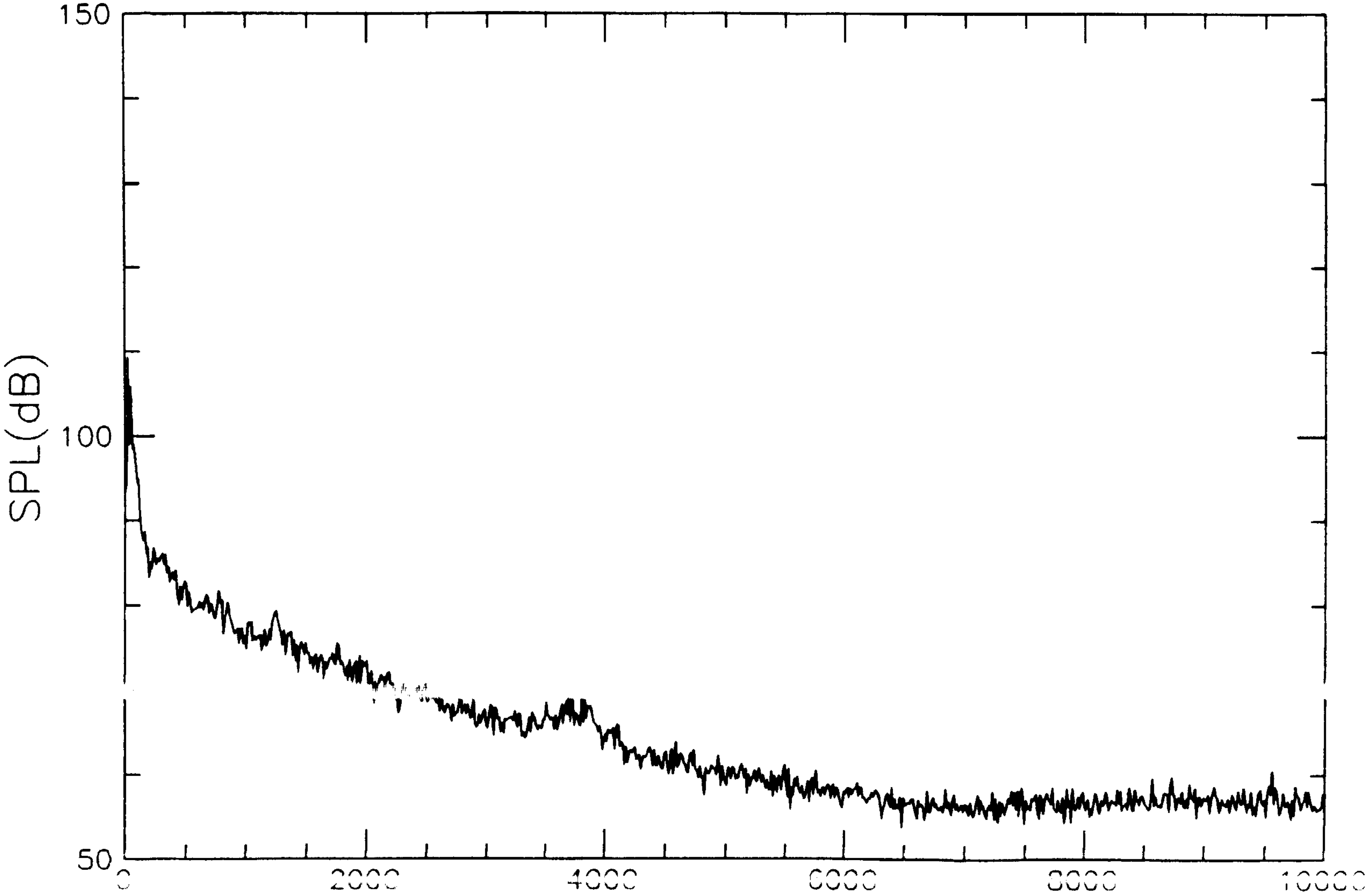

Figure 23. De-Dopplerized spectrum; $\Delta f=12.2$ Hz; $\theta_1=141.15^{\circ}$; $\Delta\theta=10.95^{\circ}$.

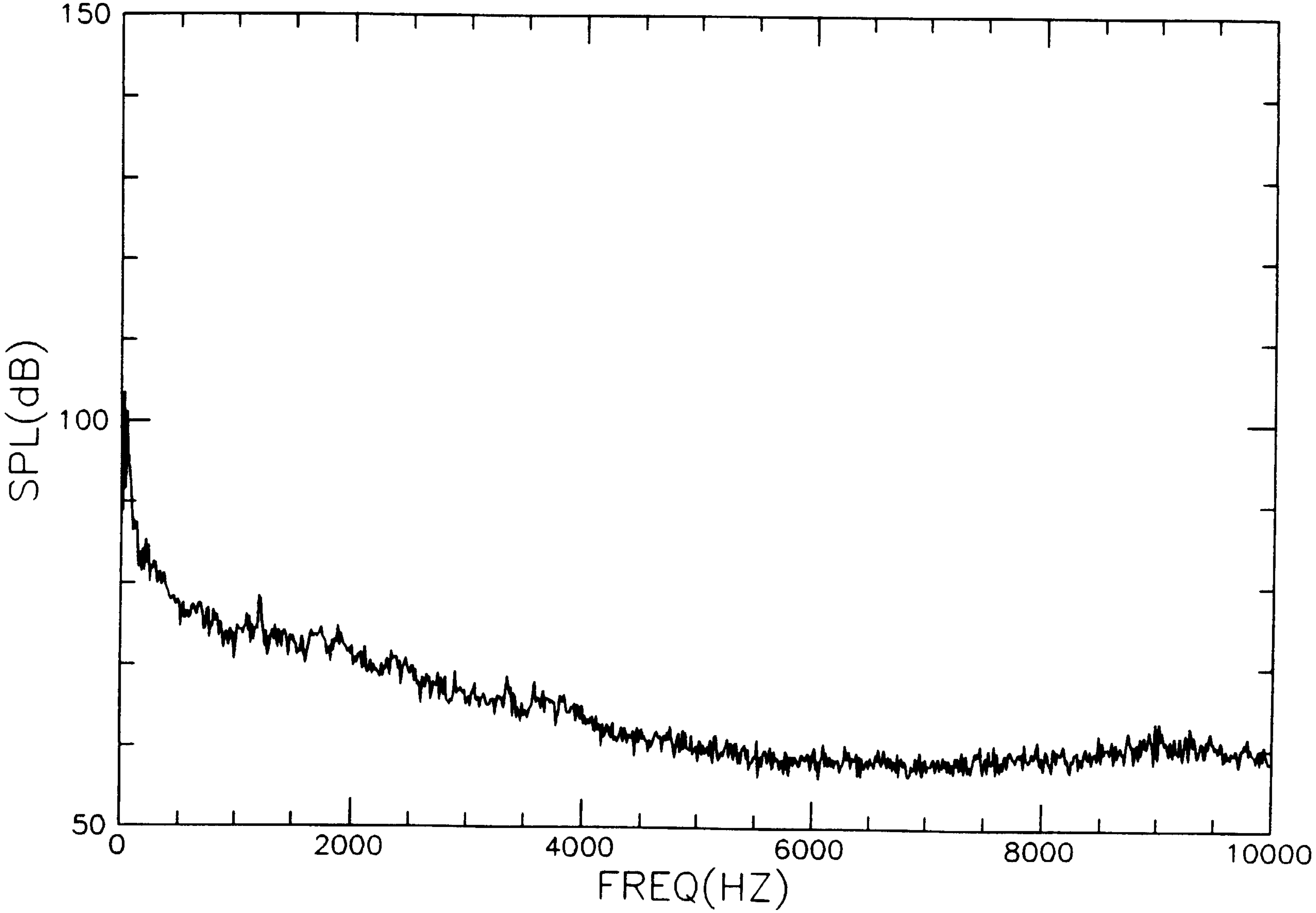

Figure 24. Doppler spectrum; Δf=1.53 Hz; $\theta_1=16.25°$; $\Delta\theta=6.25°$.

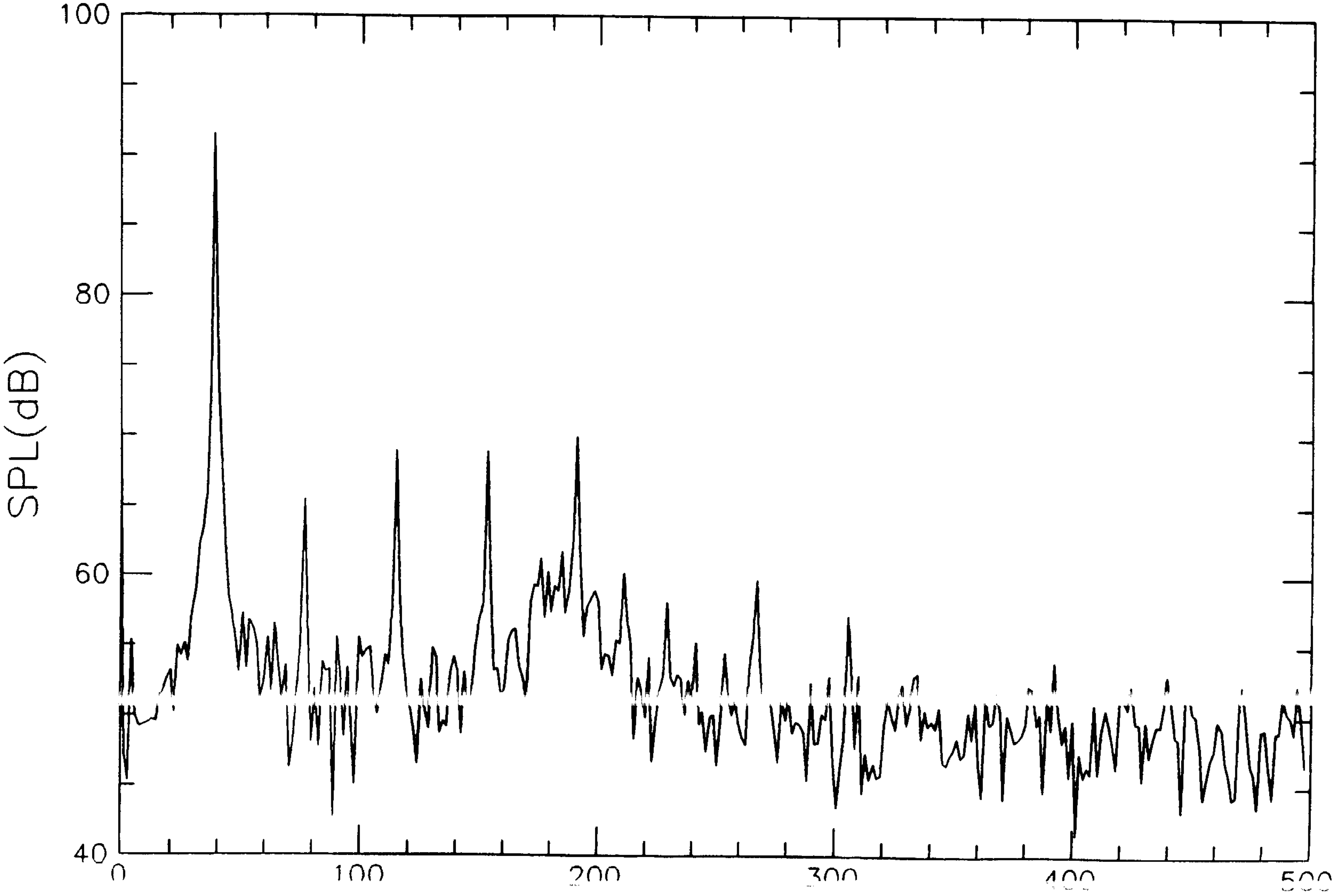

Figure 25. Doppler spectrum; $\Delta f=1.53$ Hz; $\theta_1=20.3^{\circ}$; $\Delta\theta=10.73^{\circ}$.

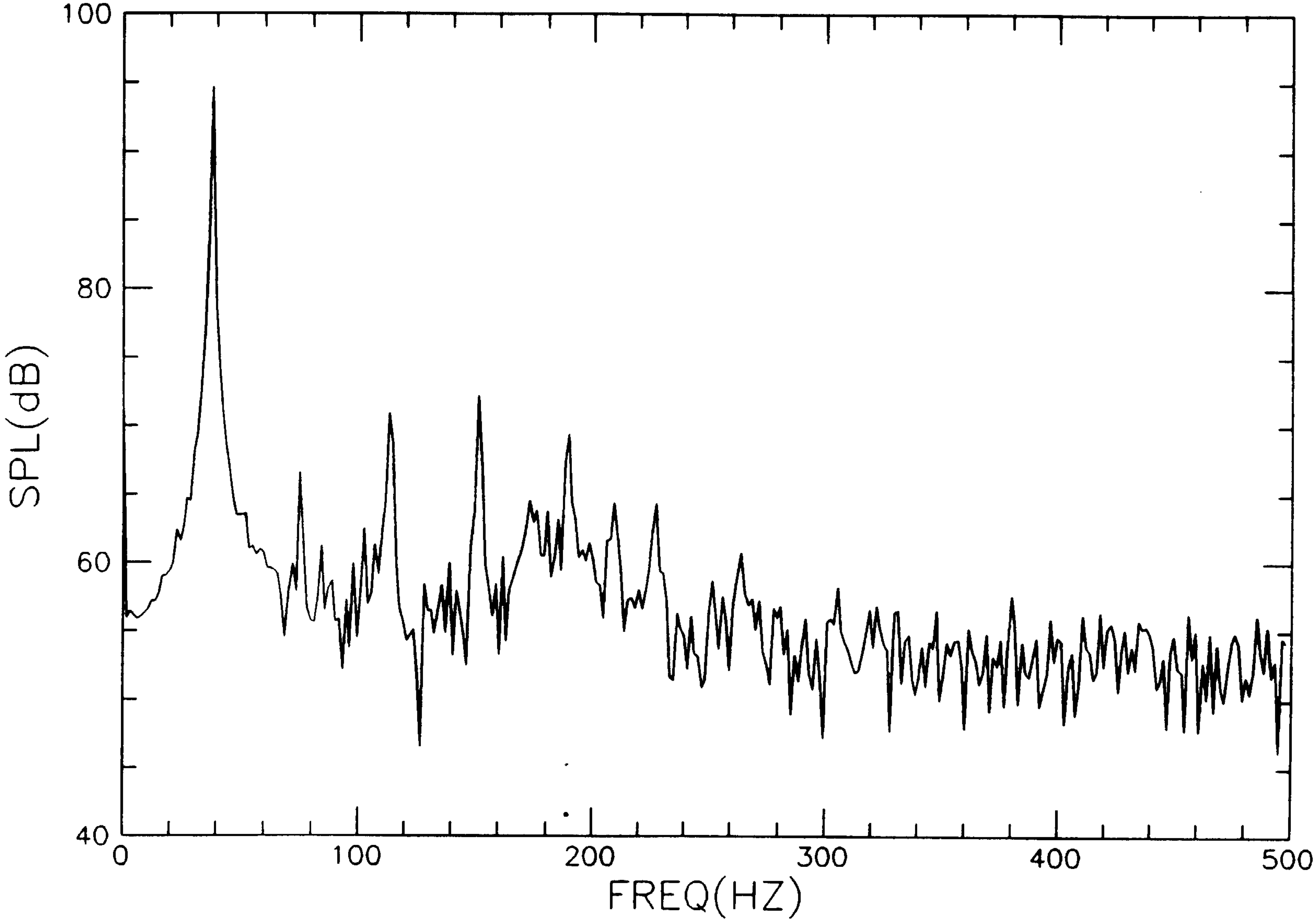

Figure 26. Doppler spectrum; Δf=1.53 Hz; θ_1=27.6°; Δθ=21.33°.

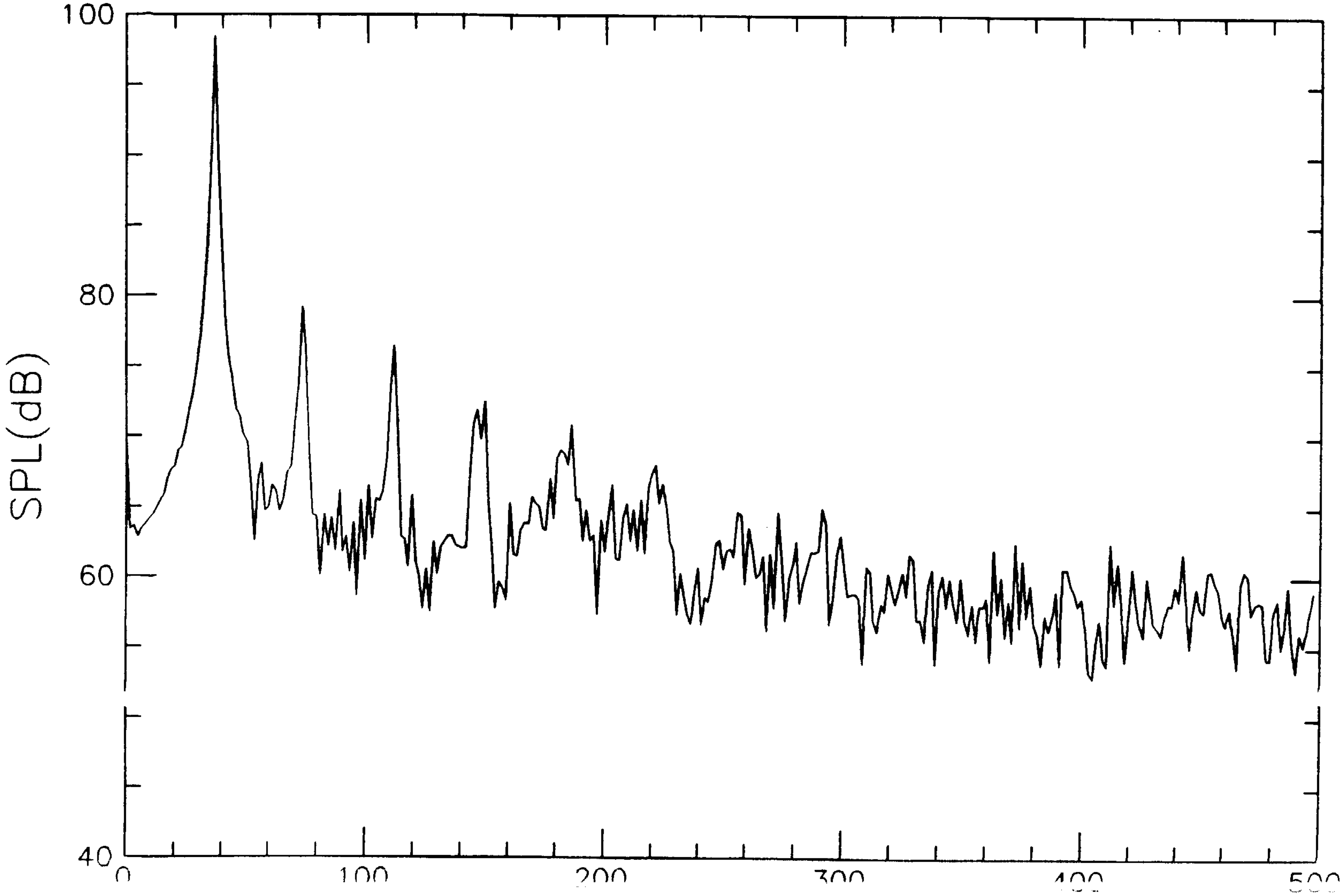

Figure 27. Doppler spectrum; $\Delta f=1.53$ Hz; $\theta_1=41.9^\circ$; $\Delta\theta=43.35^\circ$.

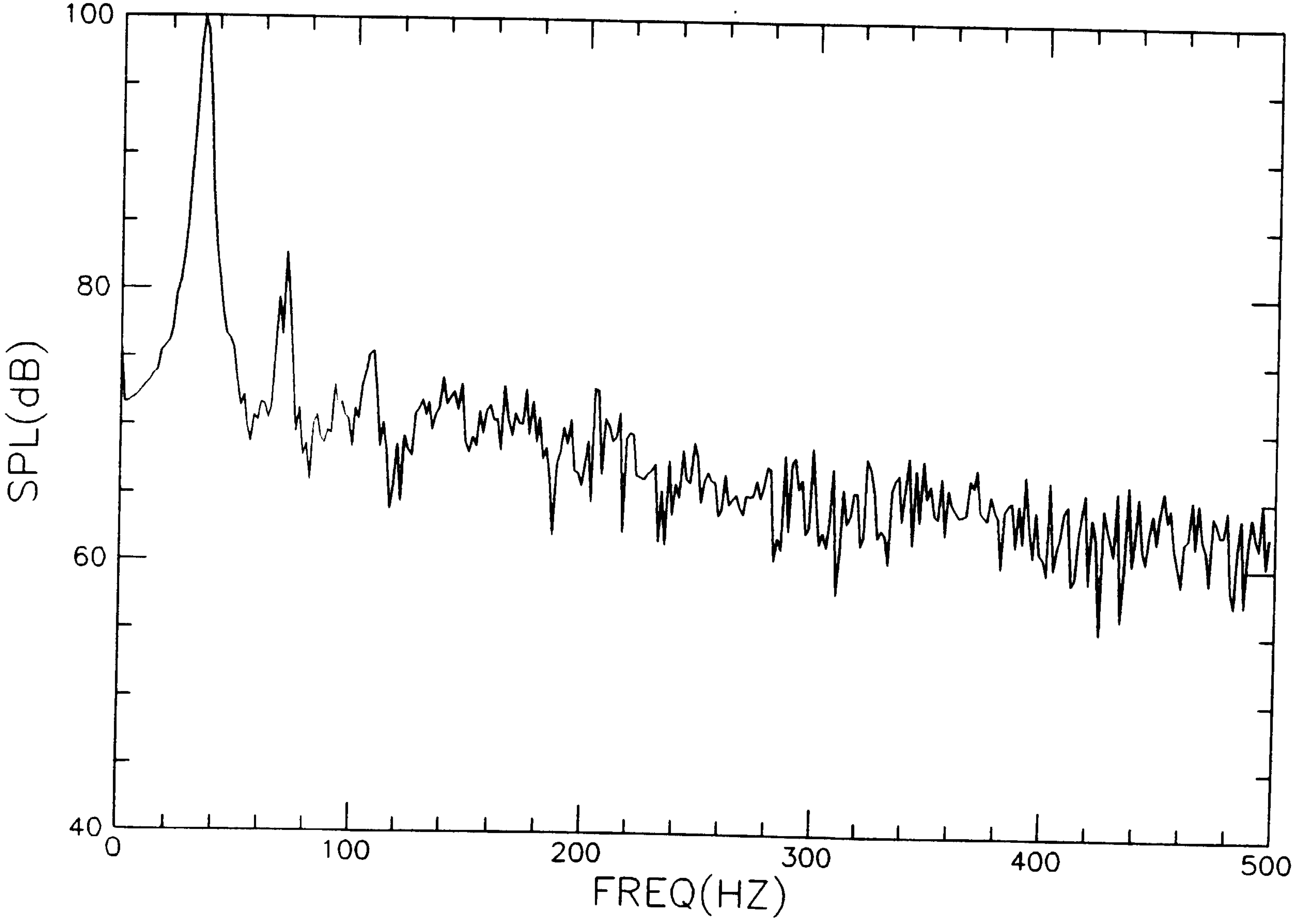

Figure 28. Doppler spectrum; $\Delta f=1.53$ Hz; $\theta_1=72.0^\circ$; $\Delta\theta=53.1^\circ$.

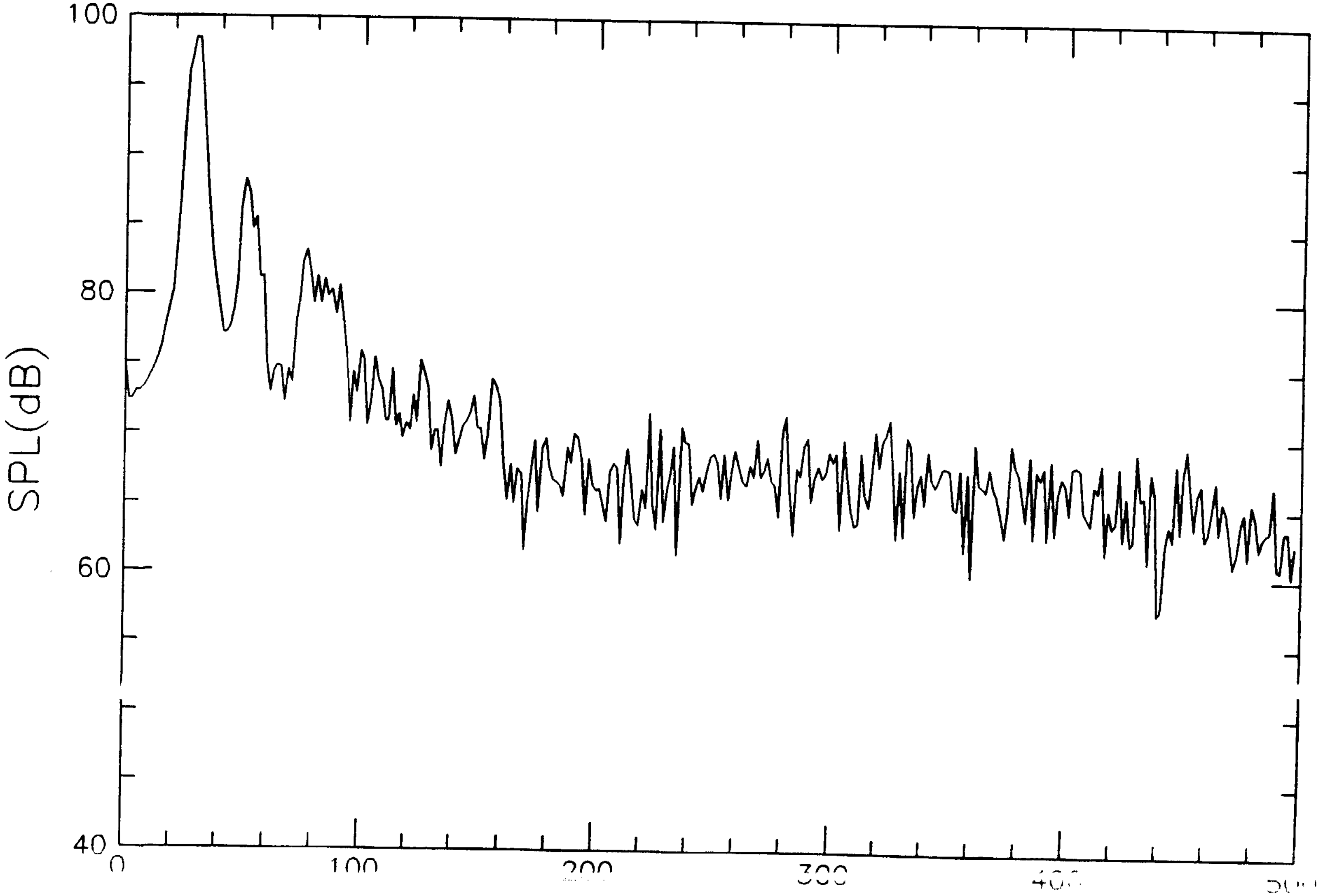

Figure 29. Doppler spectrum; $\Delta f=1.53$ Hz; $\theta_1=114.7^\circ$; $\Delta\theta=31.4^\circ$.

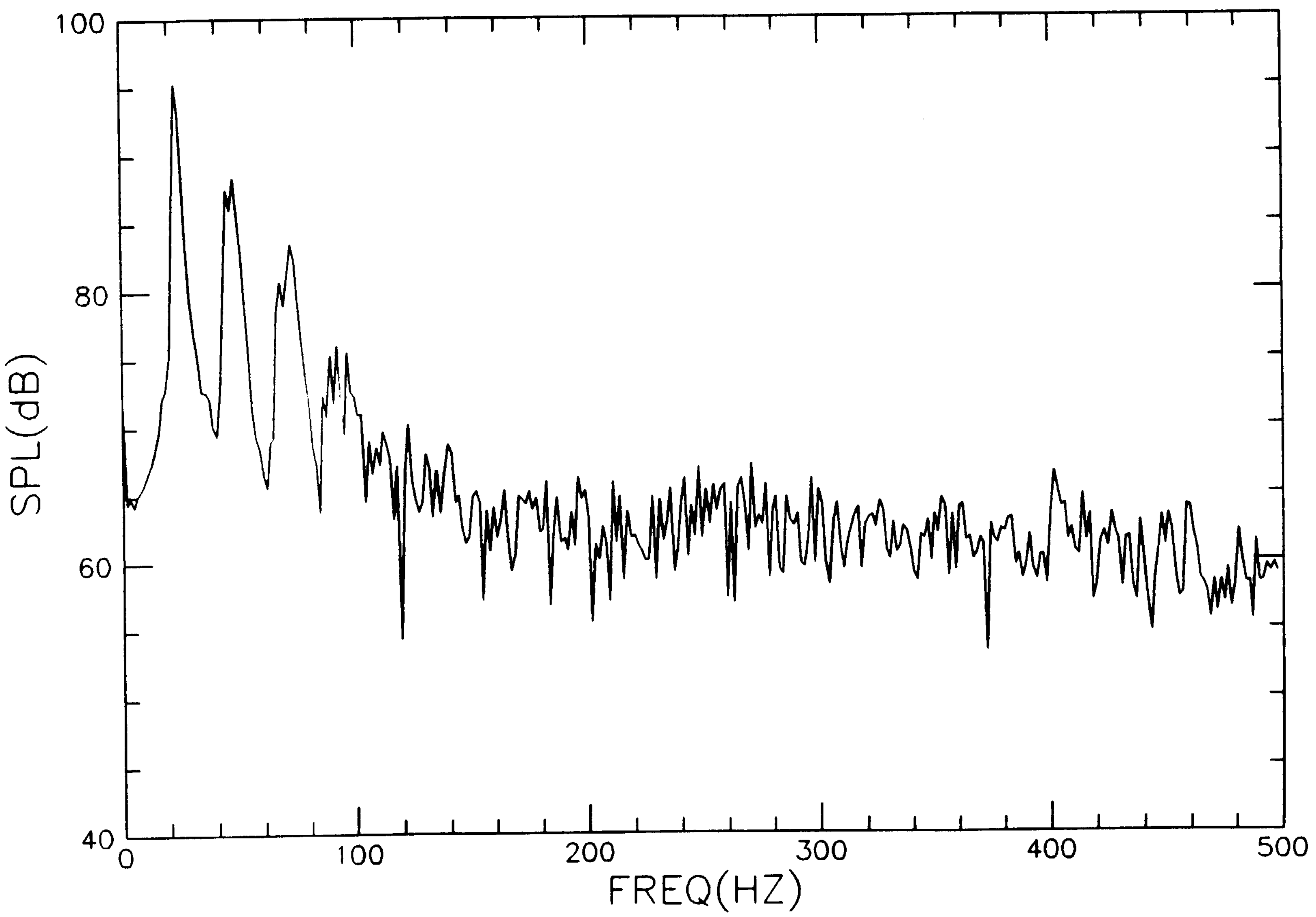

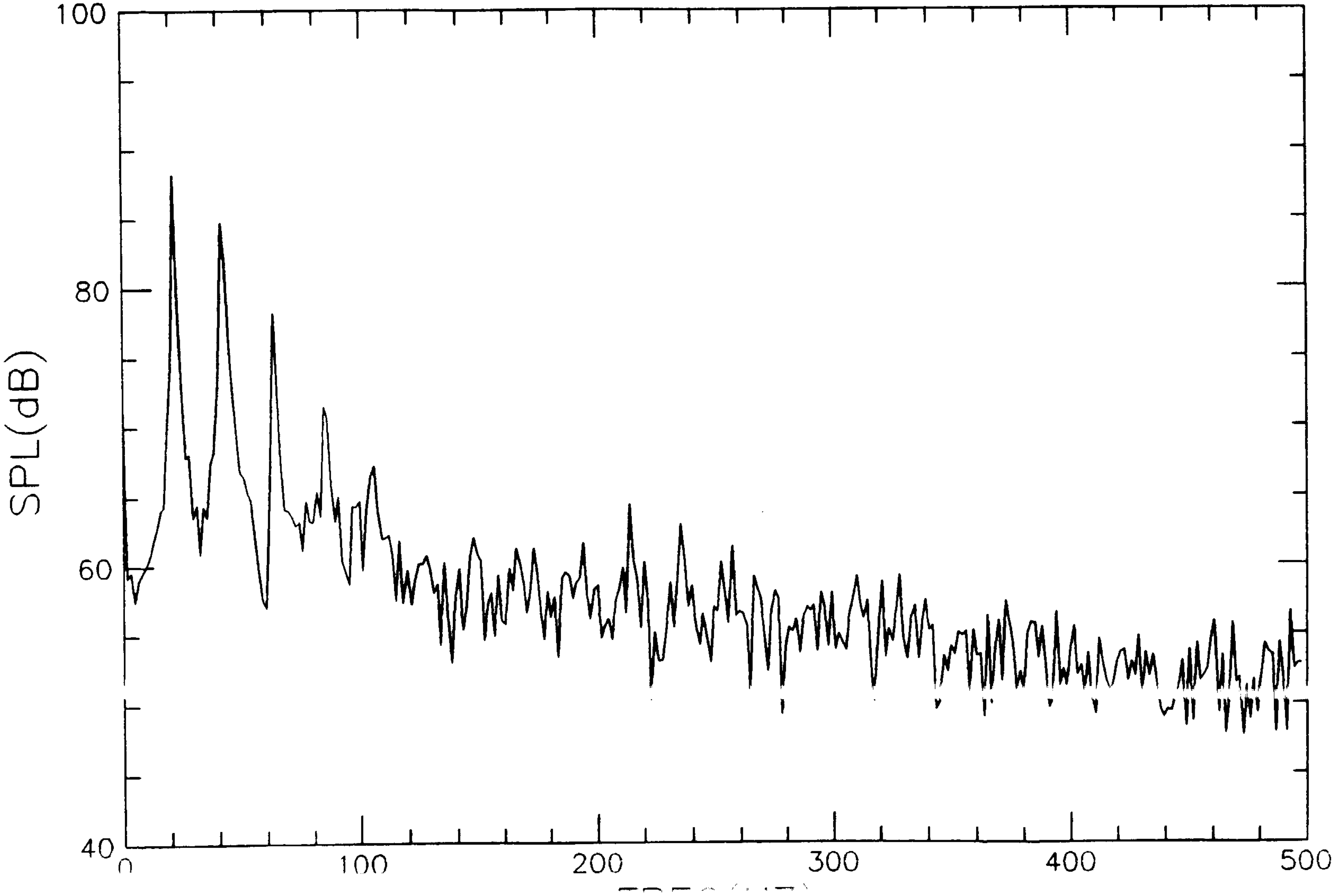

Figure 30. Doppler spectrum; Δf=1.53 Hz; θ_1=141.15°; Δθ=15.1°.

Figure 31. De-Dopplerized spectrum; $\Delta f=1.53$ Hz; $\theta_1=16.25°$; $\Delta\theta=6.25°$.

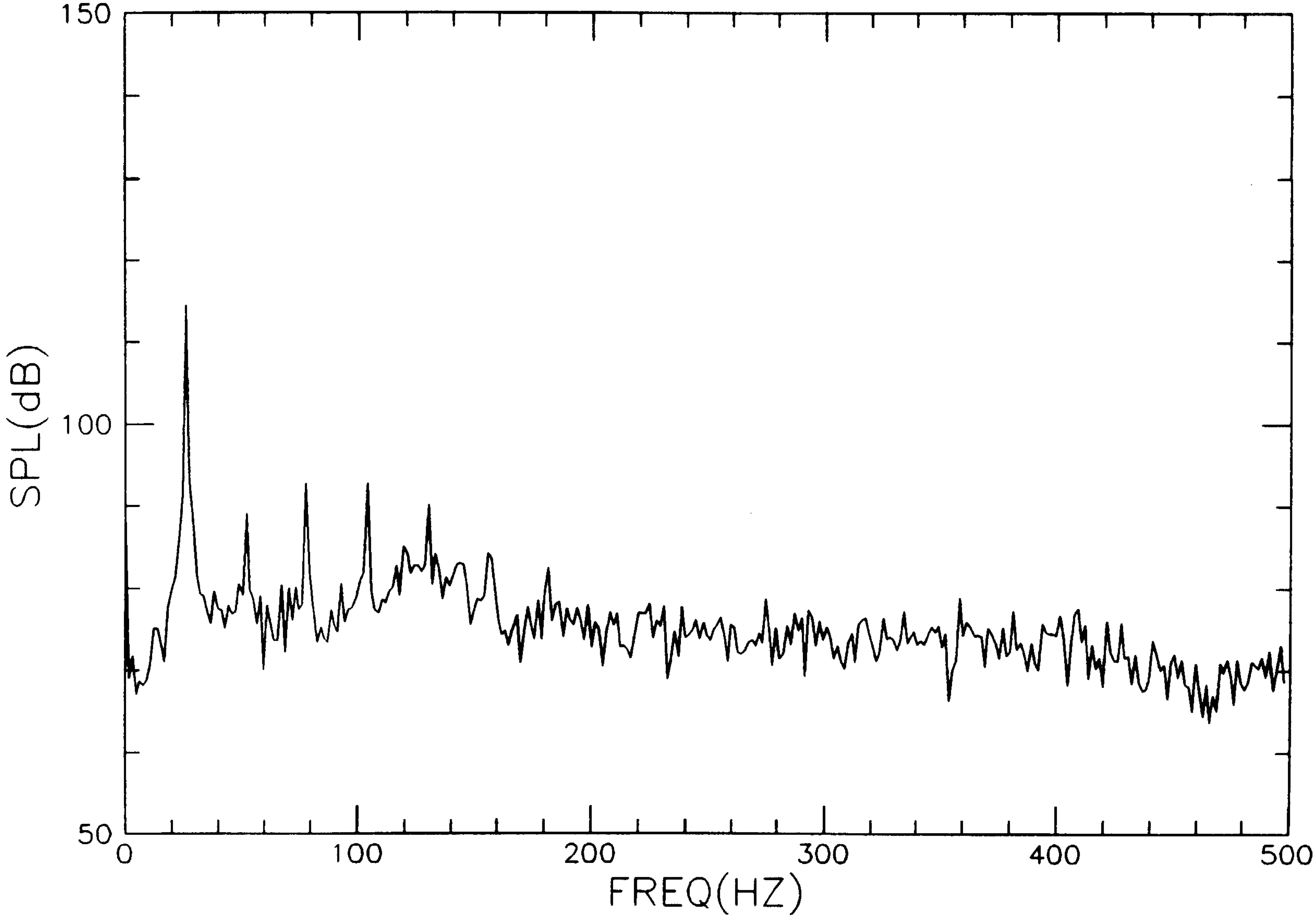

Figure 32. De-Dopplerized spectrum; Δf=1.53 Hz; θ_1=20.3°; Δθ=10.73°.

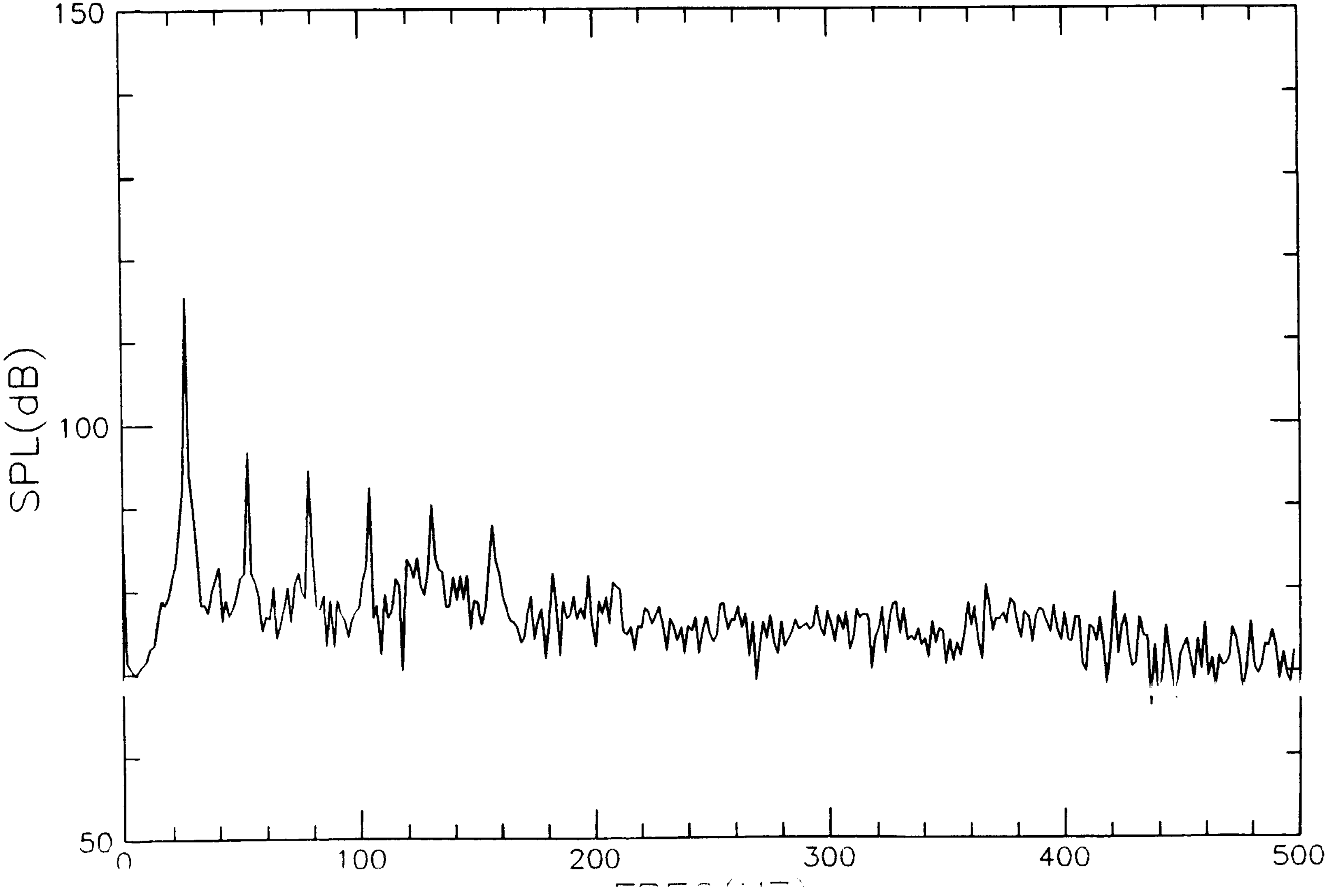

Figure 33. De-Dopplerized spectrum; $\Delta f=1.53$ Hz; $\theta_1=27.6^\circ$; $\Delta\theta=21.33^\circ$.

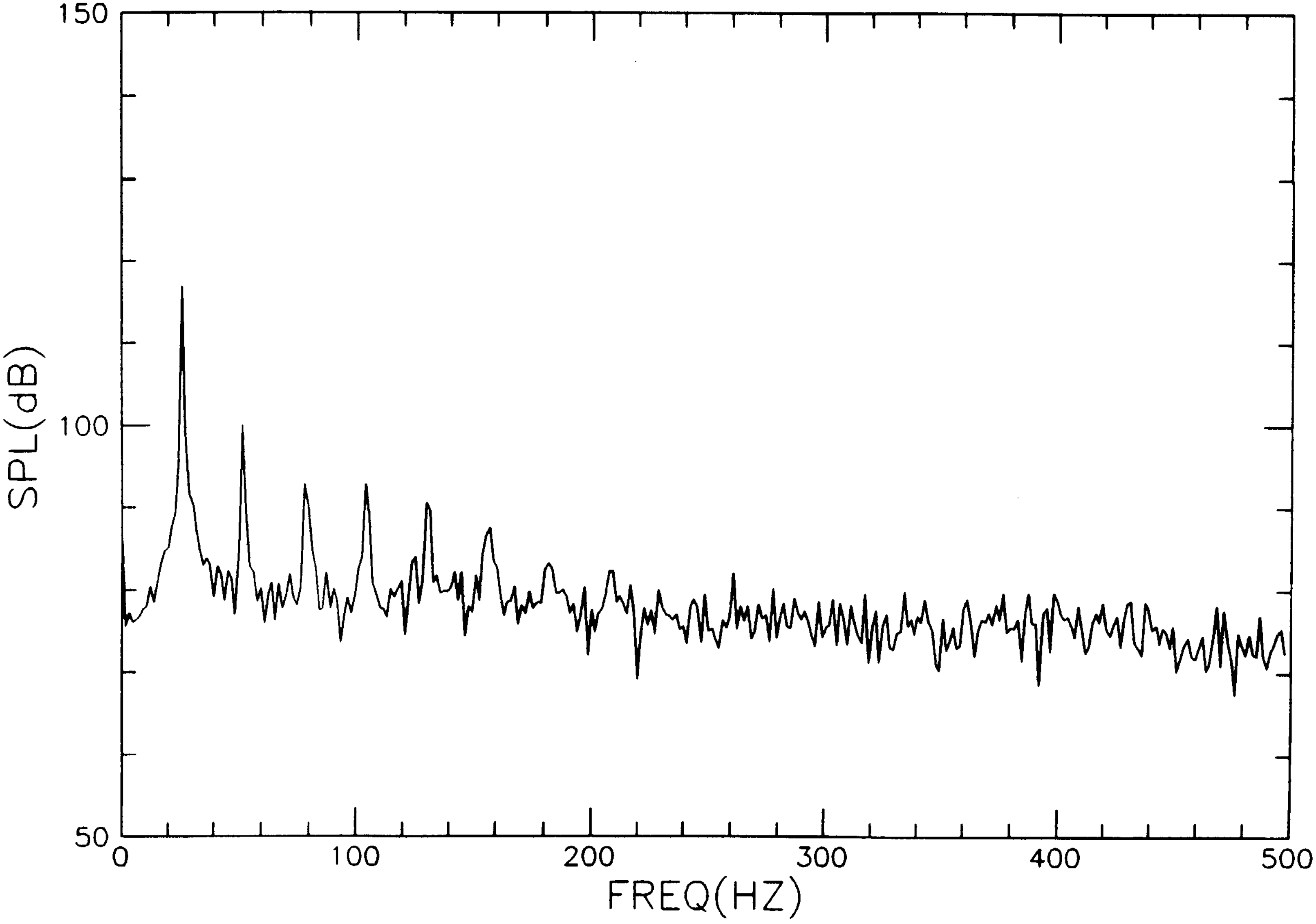

Figure 34. De-Dopplerized spectrum; $\Delta f=1.53$ Hz; $\theta_1=41.9°$; $\Delta\theta=43.35°$.

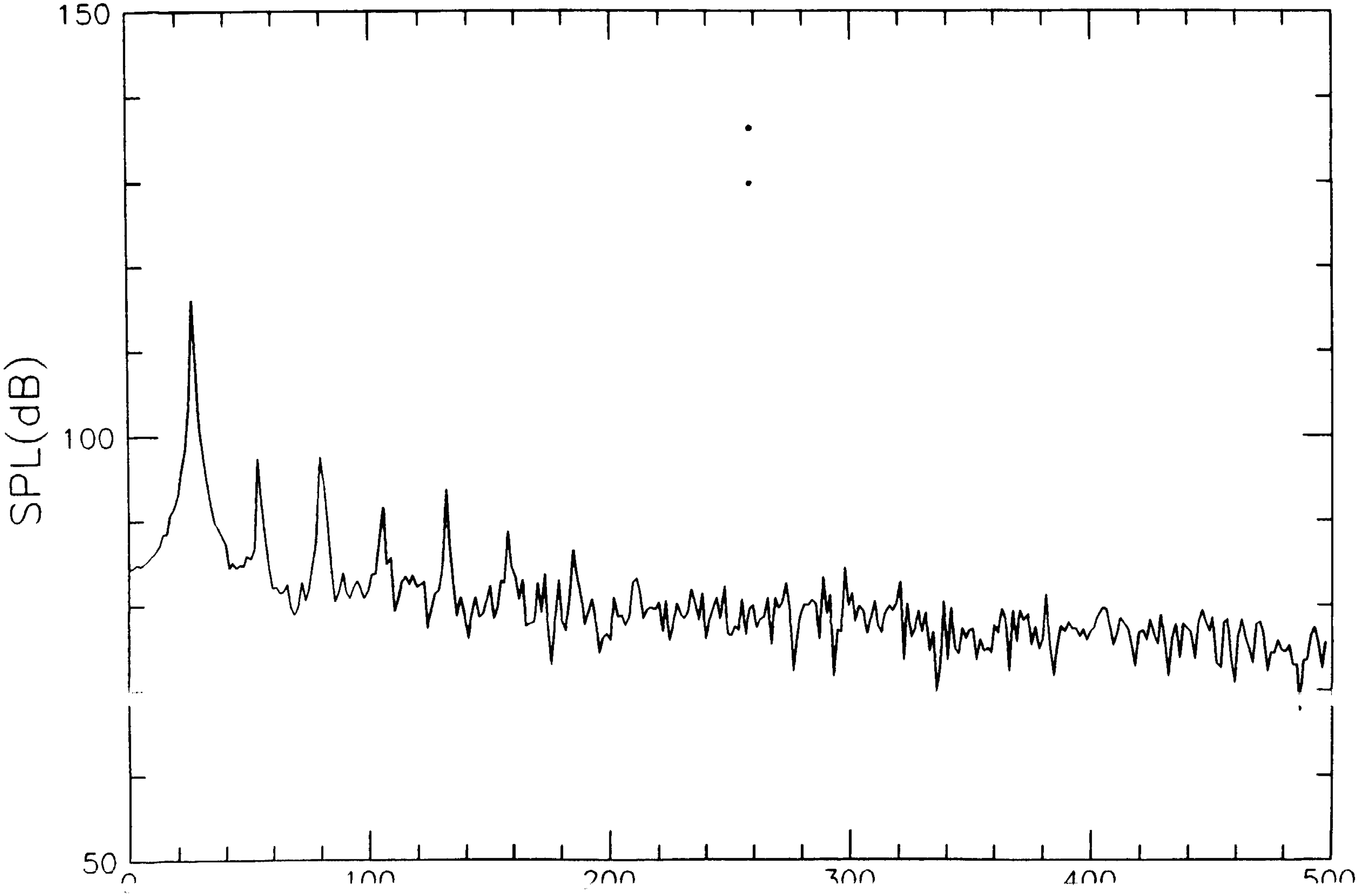

Figure 35. De-Dopplerized spectrum; $\Delta f=1.53$ Hz; $\theta_1=72.0^\circ$; $\Delta\theta=53.1^\circ$.

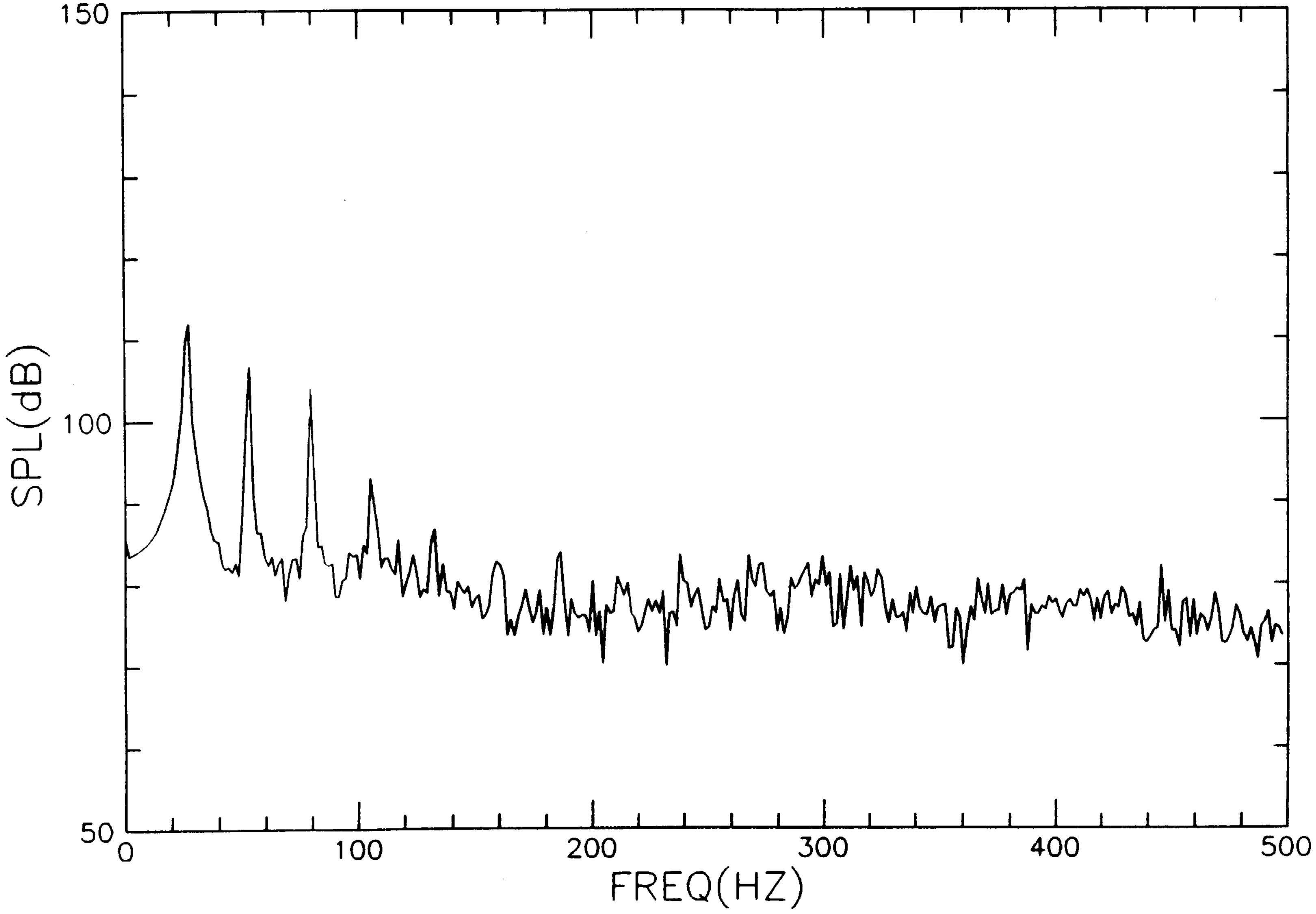

Figure 36. De-Dopplerized spectrum; $\Delta f=1.53$ Hz; $\theta_1=114.7^{\circ}$; $\Delta\theta=31.4^{\circ}$.

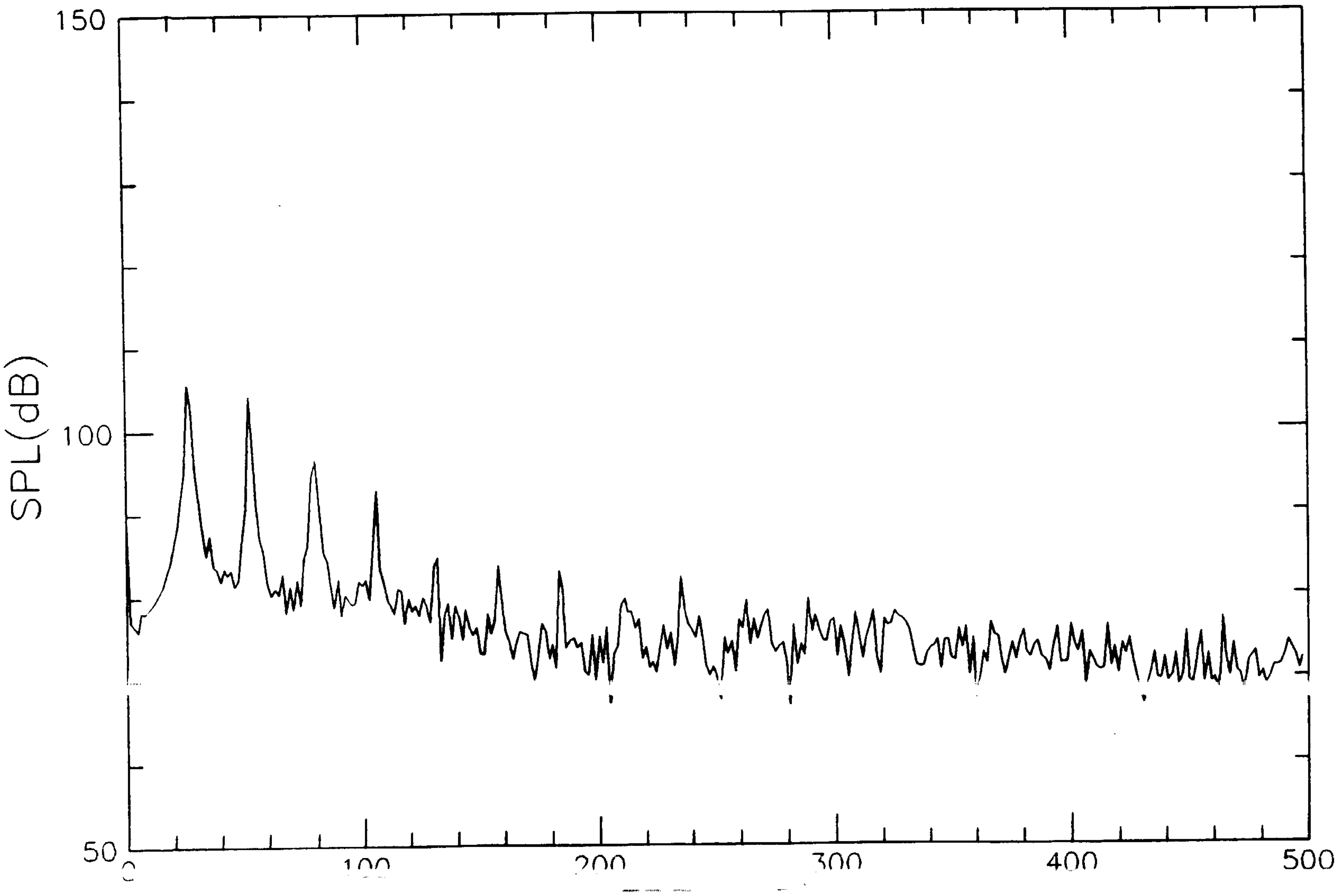

Figure 37. De-Dopplerized spectrum; $\Delta f=1.53$ Hz; $\theta_1=141.15^\circ$; $\Delta\theta=15.1^\circ$.

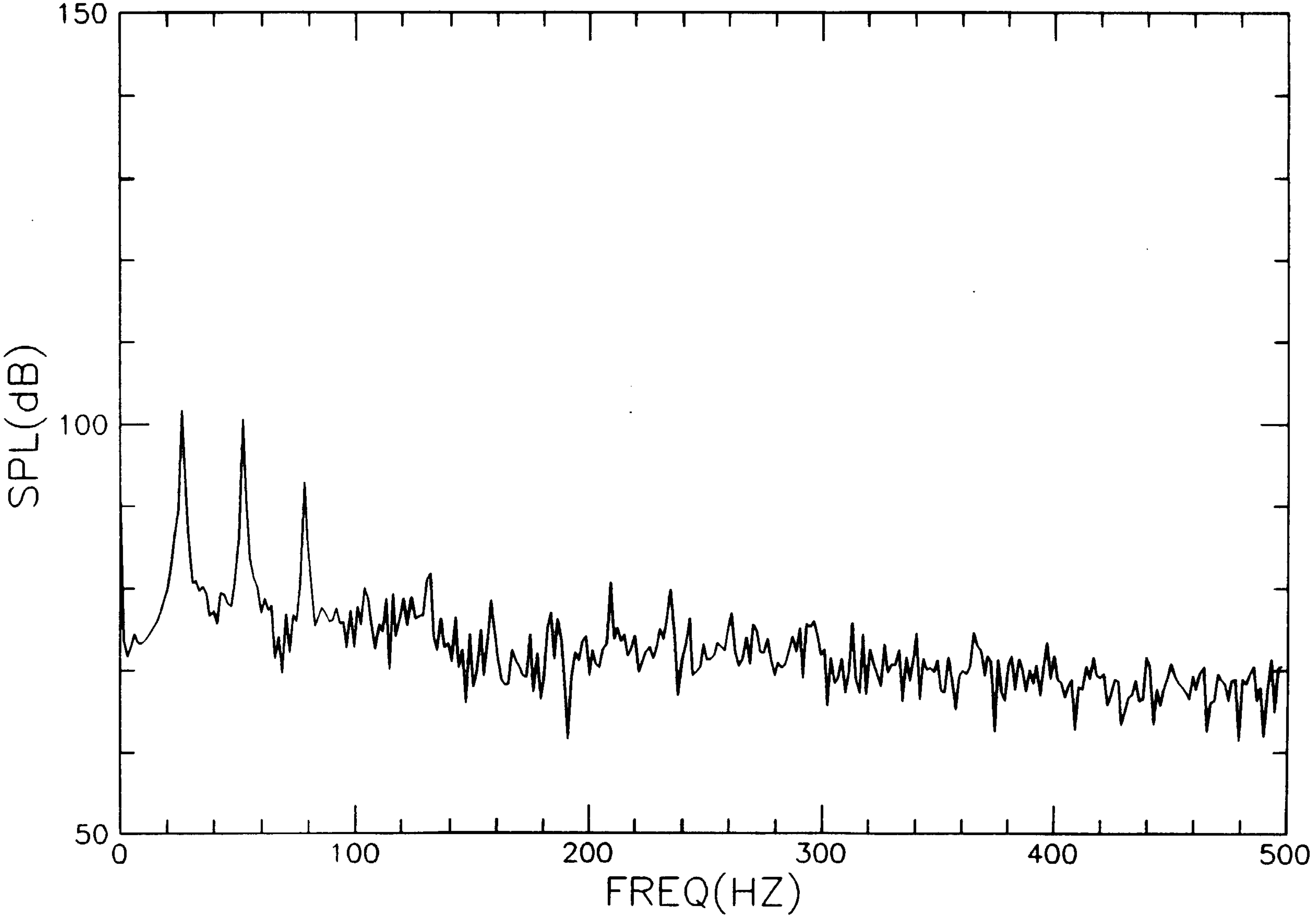

Figure 38. Simulated emission time history.

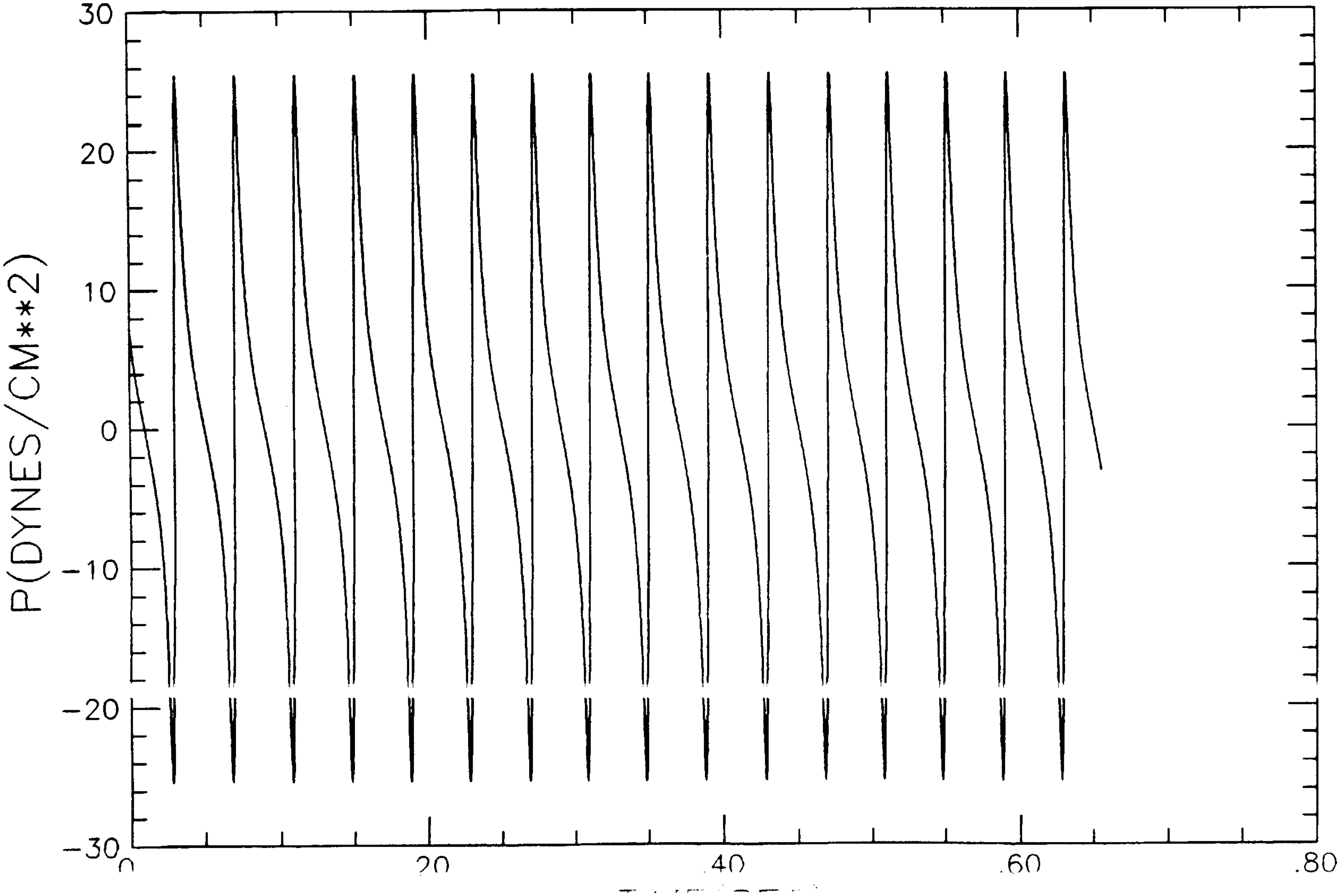

Figure 39. Simulated reception time history; $\theta_1=16.25^o$; $\Delta\theta=10.26^o$.

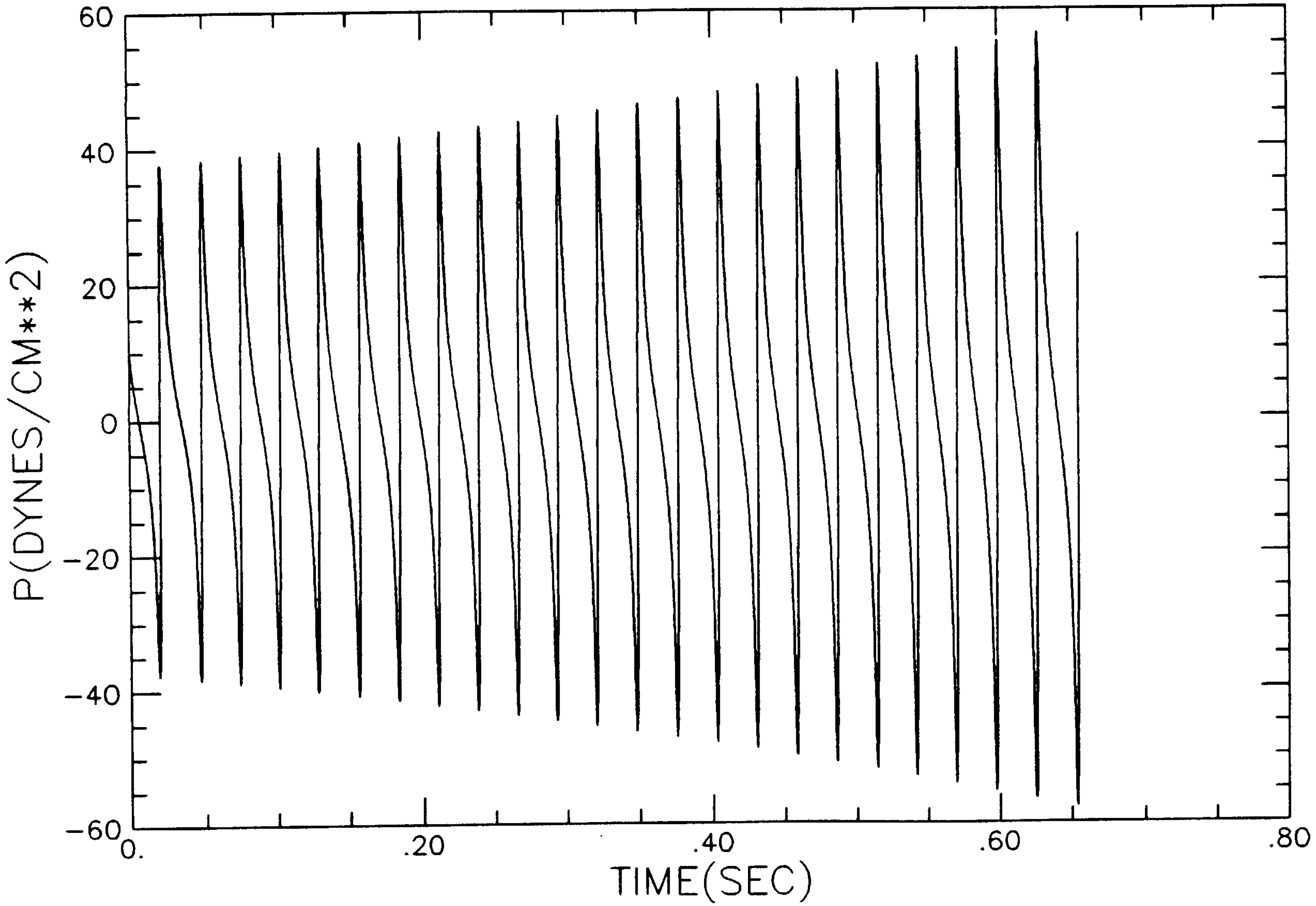

Figure 40. Simulated reception time history; $\theta_1=141.15^o$; $\Delta\theta=12.39^o$.

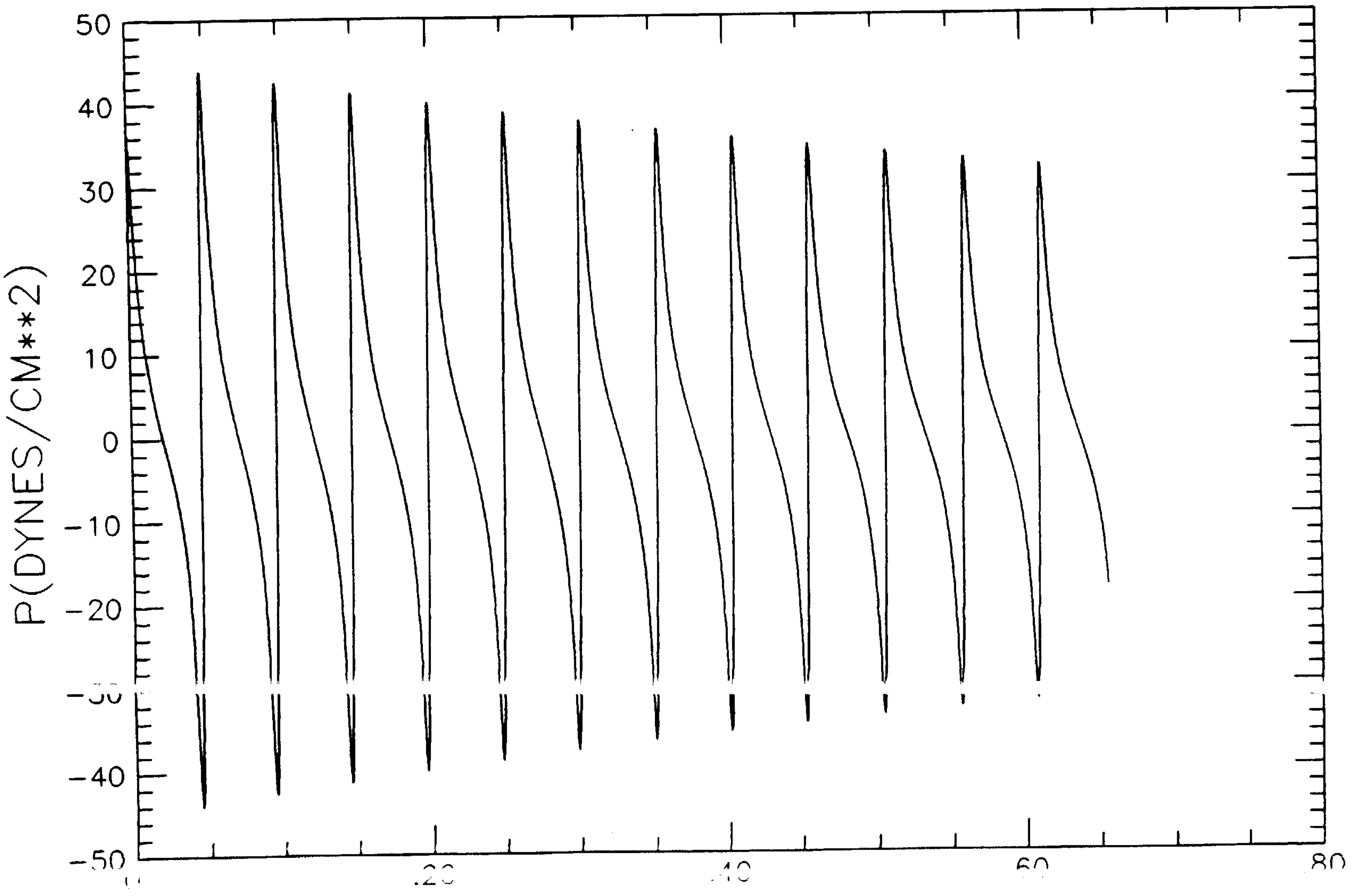

Figure 41. Simulated spectrum; $\Delta f=1.53$ Hz; $\theta_1=16.25^{\circ}$; $\Delta\theta=10.26^{\circ}$.

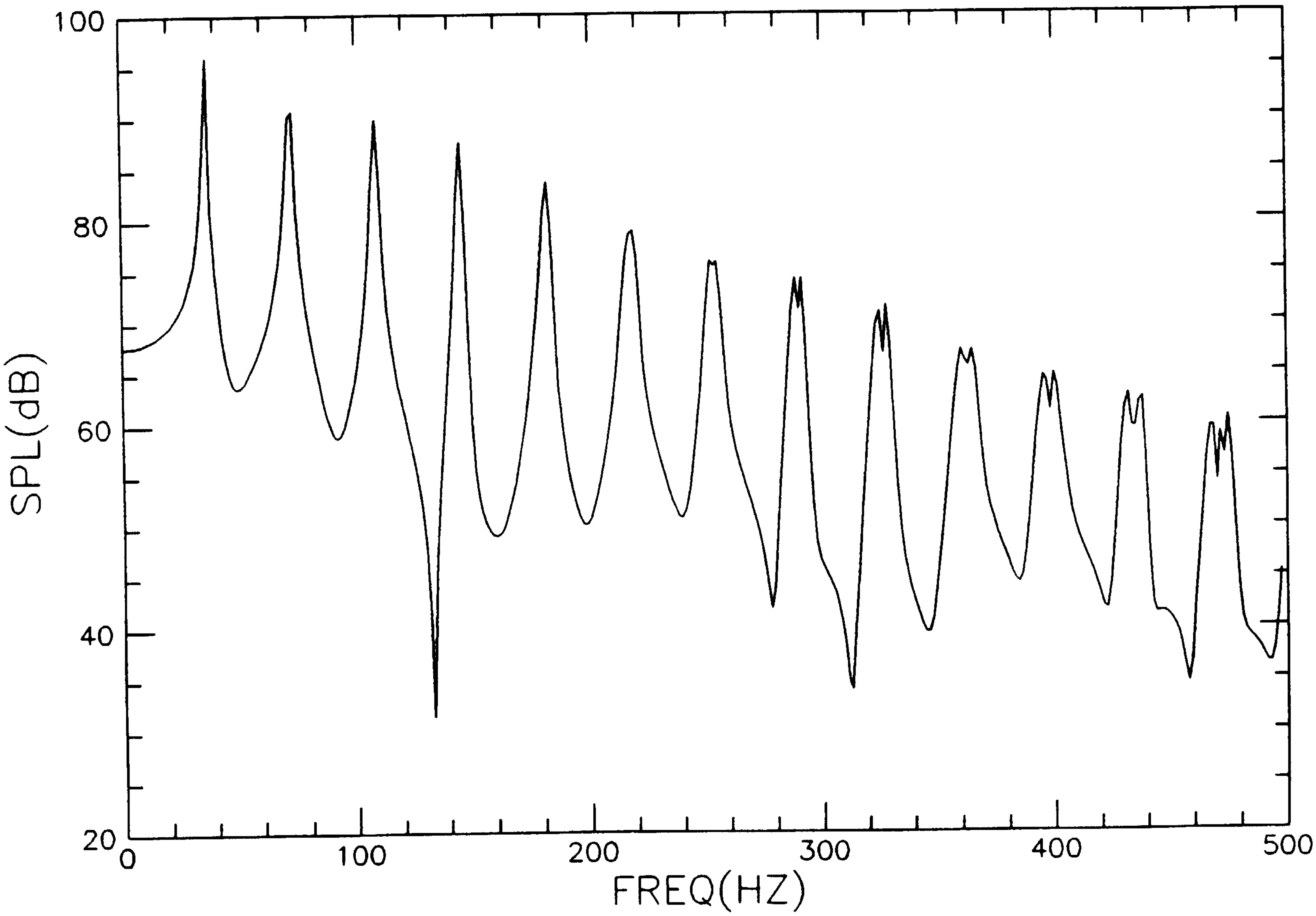

Figure 42. Simulated spectrum; Δf=1.53 Hz; θ_1=20.3°; Δθ=17.06°.

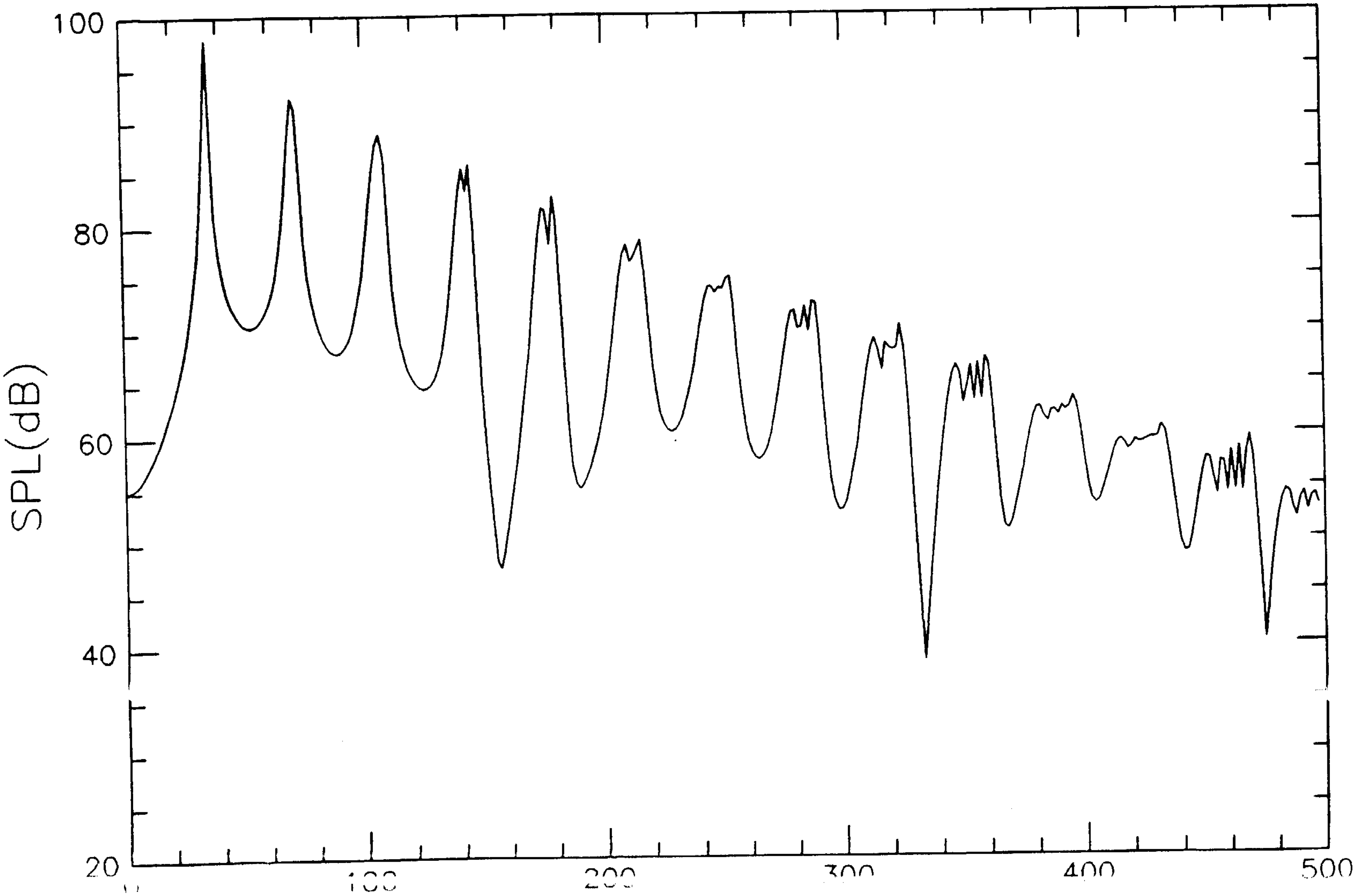

Figure 43. Simulated spectrum; $\Delta f=1.53$ Hz; $\theta_1=27.6^o$; $\Delta\theta=31.45^o$.

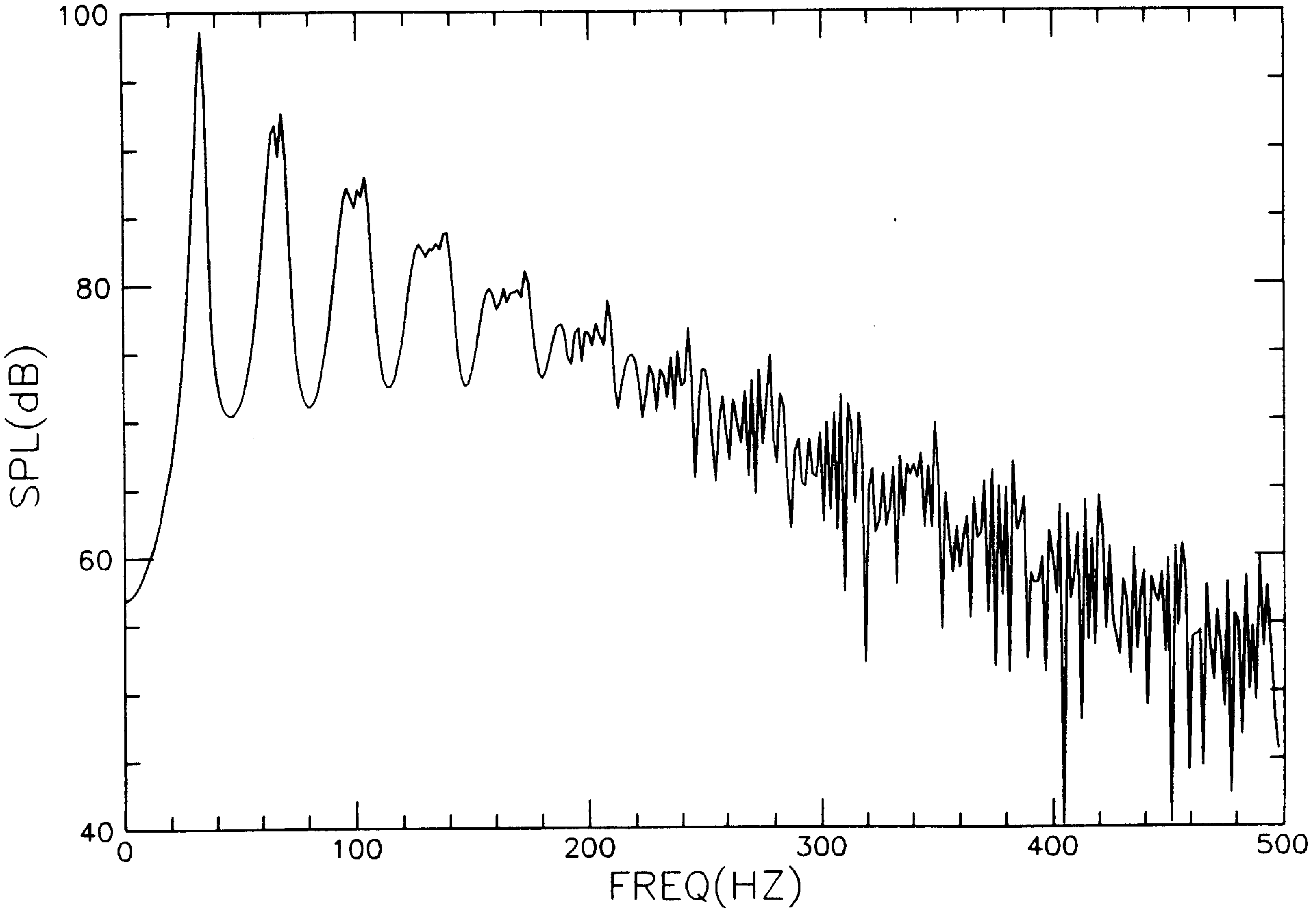

Figure 44. Simulated spectrum; Δf=1.53 Hz; θ_1=41.9°; Δθ=50.05°.

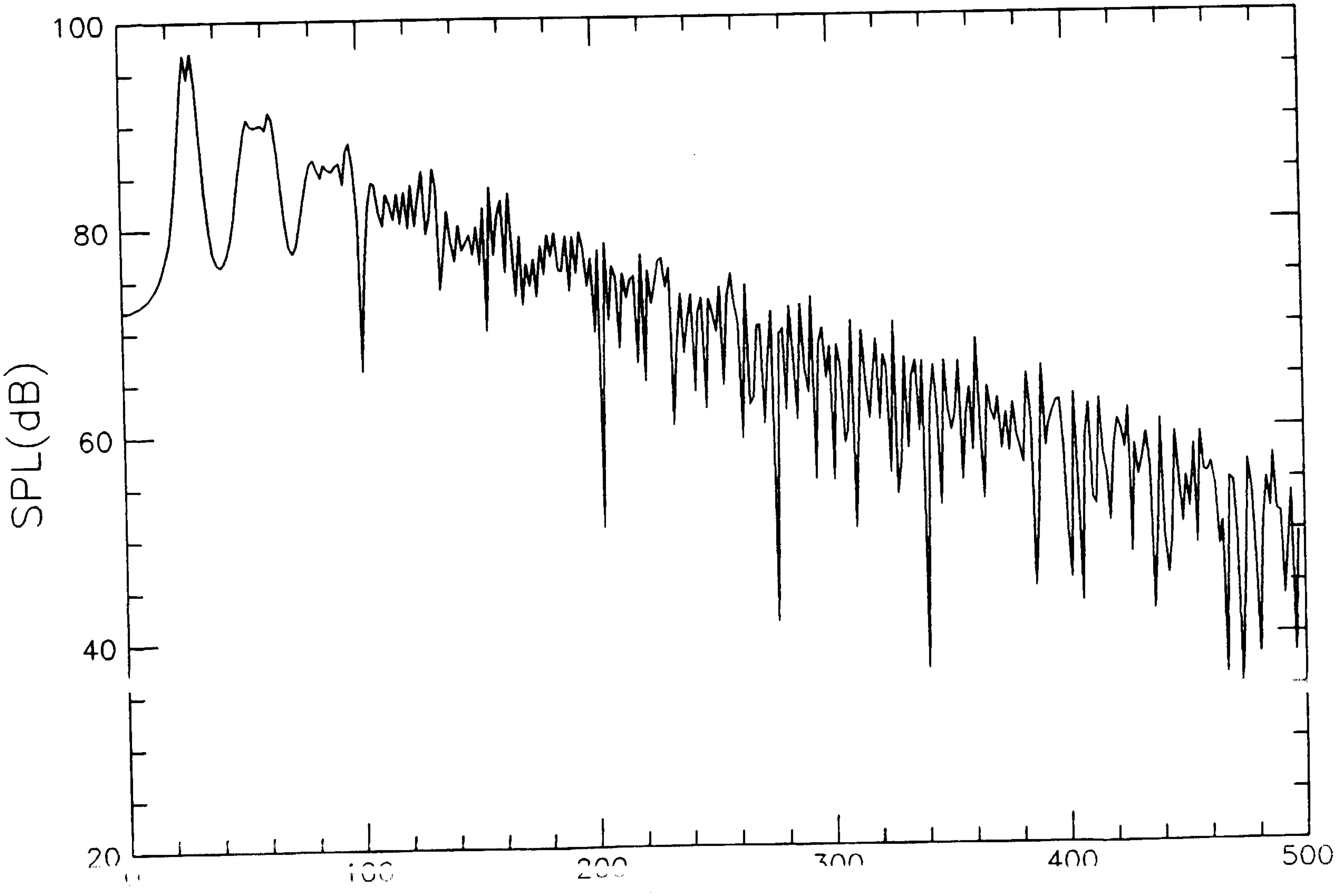

Figure 45. Simulated spectrum; $\Delta f=1.53$ Hz; $\theta_1=72.0°$; $\Delta\theta=49.69°$.

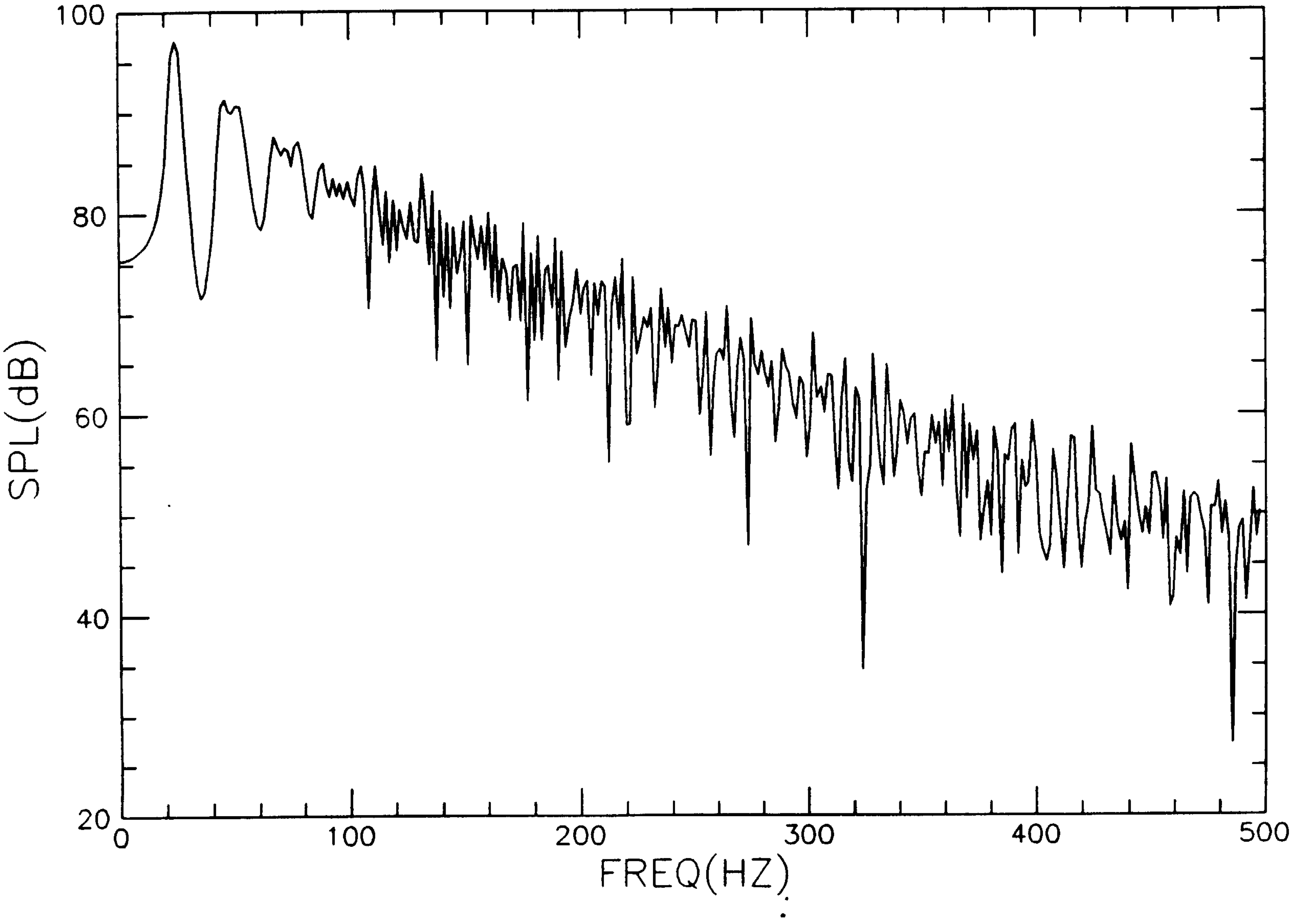

Figure 46. Simulated spectrum; $\Delta f=1.53$ Hz; $\theta_1=114.7^{\circ}$; $\Delta\theta=27.12^{\circ}$.

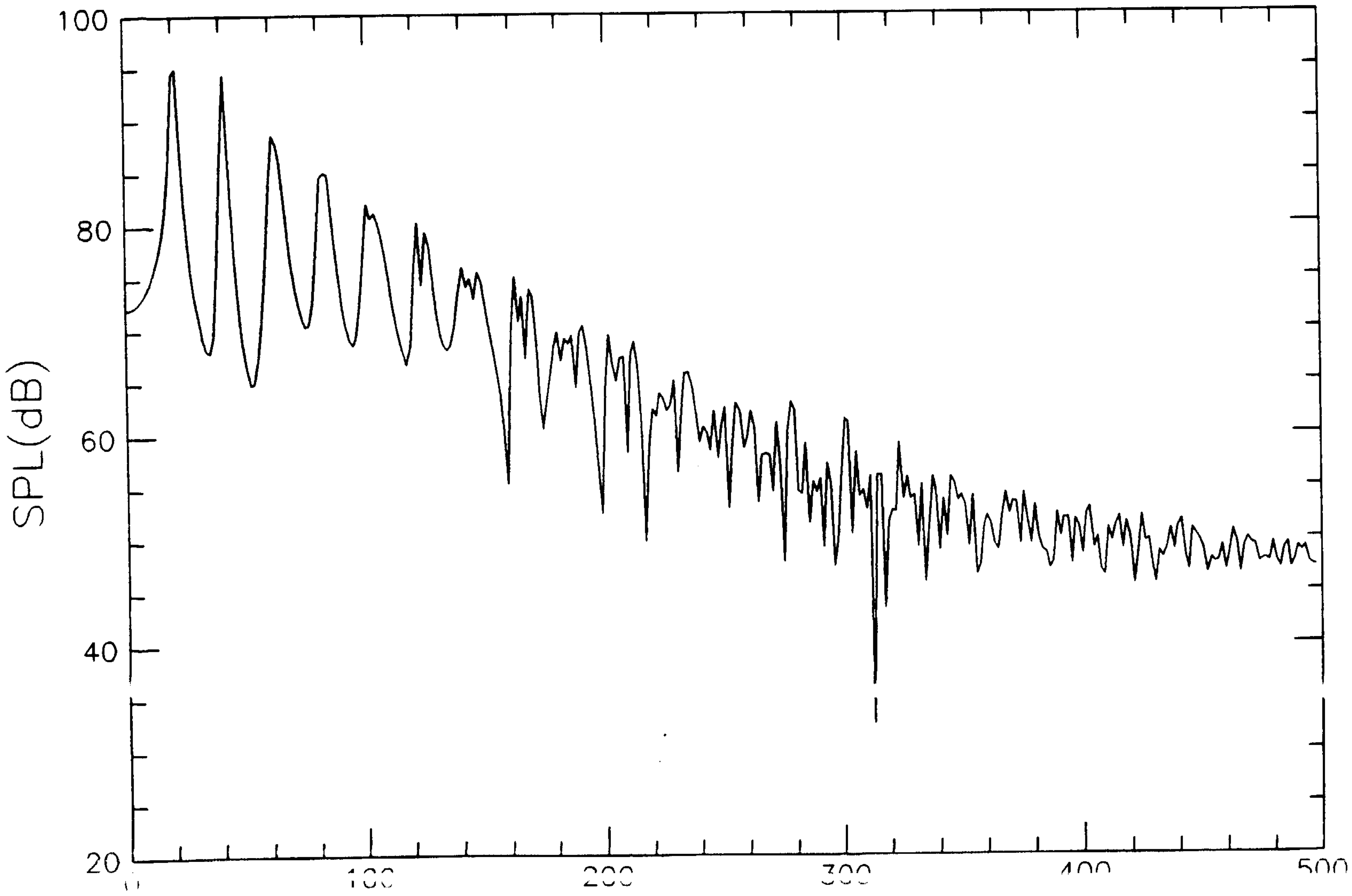

Figure 47. Simulated spectrum; $\Delta f=1.53$ Hz; $\theta_1=141.15^\circ$; $\Delta\theta=12.39^\circ$.

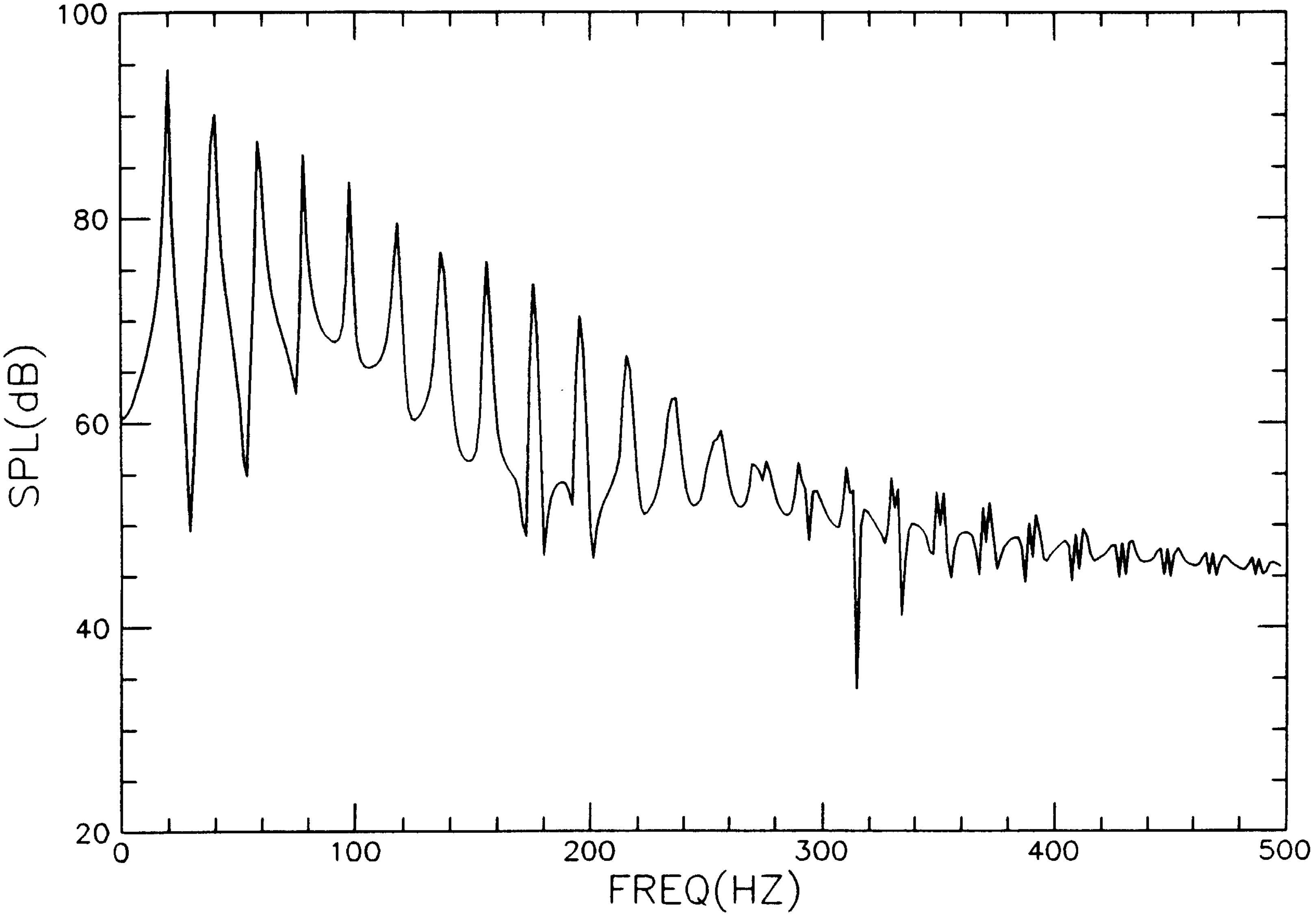

NASA
National Aeronautics and Space Administration

Report Documentation Page

1. Report No.
NASA CR-187546

2. Government Accession No.

3. Recipient's Catalog No.

4. Title and Subtitle
Signal Processing of Aircraft Flyover Noise

5. Report Date
May 1991

6. Performing Organization Code

7. Author(s)
Jeffrey J. Kelly

8. Performing Organization Report No.

10. Work Unit No.
537-03-20

9. Performing Organization Name and Address
Lockheed Engineering & Sciences Company
144 Research Research Drive
Hampton, VA 23666

11. Contract or Grant No.
NAS1-19000

13. Type of Report and Period Covered
Contractor Report

12. Sponsoring Agency Name and Address
National Aeronautics and Space Administration
Langley Research Center
Hampton, VA 23665-5225

14. Sponsoring Agency Code

15. Supplementary Notes
Langley Technical Monitor: Robert A. Golub

16. Abstract

A detailed analysis of signal processing concerns for measuring aircraft flyover noise is presented. Development of a de-Dopplerization scheme for both corrected time history and spectral data is discussed along with an analysis of motion effects on measured spectra. A computer code was written to implement the de-Dopplerization scheme. Input to the code is the aircraft position data and the pressure time histories. To facilitate ensemble averaging, a uniform level flyover is considered in the study but the code can accept more general flight profiles. The effects of spectral smearing and its removal is discussed. Using data acquired from XV-15 tilt-rotor flyover test comparisons are made showing the measured and corrected spectra. Frequency shifts are accurately accounted for by the method. It is shown that correcting for spherical spreading, Doppler amplitude, and frequency can give some idea about source directivity. The analysis indicated that smearing increases with frequency and is more severe on approach than recession.

17. Key Words (Suggested by Author(s))

De-Dopplerization
Flyover noise measurements
High Speed Civil Transport
Fast Fourier transform
Signal processing
Signal processing
XV-15 tilt-rotor
Spectral smearing
Ensemble averaging

18. Distribution Statement
Unclassified-Unlimited

Subject Category 71

19. Security Classif. (of this report)
Unclassified

20. Security Classif. (of this page)
Unclassified

21. No. of pages
85

22. Price
A05

NASA FORM 1626 OCT 86